Influence of particulate matter on observed albedo reductions on Plaine Morte glacier, Swiss Alps

Master's Thesis

Faculty of Science

University of Bern

presented by

Eva Bühlmann

2011

Supervisor:

Prof. Dr. Margit Schwikowski

Paul Scherrer Institute and Oeschger Centre for Climate Change Research

Co-Supervisor:

Prof. Dr. Martin Hoelzle

Department of Geosciences,University of Fribourg

Advisor:

Pierre-Alain Herren

Paul Scherrer Institute and Oeschger Centre for Climate Change Research

Moulin on Plaine Morte glacier, Eva Bühlmann, 2010

Table of contents

List of figures

List of tables

List of abbreviations

AWS	Automated Weather Station
BC	Black Carbon
BRDF	Bi-Directional Reflectance Function
DAPI	4' ,6-diamidino-5-phenylindole
EC	Elemental Carbon
ELA	Equilibrium Line Altitude
EPS	Extracellular Polymeric Substances
IC	Ion Chromatography
ICP-MS	Inductively Coupled Plasma Mass Spectrometer
IPCC	Intergovernmental Panel on Climate Change
IR-MS	Isotope Ratio Mass Spectrometery
LLR	Local Loose Rock
LOI	Loss on Ignition
m a.s.l.	metres above sea level
m weq	metre water equivalent
NIR	Near Infrared Spectrum
OC	Organic Carbon
PBL	Planetary Boundary Layer
PM	Particulate Matter
ppb	parts per billion
ppm	parts per million
PSI	Paul Scherrer Institute
PTFE	PolyTetraFluoroEthylene
REE	Rare Earth Elements
RF	Radiative Forcing
SDE	Saharan Dust Event
SEM	Scanning Electron Microscopy
SP2	Single Particle Soot Photometer
UTC	Coordinated Universal Time
VIS	Visible Spectrum
VSMOW	Vienna Standard Mean Ocean Water
XRD	X-ray Diffraction
λ	Wave Length
µeq	micro equivalent

List of chemical denotations

C	carbon
$C_{12}H_{22}O_{11}$	sucrose
$CaCO_3$	calcite
CO_2	carbon dioxide
H	hydrogen
HCl	hydrochloric acid
HNO_3	nitric acid
LiF	lithium fluoride
N_2	molecular nitrogen

List of ions

Ca^{2+}	calcium
Cl^-	chloride
CO_3^{2-}	carbonate
H^+	hydrogen ion
K^+	potassium
Mg^{2+}	magnesium
Na^+	sodium
NH_4^+	ammonium
NO_3^-	nitrate
SO_4^{2-}	sulphate

List of rare earth elements (REE)

Ce	cerium
Eu	europium
La	lanthanum
Nd	neodymium
Pr	praseodyimum
Sc	scandium
Sm	samarium
Yb	ytterbium

List of trace elements

Ag	silver
Al	aluminum
Ba	barium
Bi	bismuth
Ca	calcium
Cd	cadmium
Co	cobalt
Cr	chromium
Cs	cesium
Cu	copper
Fe	iron
Li	lithium
Mg	magnesium
Mn	manganese
Mo	molybdenum
Na	sodium
Ni	nickel
Pb	lead
Rb	rubidium
Sb	antimony
Sr	strontium
Th	thorium
Ti	titanium
Tl	thallium
U	uranium
V	vanadium
W	tungsten
Zn	zinc
Zr	zirconium

Summary

In the face of global warming and subsequent glacial retreat, studies on the snow/ice-albedo feedback mechanisms have gained importance within the climate science community. Deposition of impurities on snowpacks or glaciers was found to reduce their surface albedo and therefore enhance melting and contribute to global warming by additional light-absorption. So far, soot from fossil fuel combustion was most emphasised due to its strong absorption properties and its anthropogenic origin. However, supra-glacial particulate deposits, generally termed cryoconite, have been shown to contain a diversity of additional absorbing components, including mineral dust, living microorganisms and decomposing organic matter. Although a variety of studies were conducted to determine driving forces behind observed glacial albedo reductions, knowledge about the relative contribution of different cryoconite components remains scarce, especially in the Alpine region.

The present study aimed to investigate the origin and biogeochemical composition of cryoconite on Alpine glaciers and to contribute to a more profound understanding of relative effects of different cryoconite components to observed estival albedo reductions. The study site at Plaine Morte glacier (46°23'N, 7°29'E) is situated in the western Swiss Alps and has been previously reported to be characterised by exceptional sensitivity towards changes in the energy budget. In the course of the ablation season in 2010, broadband albedo and spectral reflectance measurements were performed during four individual days of field campaign (1 June, 6 July, 20 July and 25 August). Snow samples, particulate matter and ice samples were collected and transferred to the laboratories of the PSI for biogeochemical analyses. Major ions and trace elements were used to identify impurity sources within the snowpack. The bulk mineralogy, the organic fraction and the EC content of cryoconite were determined. Biogenic matter and microorganisms were additionally assessed qualitatively by microscopic techniques. The obtained cryoconite composition was then related to the observed albedo of Plaine Morte glacier to quantify the relative contribution of each of the cryoconite compounds.

Cryoconite was found to be dominated by mineral dust of local origin and outcropping dust layers within the melting glacier ice instead of dust from long range transport i.e. Saharan dust. The organic matter fraction was substantially higher than found in local loose rock, indicating enhanced biological activity. So far, no methods exist to quantitatively assess the contribution of microorganisms to the observed albedo reduction. EC showed only minor mass-contribution to the total cryoconite load, but seemed to be subject to strong multi-annual enrichment. Although no suitable model was found for snow and ice albedo under the influence of impurities, the results indicated substantial EC induced albedo reductions. Additionally, dark humic substances were presumed to be of major importance, whereas mineral dust and living organisms were found to have a limited effect on the surface albedo of Plaine Morte glacier. Overall, the largest impact of cryoconite seemed to be caused by triggering of a positive feedback mechanism including enhanced strongly light-absorbing liquid water content. This project demonstrates the local importance of cryoconite accumulations to the energy balance of a glacier and highlights the need for further research concerning humic substances and their relative contribution to albedo changes.

Zusammenfassung

Seit sich die Klimaforschung mit der globalen Erwärmung und dem damit verbundenen Abschmelzen der Gletscher auseinandersetzt, ist auch der Schnee/Eis-Albedo Feedbackmechanismus in ihren Fokus gerückt. Die Albedo stark reflektierender Schnee- oder Gletscheroberflächen wird durch die Ablagerung dunkler Partikel reduziert. Dabei kommt es zu erhöhter Absorption von Strahlung, die den Schmelzprozess vorantreibt. Dies trägt indirekt zur Erwärmung der Atmosphäre bei. Supra-glaziale Partikelablagerungen werden generell als Kryokonit bezeichnet und enthalten neben Russ nachweislich weitere absorbierende Bestandteile, wie zum Beispiel Mineralstaub, Mikroorganismen und zersetzte organische Materie. Wegen der starken Absorptionseigenschaften und der anthropogenen Quelle wurde der Schwerpunkt der Forschung bisher vor allem auf Russpartikel aus der Verbrennung fossiler Brennstoffe gelegt. Obwohl einige Studien zu einem umfassenderen Verständnis beobachteter Albedo-Reduktionen beigetragen haben, bestehen noch immer viele Unklarheiten, welcher Anteil daran den verschiedenen Kryokonit-Bestandteilen zugeschrieben werden muss. Insbesondere in den Alpen besteht weiterhin Forschungsbedarf.

Die vorliegende Studie verfolgte das Ziel, die Herkunft und biogeochemische Zusammensetzung von Kryokonit auf einem alpinen Gletscher zu bestimmen. Sie soll zu einem vertieften Verständnis der albedo-relevanten Komponenten und ihrem relativen Effekt auf die sommerliche Albedo-Reduktion beitragen. Die Forschungsregion um den Plaine Morte Gletscher (46°23'N, 7°29'E) liegt in den westlichen Schweizer Alpen. Dieser Gletscher scheint besonders sensibel auf Veränderungen in der Energiebilanz zu reagieren. An vier einzelnen Tagen während der Ablationsphase im Sommer 2010 (1. Juni, 6. Juli, 20. Juli und 25. August), wurden bei der Feldarbeit Breitbandalbedo- und spektral aufgelöste Reflektanzmessungen durchgeführt. Gleichzeitig wurden Schneeproben, Kryokonit-Material und Eisproben entnommen und für biogeochemische Analysen in die Labors des PSI gebracht. Mittels Ionen und Spurenelementen wurde versucht, die Herkunft von Verunreinigungen innerhalb der Schneedecke zu bestimmen. Die mineralische Zusammensetzung, der organischen Anteil sowie der EC-Gehalt von Kryokonit wurden ermittelt. Zusätzlich erfolgten qualitative mikroskopische Untersuchungen von biogener Materie und Mikroorganismen. Anschliessend wurde versucht, die beobachtete Kryokonit-Zusammensetzung mit der erfassten Albedo-Veränderung auf dem Plaine Morte Gletscher in Verbindung zu bringen, um den jeweiligen Beitrag der unterschiedlichen Kryokonit-Bestandteile zu quantifizieren.

Kryokonit wurden durch lokalen Mineralstaub und durch ausschmelzende Staubschichten innerhalb des Gletschereises dominiert. Der Gehalt organischer Materie auf der Gletscheroberfläche war im Vergleich zu lokalem Lockergestein wesentlich erhöht. Dies deutet auf gesteigerte biologische Aktivität hin. Leider sind bekannte Methoden unzureichend, um den Anteil der Mikroorganismen an der beobachteten Albedoreduktion quantitativ zu bestimmen. Der Masseanteil des elementaren Kohlenstoffs am gesamten Kryokonit ist relativ gering, scheint aber weiter akkumuliert zu werden, da er keinen Abbauprozessen unterliegt. Obwohl kein adäquates Modell zur Simulation von Schnee- und Eisalbedo unter dem Einfluss verschiedener Verunreinigungen gefunden wurde, deuteten die Resultate darauf hin, dass EC einen beträchtlichen Einfluss auf die Albedo-Reduktion hat. Zusätzlich schienen dunkle humusähnliche Substanzen von grosser Bedeutung für die Albedo des Plaine Morte Gletschers zu sein, wohingegen der direkte Effekt von Mineralstaub und Mikroorganismen als gering eingeschätzt werden kann. Insgesamt wird angenommen, dass

der grösste Einfluss von Kryokonit darin besteht, einen Feedbackmechanismus auszulösen, der verstärktes Auftreten von stark lichtabsorbierendem Flüssigwasser zur Folge hat. Diese Studie verdeutlicht die Bedeutung von Kryokonit für die Energiebilanz eines Gletschers. Sie unterstreicht weiterhin den Bedarf nach vertiefenden Untersuchungen der humusähnlichen Substanzen und deren Beitrag zu Veränderungen in der Albedo.

1. Introduction

Climate change is among the most relevant environmental issues of the 21st century, due to its global long-term impacts. The discourse on climate change entails scientific debates about the climatic relevance of different aerosol species. While light-scattering aerosols (principally sulphuric species) are considered to directly and indirectly exert a cooling influence on the atmosphere (Charlson et al., 1992), carbonaceous aerosols in contrast show reverse effects (Ramanathan et al., 2007). In this respect, soot from fossil fuel combustion and biomass burning is among the most important particles within aerosols, since its origin is primarily anthropogenic. Soot aerosols affect the radiation balance and alter the atmospheric temperature by strongly absorbing long- and shortwave radiation (Forster et al., 2007). Black carbon (BC), which is produced by incomplete combustion and constitutes the main component of soot, is primarily responsible for this strong absorption behaviour (Jacobson, 2004). The radiative forcing (RF) potential of BC in the atmosphere was extensively discussed for the first time in the second assessment report of the Intergovernmental Panel on Climate Change (IPCC; Schimel et al., 1995). Although recognised earlier (Warren and Wiscombe, 1980), its consecutive warming effect after the deposition to a snowpack or other bright surfaces was not accounted for until the fourth IPCC assessment report of the year 2007 (Forster et al., 2007). When BC particles are deposited they may lower the surface albedo and cause direct surface warming due to additional absorption (Jacobson, 2004). Figure 1 depicts the snow-albedo feedback mechanism, intensified by BC in snow and ice. In 2007, a "low level of scientific understanding" (Forster et al., 2007: p. 85) was still assigned for the RF of BC in snow and ice. Based on the early findings of Warren and Wiscombe (1980), several studies have recently been conducted to close this research gap (e.g. Hansen and Nazarenko, 2003; Jacobson, 2004; Flanner et al., 2007; Gardner and Sharp, 2010; Yasunari et al., 2010; Aoki et al., 2011). The surface albedo has been reported to be of particular importance to the energy budget of glaciers (Oerlemans, 2010; c.f. section 2.1). In addition to BC, other compounds, such as microorganisms and decomposing organic matter (Kohshima et al., 1993; Kohshima, 1994; Thomas and Duval, 1995; Takeuchi, 2001, 2002b, a, 2009) and mineral dust (Oerlemans et al., 2009; Bøggild et al., 2010) have recently been identified to contribute to supra-glacial particulate matter (PM) accumulations termed "cryoconite" (c.f. section 2.2). Since these compounds substantially reduce the albedo, these studies also contribute to a more profound understanding of the estival albedo reduction on glaciers and ice sheets. Around 10% of the earth's surface is covered by glacier ice, of which roughly 99% is located in the large ice sheets at the poles (Paterson, 1994). On a global scale, the snow/ice-albedo feedback shows largest effects in the northern hemispheric polar region with large snow or (sea) ice extent (Jacobson, 2004). Therefore, it is not surprising that little research has been done so far to determine the biogeochemical composition of dust and debris covering Alpine glaciers and to determine its albedo-relevance. However, due to larger mass turnover, a higher level of solar irradiation and the proximity to pollution sources, mid-latitude valley glaciers might be more vulnerable to the feedback mechanism induced by PM deposits (Doherty et al., 2010; Oerlemans, 2010). At the same time, these characteristics turn high Alpine glaciers into scarce but valuable climate archives (Schwikowski and Eichler, 2010), since the emission history during the industrial period is preserved in annual layers, compensating the lack of instrumental data for that period (Legrand et al., 2007). Even more importantly, Alpine glaciers act as water reservoirs, determining summer discharge of various

streams within Europe (Braun et al., 2000; Weingartner, 2007). Therefore, knowledge about glacial response to changing environmental conditions is of great importance to water resource management. In addition, Alpine glacier surfaces have been found to accumulate extraordinary dark matter in recent years (personal communication M. Schwikowski, PSI; Paul et al. 2005). Thus, mechanisms behind PM deposition and resulting albedo changes on Alpine glaciers are worth closer investigations, even if their climate impact seems to be limited to local or continental spatial scales (Forster et al., 2007).

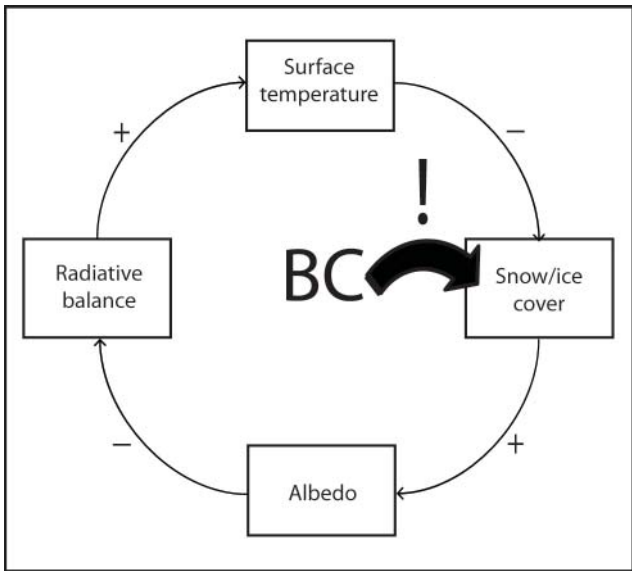

Figure 1: Schematic depiction of the snow-albedo feedback mechanism (modified after Stocker, 2009). The symbols next to the arrows indicate whether the quantities in the boxes are correlated positively (+) or negatively (-). The deposition of BC (or other impurities) intensifies the effect of the snow-albedo feedback.

1.1. State of knowledge and research motivation

So far, most studies have focussed on the albedo effect of a single cryoconite component. Due to its outstanding absorption behaviour, BC was certainly most emphasised in this respect. However, in the past few years more and more research was dedicated to the formation processes of cryoconite deposits, the microbial community within cryoconite or its effect on the albedo evolution of a glacier surface.

Black carbon

Flanner et al. (2007) identified that the Tibetan plateau suffered from strongest BC induced RF due to its proximity to large emission sources like India and Southeast Asia and a higher level of solar irradiation. Consequently, attention was drawn to this region, resulting in various studies on BC concentrations and albedo feedback mechanisms in the Himalayas, where enhanced glacial melt was attributed to increased BC concentration (e.g. Ming et al., 2009; Kaspari et al., 2011). As suggested by Jacobson (2004), field studies in the sub-polar regions of the northern hemisphere revealed a significant acceleration of snow melt and the subsequent retreat of the annual snow extent by presence of BC in snow (e.g.: Doherty et al., 2010; Aamaas et al., 2011). These authors observed substantial BC enrichment at the surface during the snowpack melt. To improve model simulations, Brandt et al. (2011) carried out an experimental study on albedo reduction efficiency of BC considering complex interactions between different albedo relevant parameters. This study proved that modelling of relatively small BC concentrations is extremely delicate and that still more profound experimental research needs to be done to assess the viability of model calculations.

Mineral dust

Although highly variable, mineral dust was reported to be near-transparent, except for strongly absorbing inclusions like iron oxides (Warren and Wiscombe, 1980). Various estimates exist on the absorption efficiency of mineral dust (Warren and Wiscombe, 1980; Doherty et al., 2010; Gardner and Sharp, 2010), generally attributing comparatively low effects compared to BC. Nevertheless, different dust sources were reported to affect the albedo of glaciers on different time-scales. While dust input from long-range transport e.g. Saharan dust (Oerlemans et al., 2009) or occasionally volcanic ash (Conway et al., 1996) cause short term albedo reductions,

outcropping dust layers (Wientjes and Oerlemans, 2010) and mineral dust from local sources (Bøggild et al., 2010) were found to reduce the albedo on longer timescales. Debris cover from adjacent slopes seems to be more complexly related to the albedo and melt behaviour of a glacier. Depending on the texture and thickness of the debris cover, thermal heat conduction can be hindered, shielding the glacier surface from direct radiation. Consequently, the albedo reduction can be outweighed by the shielding mechanism, causing the diurnal melt rates to decrease (Reznichenko et al., 2010). For more details on particle deposition mechanisms see section 2.3.

Biogenic matter

The influence of biota on the albedo of a glacier was first investigated by Kohshima et al. (1993) and can be divided into primary and secondary effects. The primary effect is attributed to direct absorption of certain snow algal species, i.e. predominantly *Chlamydomonas nivalis*. *Chlamydomonas nivalis* is known to reduce the spectral reflectance in the range of carotenoid (400-600 nm) and chlorophyll (670-680 nm) absorption bands (Thomas and Duval, 1995). However, it has been reported to reduce the albedo on very limited temporal and spatial scales (Kohshima et al., 1993; Thomas and Duval, 1995; Takeuchi, 2002b). The secondary effect is due to the microbial decomposition of organic matter to brown organic carbon (OC) and dark humic substances, which has been reported to substantially alter the absorption properties of cryoconite matter (Takeuchi et al., 2001). In addition to *in-situ* decomposition, aerosol deposition might contribute substantially to the total absorbing organic fraction as aerosol research by Krivácsy et al. (2001) suggests. However, except for estimates from elemental ratios (Andreae and Gelencsér, 2006) and titrimetric quantification of humic acids (Takeuchi et al., 2001), no reliable quantification method has been developed for humic substances so far. Therefore also the quantitative albedo-relevance of the absorbing organic fraction remains unclear. The distribution of cryoconite on the glacier surface is strongly heterogeneous (Oerlemans, 2010). Bøggild et al. (2010) and Takeuchi (2009) indicated the albedo-relevance of cryoconite hole formation. Glue like extracellular polymeric substances (EPS) were found to cause initial aggregation of algal cells and mineral dust particles, while filamentous cyanobacteria were reported to physically strengthen this adhesion (Takeuchi et al., 2001; Hodson et al., 2010; Langford et al., 2010). Langford et al. (2010) suggested that, in addition to humic substances, BC might contribute to the dark colouration of the granules amplifying the albedo effect of the granule structures. To best knowledge, however, no integrative study on the biogeochemical cryoconite components (including BC) and their relative albedo-effect has so far been carried out.

Modelling

Parameterizations of snow and ice albedo for global climate models are a complex issue, involving a series of effects, especially for glacier ice (e.g. snow grain size, snow depth, solar zenith angle, surface morphology, dust and soot concentrations, crystal structure or liquid water content; Oerlemans, 2010). Most early or simple albedo and climate models only account for clean snow or ice condition (Wiscombe and Warren, 1980; Curry et al., 2001; Oerlemans, 2010; Negi and Kokhanovsky, 2011). More sophisticated models include the effect of BC (Gardner and Sharp, 2010) and absorbing mineral dust (Warren and Wiscombe, 1980; Aoki et al., 2011; Yasunari et al., 2011). However, most models are restricted to modelling of snow and sea ice albedo (i.e. based on snow grain size), which makes them unsuitable for albedo modelling of glacier ice. Overall, the findings of the literature on cryoconite suggest that other impurities might need to be included in RF modelling of the snow/ice-albedo feedback (e.g. brown OC or

humic substances). Moreover additional research is needed to assess the contributions of natural versus anthropogenic forcings within the snow/ice-albedo feedback mechanism.

Study regions

Cryoconite has been investigated on glaciers around the world. A vast majority of the corresponding studies emphasised the polar and sub-polar regions and the community structure of cryoconite. As can be seen in Table 1, investigations on cryoconite are scarce in the Alpine region. However, in the past decade some glacier albedo studies have been conducted using remote sensing technologies (Klok et al., 2003; Paul et al., 2005) or *in-situ* monitoring (Brock et al., 2000; Oerlemans et al., 2009). Oerlemans et al. (2009), for example, found increased drought induced dust input from exposed side moraines to Morteratsch glacier in the eastern Swiss Alps. The supplementary dust input was suggested to trigger a feedback mechanism including enhanced biological activity and melt rates, leading to a forcing calculated to be equivalent to a temperature rise of 1.7 °C. Paul et al. (2005) used satellite images to assess albedo changes of western Alpine

Table 1: Compilation of studies contributing to cryoconite and albedo investigations (incomplete), with their respective study region and focus.

Author	***Year***	***Climatic zone***	***Study region***	***Thematic focus***
Anesio et al.	*2009*	*sub-polar*	*Greenland, Svalbard*	*community respiration*
Säwström et al.	*2002*	*sub-polar*	*Svalbard*	*community structure*
Takeuchi	*2002b*	*sub-polar*	*Alaska*	*albedo*
Stibal et al.	*2006*	*sub-polar*	*Svalbard*	*community structure*
Stibal et al.	*2008*	*sub-polar*	*Svalbard*	*community structure*
Bøggild et al.	*2010*	*sub-polar*	*Greenland*	*albedo*
Hodson et al.	*2010*	*sub-polar*	*Svalbard*	*biogeochemistry*
Langford et al.	*2010*	*sub-polar*	*Greenland, Svalbard*	*biogeochemistry*
Uetake et al.	*2010*	*sub-polar*	*Greenland*	*algae and cyanobacteria*
Bagshaw et al.	*2007*	*polar*	*Antarctica*	*cryoconite holes*
Fountain et al.	*2004*	*polar*	*Antarctica*	*meltwater runoff*
Porazinska et al.	*2004*	*polar*	*Antarctica*	*bio-diversity*
Takeuchi	*2000*	*mid-latitude*	*Himalaya*	*cryoconite holes*
Takeuchi et al.	*2001a*	*mid-latitude*	*Himalaya*	*albedo*
Kohshima	*1993*	*mid-latitude*	*Himalaya*	*enhanced melt*
Takeuchi et al.	*2001b*	*mid-latitude*	*Andes*	*biogeochemistry*
Kohshima et al.	*2007*	*mid-latitude*	*Andes*	*dating of ice core*
Takeuchi et al.	*2006*	*mid-latitude*	*Altai*	*community structure*
Kohshima	*1994*	*mid-latitude*	*Japan*	*bio-diversity*
Margesin et al.	*2002*	*mid-latitude*	***Alps***	*community structure*
Paul et al.	*2005*	*mid-latitude*	***Alps***	*albedo (remote sensing)*
Klok et al.	*2003*	*mid-latitude*	***Alps***	*albedo (remote sensing)*
Oerlemans et al.	*2009*	*mid-latitude*	***Alps***	*albedo*
Brock et al.	*2000*	*mid-latitude*	***Alps***	*albedo*

glaciers under extreme meteorological conditions. Thereby an extraordinarily low albedo was observed on Plaine Morte glacier during the prolonged heat wave in summer 2003, causing a negative mass-balance of -5.6 m for that particular year. However, the albedo reduction was presumed to partly be caused by the presence of meltwater and the performed mass-balance calculations were suspected to be of insufficient accuracy, leading to an overestimation of mass loss. Nevertheless, Plaine Morte glacier was concluded to be highly sensitive to small changes in the energy budget.

1.2. Research questions

As detailed in the section above, albedo changes on glacier surfaces can substantially impact global climate. Yet, mechanisms behind albedo reductions and subsequent feedbacks remain unclear. So far, little attention has been paid to the contributors to albedo reductions on Alpine glaciers. The recently observed surface darkening on several Alpine glaciers (Paul et al., 2005; personal communication M. Schwikowski, PSI; Oerlemans et al., 2009) illustrate the need for investigations in the Alps. The extreme conditions observed on Plaine Morte glacier in summer 2003, combined with its high sensitivity towards changes in energy budget have drawn special interest to this mid-sized plateau glacier in the western Swiss Alps. The study of Paul et al. (2005) demonstrated the actuality of the issue for this glacier and evoked a set of unanswered questions. Another reason for studying Plaine Morte glacier, was the touristic infrastructure facilitating field work logistics and at the same time constituting local anthropogenic influence on the glacier. Hence, the present study investigates the biogeochemical composition of dust accumulating on the surface of Plaine Morte glacier during summer 2010 and aims to assess its effect on the albedo of the glacier.

Following research questions are addressed:

- ***Can individual impurity sources be identified and their input inventory and accordingly their contribution to cryoconite accumulation be quantified from the analyses of seasonal snow?***
- ***What is the typical biogeochemical cryoconite composition on Plaine Morte glacier?***
- ***How do the different constituents of cryoconite matter influence the temporal and spatial evolution of the surface albedo of the glacier during the ablation season?***

1.3. Project design

Throughout the ablation season 2010, a field campaign consisting of 4 individual days of fieldwork (1 June, 6 July, 20 July and 25 August) was carried out on Plaine Morte glacier. To study the albedo effect of cryoconite, broadband albedo and spectral reflectance were measured and different types of samples (i.e. snow, PM and ice samples) were extracted from the glacier surface. Different approaches were chosen, to answer the research questions:

- The snow samples were analysed for their stable oxygen isotope ratio, ionic composition, trace elements, bulk mineralogy and the elemental carbon (EC, c.f. section 2.5) content, primarily to investigate the contribution of impurity inputs and their sources during the accumulation season.
- The ice samples from the snow free surface offered the opportunity to investigate the cryoconite composition with reference to the surface area. In addition to the bulk mineralogy, the organic fraction and the EC content were quantified. Microorganisms and biogenic matter were qualitatively investigated by light-microscopy, using cryoconite granules as a proxy for biological activity.

- The measured albedo was compared to modelling results, to assess the albedo-relevance of grain size changes and EC. Additionally, the remaining unexplained albedo reduction was related to the cryoconite composition and field observations to identify further relevant absorbing components on the glacier surface.

In many respects this project is a reconnaissance study to investigate different methods of biogeochemical analyses as well as albedo and spectral reflectance measurements. Obtained results are expected to add to more profound knowledge on the cryoconite composition and its formation processes on Plaine Morte. In a broader context, the outcome of this study might potentially contribute to the identification of driving forces behind the albedo feedback on Alpine glaciers and indicate its nature (natural or anthropogenic). Additionally, the observations during the field campaign might reveal whether the 2003 albedo on Plaine Morte was a single extreme event or whether albedo triggering mechanisms are evolving trend characteristics.

1.4. Thesis outline

Section 1 introduces the topic of the snow/ice-albedo feedback under the influence of BC and other impurities, giving an outline on the state of knowledge and evincing the research motivation and research questions. In section 2, basic terms, concepts and processes are defined. This includes a brief introduction to the energy balance of glaciers, the definition, deposition mechanisms and source identification of PM and cryoconite and a clarification of terms used for the carbonaceous fraction of soot. Section 3 describes the geographical setting of the study site at Plaine Morte glacier with its glaciological and hydrological characteristics. Additionally a brief overview on its geological and climatic environment is given. Section 4 introduces the fieldwork procedure and all analytical methods applied. The results of the field work and laboratory analyses are presented in section 5. In section 6 the biogeochemical composition of cryoconite is related to observed changes in surface albedo. Additionally, the results are compared with findings of previous studies, discussing their relevance with respect to the research questions. The tripartite set of research questions guides the structure of the thesis in the results as well as in the discussion section (sections 5 and 6, respectively). Section 7 contains concluding remarks and suggestions for subsequent studies as an outlook.

2. Basic terms, concepts and processes

2.1. Energy balance and albedo of glaciers

The mass-balance of a glacier is largely determined by the climatic parameters temperature, precipitation and most importantly the radiation balance. The albedo (α) is defined as the ratio of outgoing to incoming solar radiation (S_{in}), integrated over the entire solar spectrum and thus a measure of surface reflectance. Typical broadband albedo values for fresh snow and clean ice are 0.84 and 0.4, respectively, while the albedo of ice with high dust load can show values as low as 0.15 (Paterson, 1994). The following equation describes the net glacial energy balance (E_{net}):

$$E_{net} = S_{in}(1-\alpha) + L_{in} + L_{out} + H_s + H_l \quad (2.1)$$

The terms L_{in} and L_{out} denote incoming and outgoing long wave radiation, which are generally reasonably well balanced over a glacier surface and therefore of minor importance to the total energy flux. H_s and H_l describe the turbulent sensible and the latent heat flux, respectively. Both have a limited impact on the net energy balance, except for the latent heat flux caused by meltwater percolation and refreezing. Thus, the albedo constitutes a controlling factor in the energy budget of a glacier. For more details on the glacial energy balance see Oerlemans (2010) or Paterson (1994). If cryoconite deposits cover the glacier surface, most of the additional absorption energy is available for melting snow or ice, since glaciers cannot change their surface temperature to adjust to the change in energy balance (Oerlemans et al., 2009). Overall, the albedo effect of impurities is strong but temporally limited in the accumulation area. There, particle accumulation on the snowpack is mostly restricted to atmospheric fall out and enrichment due to annual snow melt and is sporadically interrupted by summer snowfall events. In contrast, particle accumulation in the ablation zone is enhanced by additional sources (c.f. section 2.3) and proceeds continuously throughout the ablation season. Consequently, a rise in equilibrium line altitude (ELA), denoting the annual snow line and the transition between accumulation and ablation area, can trigger a positive feedback by increasing the cryoconite-influenced surface area.

2.2. Cryoconite

Supra-glacial impurity accumulations are by no means restricted to mineral dust inputs, although this is the most obvious particulate constituent. Soot and biogenic matter (like pollen, spores, algae or decomposing plant-fragments) can be deposited to a glacier surface, but typically in substantially lower mass concentrations. Additionally, dust deposits have been reported to act as substrate for microbial activity, adding substantial amounts of living and dead organic matter to the glacier surface (Bagshaw et al., 2007; Oerlemans et al., 2009). The resulting ensemble of dark organic and inorganic matter is generally referred to as cryoconite. This term was first introduced by the Swedish polar explorer Nordenskjöld in the year 1875 (Takeuchi et al., 2001). Cryoconite has been reported to co-determine the surface structure of glaciers mainly by accumulation of matter with subsequent formation of sediment and water filled depressions named cryoconite holes. The strong absorption behaviour of cryoconite matter is the driving force behind cryoconite hole formation, which leads to additional heat release to the ice surface with consequential enhanced melt (Wharton et al., 1985). These characteristics illustrate the importance of cryoconite to the surface albedo of a glacier.

2.3. Atmospheric transport and deposition mechanisms of PM

Particles are transported to the glaciated areas by aeolian processes or by deposition from local sources. The concentrations of aerosols are thereby strongly influenced by seasonal or long-term emission patterns. However, transport mechanisms and atmospheric stability are additional controlling parameters regarding aerosol deposition to Alpine glaciers. Due to seasonal shifts in planetary boundary layer (PBL) height, high Alpine sites of more than 3100 metres above sea level (m a.s.l.) are characterised by bimodal aerosol input (Baltensperger et al., 1997). In summer, convection induced vertical mixing transports polluted air masses from the surrounding valleys to the higher Alpine regions. In winter stable atmospheric conditions hinder vertical mixing and cause a decoupling of the higher altitudes from the PBL. Since air masses at higher Alpine sites can be diluted by mixing with cleaner air from the free troposphere, concentrations of pollutants can be significantly reduced compared to mean PBL values (Schwikowski and Eichler, 2010).

The atmospheric impurity deposition on glacier surfaces is governed by two mechanisms: wet deposition and dry deposition (Warren and Wiscombe, 1980). During the accumulation season impurity deposition predominantly occurs by wet deposition, since ice crystals are extremely efficient scavengers (Warren and Wiscombe, 1980; Hadley et al., 2010). During the ablation season, however, deposition mechanisms are more likely to be dominated by dry deposition (fall out) and accumulation of particles from the melting snowpack. As mentioned in section 1, outcropping dust from the melting glacier ice (Oerlemans et al., 2009; Wientjes and Oerlemans, 2010), scree input from the adjacent slopes (Reznichenko et al., 2010) and biological activity (Takeuchi 2002b; Langford et al. 2010) may additionally contribute to the total dust accumulation.

2.4. Sources of PM and their identification

Aerosols from the PBL may include biogenic matter from vegetation and agriculture as well as anthropogenic pollution from traffic and industry. In addition to biogenic and anthropogenic aerosols from the PBL, local and remote mineral dust sources contribute to the cryoconite accumulation on glaciers. Mineral dust stems predominantly from loose rock in the vicinity of the glacier, but Saharan dust events (SDE) from long-range transport across the Mediterranean Sea and/or the Atlantic Ocean are reported to episodically add to total dust concentrations on high Alpine glaciers (Schwikowski et al., 1999). Additionally the eruptions of the Icelandic volcano Eyjafjalla from March to May 2010 might have caused ash deposition to Alpine glaciers during the study period. Ionic species and trace elements within a snowpack are generally assumed to reflect the atmospheric composition during the time of snow deposition (Schwikowski and Eichler, 2010). Since many of these species can be attributed to a specific source, ions and trace elements can help to identify source regions. Secondary aerosol species (nitrate (NO_3^-) and sulphate (SO_4^{2-}) from fossil fuel combustion in traffic and industry and ammonium (NH_4^+) from agriculture) can be attributed to anthropogenic pollution (Schwikowski and Eichler, 2010). Sodium (Na^+) and chloride (Cl^-) mostly show high correlation and the characteristic Cl^-/ Na^+ ratio of 1.16 indicating sea spray as predominant source (Eichler et al., 2001). Finally, increased calcium (Ca^{2+}) or iron (Fe) concentrations (Schwikowski et al., 1999; Kaspari et al., 2011) (and to a lesser extent also potassium (K^+) and magnesium (Mg^{2+})) can be used as dust markers.

Saharan dust is dominated by the clay mineral fraction and consists of roughly 90% illite, kaolinite and montmorillonite (Collaud-Coen et al., 2004). However, Saharan dust mineralogy and consequently its chemical composition strongly depend on the

geological source region within the desert as well as on weathering and transport history (Moreno et al., 2006; Kandler et al., 2007). In addition to high Ca^{2+} concentrations, excess Cl^- and SO_4^{2-} (Wagenbach et al., 1988), have been reported to represent SDE. Other authors, however, used the same species, combined with increased fluoride concentrations, as volcanic ash markers (Legrand and Mayewski, 1997; Ginot et al., 2010). Thus, SDE do not produce an easily identifiable signal.

Moune et al. (2006) investigated snow samples with ash deposits from the eruptions of the Icelandic volcano Hekla in the year 2000. The resulting rare earth element (REE) and trace element composition was stated to be characteristic for Icelandic volcanic ash. Therefore the REE composition from Hekla ash is suitable to indicate Eyjafjalla ash depositions within the snowpack. Similarly, Bukowiecki et al. (2011) and Tobler et al. (2011), investigated snow samples from the high Alpine site Jungfraujoch (3454 m a.s.l.), situated 40 km north-east of Plaine Morte glacier. These studies compared the trace element and ion concentrations after the overpass of the Eyjafjalla ash plume to the baseline values of the snowpit and found enrichments exceeding factor 20 for most REE and SO_4^{2-}. This threshold serves as additional indication for Eyjafjalla ash.

In addition to source identification, simple budget equations of e.g. trace elements or EC can be used to estimate the impurity input during the accumulation season, in comparison to total impurity inventory on the glacier surface at the end of the ablation season.

2.5. Carbonaceous fraction of soot

As elucidated above, soot is attributed a decisive role in the snow/ice-albedo feedback, due to its absorption efficiency (c.f. Figure 1). Soot consists of amorphous carbonaceous particles showing varying carbon (C) to hydrogen (H) ratios (Perron, 2010) and mostly pronounced hydrophobic properties (Doherty et al., 2010). Its most dominant feature, however, is the constant absorbance over all wavelengths of the visible spectrum (VIS; Warren and Wiscombe, 1980). Due to its complex physical and chemical properties, various definitions exist for the strongly absorbing carbonaceous soot particles, originating from the combustion of fossil fuels and biomass burning. BC and EC are assumed to represent the absorbing and the elemental fraction of soot, respectively. The definition of the two terms is largely method-dependant, which will be briefly discussed in section 4.5.3 of this study. Literature on the albedo effect of soot preferentially uses the term BC with its optical definition. In this study soot was measured as EC, which leads to limited inter-comparability regarding measured concentrations and absorption behaviour of soot. Kaspari et al. (2009) found substantial deviations between concentrations determined by the respective methods, which were reported to be non-systematic, hindering simple conversion between the two terms (Andreae and Gelencsér, 2006). Nevertheless EC concentrations were used as a rough approximation in the context of albedo reduction. Note that this might influence the outcome of this study. Consequently both terms, BC and EC, will be utilized, since they cannot be used synonymously. For more details on the differentiation of various existing soot definitions, see Gelencsér (2004) or Andreae and Gelencsér (2006).

3. Study site

3.1. Geographical setting

The Plaine Morte glacier (46°23'N, 7°29'E) is situated in the western Swiss Alps, at the boundary between the cantons of Berne and Valais (c.f. Figure 2a,b). The glacier forms an extensive plateau with a mean altitude of 2750 m a.s.l. showing no distinct tongue and little gradient. With an area of roughly 8.5 km^2 (Farinotti, 2010), Plaine Morte glacier is the largest individual glacier in the glaciated environment of the Wildstrubel. As the region is developed for tourism, the glacier is accessible by cable car throughout the year. During winter time, a ski lift connects several slopes on the glacier surface to the main skiing area on the southern slopes of the Crans-Montana region. Thus, the Plaine Morte glacier is strongly influenced by human activities and pollutant concentrations in ambient air might be increased due to local emissions.

3.2. Climate and meteorology

The Plaine Morte is situated on a crest dividing the wetter north of Switzerland from the dry, east-west oriented valley Valais (Frei and Schaer, 1998). Consequently the Plaine Morte can potentially be influenced by both climate regimes. In order to understand the obtained chemical composition of the snowpack, weather and climate data from the study site are of great importance. Unfortunately it was not possible to run an automated weather station (AWS) on the glacier during the course of this study. Therefore no meteorological data is available for the study period. The closest permanent stations, Lenk to the north and Montana to the south, are each 10 km away and are located at an altitude of 1000 and 1500 m a.s.l., respectively (c.f. Figure 2b). Both stations provide continuous precipitation data. Since precipitation patterns in the Alps seem to be complexly influenced by shielding and lifting processes, no uniform height gradient can be applied (Spreafico and Weingartner, 2005). Thus for a basic overview of the climatic conditions, extrapolated statistical values of the period 1971-1990 were used (data from Atlas der Schweiz, 2.0). At Plaine Morte glacier, mean annual precipitation amounts to roughly 2000 mm and seasonal variations are rather small. From October to April mean temperatures are well below zero, with their minimum in January (-9.5°C). If this is regarded to be the snow accumulation season, the mean snowpack depth amounts to roughly 1.1 metre water equivalent (m weq) at the end of the accumulation season. Summer temperatures rise to a monthly mean of 7.5°C in July and are generally accompanied by slightly higher monthly precipitation rates throughout June, July and August. Wind fields and wind strengths are highly variable in mountainous areas and cannot be determined from the data available. However from an orographic point of view, snowdrift seems to be of minor importance to total snow accumulation on this extensive plateau. Although Plaine Morte glacier does not belong to the high Alpine sites, it is expected to be influenced by shifts in PBL height and thus show bi-modal aerosol input to the glacier surface. Due to the touristic infrastructures in the vicinity of Plain Morte glacier, snow groomers might enhance soot depositions.

3.3. Glaciology and hydrology

Figure 2 (b and c) show the glaciated area in the Plaine Morte region. The Plaine Morte glacier has a mean thickness of 96 m (data kindly provided by M. Huss, University of Fribourg). The only ice outflow from the plateau is oriented northwards, forming the Raetzli-glacier tongue. In the past century, this tongue was subject to fast retreat, resulting in a length reduction of more than 1 km within the period from 1925 to 2000 (SCNAT, 2011). With a

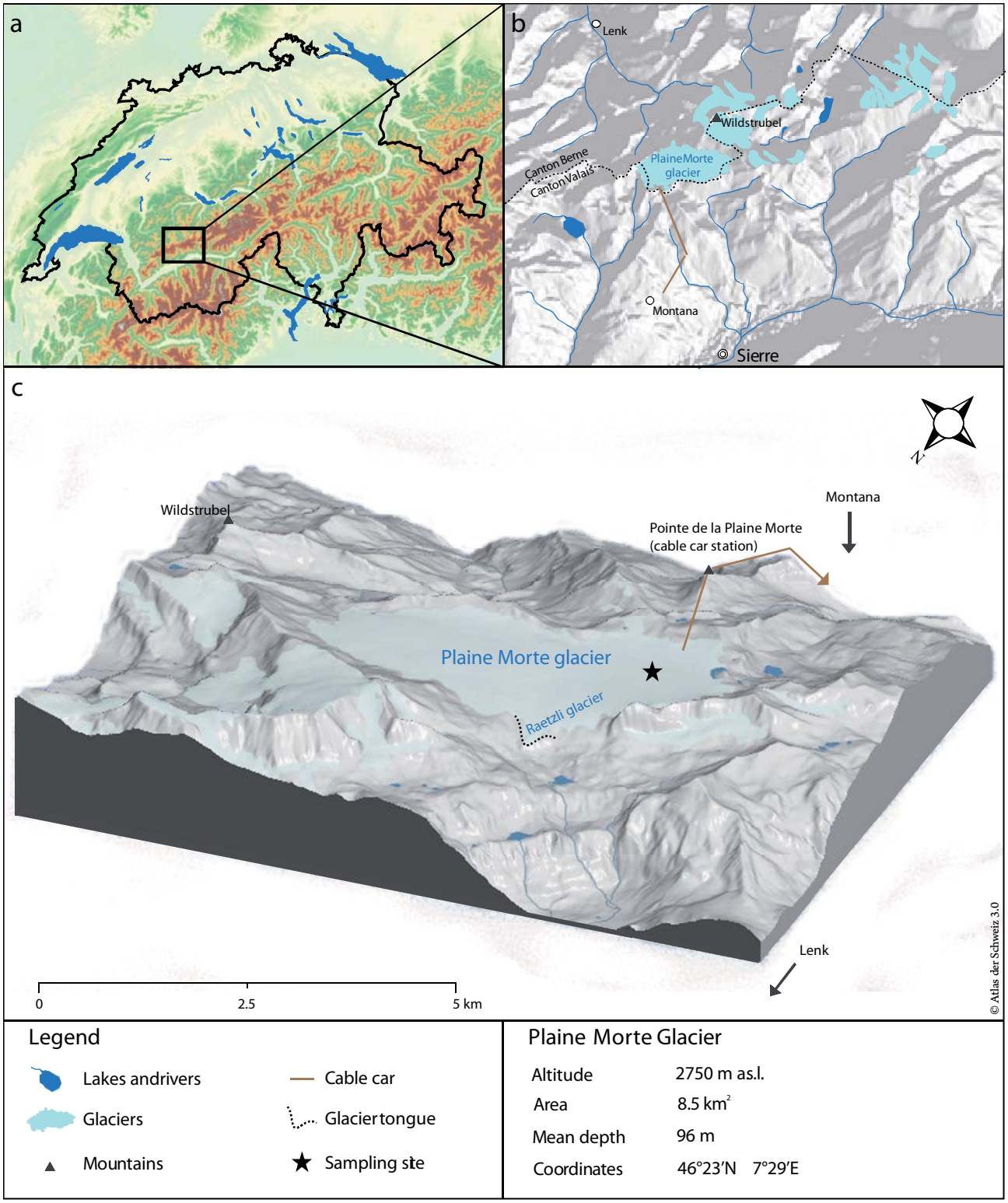

Figure 2: Geographical setting of the study site within Switzerland (a), overview over the region Montana – Lenk (b) and block image of Plaine Morte glacier and its close vicinity (c). Note that (c) is not oriented northwards (see wind rose). Lakes are displayed in dark blue, glaciated areas in light blue. The brown lines depict the cable car facilities (b, c) and the approximate location of the sampling site on Plaine Morte glacier is marked by the asterisk (c). The details on surface area and mean depth are based on data from Farinotti (2010; c.f. section 3.1) and M. Huss (c.f. section 3.3), respectively.

current length of a few hundred meters measured from the edge of the plateau, the Raetzli glacier is of minor importance to the glacio-physical properties of that glacial system, especially considering the remarkable thickness of Plaine Morte glacier. In the present state, the Plaine Morte glacier is a temperate plateau glacier, which is characterised by little gradient. As mentioned in section 1.1 the latter feature results in an exceptional sensitivity with respect to small changes in ELA. In recent years, melting processes dominated the entire glacier surface (Paul et al., 2005), which suggests that the ELA has shifted to altitudes exceeding the highest point of the glacier (2900 m a.s.l.) and that the glacier is currently in a state of retreat (Bonriposi, 2011). In addition to changes in ELA, enhanced surface darkening by dust deposits has been reported to strongly alter the energy budget and the mass-balance of Plaine Morte glacier (Paul et al., 2005). Indeed, accumulation and ablation observations, carried out by the Department of Geosciences at the University of Fribourg, revealed a significant mass loss during the ablation season in 2010, accounting for a negative mean net mass-balance of minus 1 m weq for that particular year (data kindly provided by M. Huss). Unfortunately no longer time series of glaciological parameters is available for Plaine Morte glacier.

The Plaine Morte glacier has a relatively complex and poorly understood karst induced drainage system with several surface and subsurface outflows towards both the north and the south. Due to seasonal water scarcity on the southern slopes of the Valais (Weingartner, 2007), the glaciological properties and its implications for discharge from the plateau are currently studied by a research group from the Department of Geosciences at the University of Fribourg (Voinesco, thesis in preparation) in collaboration with research groups from the University of Lausanne. This study is part of the trans-disciplinary research project "MontanAqua", which investigates water availability, usage and distribution in the Crans-Montana region (Schneider, 2010; Voinesco, thesis in preparation). With respect to climate change and glacial retreat, issues concerning seasonal runoff and water distribution potentially gain importance in the near future (Wyer, 2008), especially due to the diverse and intensive usage of the water resources in that region (e.g. for domestic and agricultural purposes as well as for hydropower and artificial snow production).

3.4. Geology

Local geology is dominated by calcareous bedrock, which is strongly weathered, forming characteristic loose rock slopes with little to no vegetation. The sub-glacial bedrock is likely affected by extensive karst formations (Maire, 1978). By far most dominant are Mesozoic sediments, intruded by some Tertiary sediment to the north of the glacier. Lithology of the close proximity of the glacier is characterised by limestone with marl beds and calcareous phyllite and marly shale. Phyllite is a designation for clay shale with metamorphic overprint, largely consisting of mica with contributions of quartz, feldspars, chlorite, augite and tourmalines (from Atlas der Schweiz, 2.0). Since limestone is preferentially weathered chemically by calcite ($CaCO_3$) dissolution, phyllite, marl and marly shale are expected to dominate supply of physically weathered particles in the aeolian dust size-bin. Therefore, dust deposits of local origin most probably show the mineralogical footprint of these loose rock species. Other lithological entities in the more distant vicinity of the glacier are clays, silts and sandstones, but these do not show a distinct characteristic mineralogy and were therefore not considered in this study.

4. Methods

4.1. Fieldwork

4.1.1. Sampling procedure

The field campaign at Plaine Morte consisted of four individual sampling days throughout summer 2010 (1 June, 6 July, 20 July and 25 August). During the field campaigns five different types of samples were extracted from the Plaine Morte glacier: snow samples from the snowpits (c.f. Figure 3a), random samples of PM (c.f. Figure 3b), and ice samples from the glacier surface (c.f. Figure 3c). Additionally samples of local loose rock (LLR, c.f. Figure 3d) and meltwater were collected. The sampling method applied on the snow covered glacier differed from the procedure followed on bare ice. The thickness of the snowpack in early June and July amounted to 2.6 m and 1.2 m, respectively. On both dates a snowpit was dug to expose the entire snow column for the sampling procedure (1 June: snowpit 1; 6 July: snowpit 2, c.f. Figure 3e). Due to technical difficulties, the snow profile was only sampled to a depth of 2.1 m on 1 June. At the far end of the snowpit, the pit-wall was smoothed with a pre-cleaned spatula to form a vertical snow face. This snow face, with its visible layers of different snowfall or melt events, was photographed for documentary purposes. Then a Teflon-coated panel was inserted horizontally at a depth of 10 cm. The samples for ion and EC analysis were collected by directly scooping portions of the 10 cm snow layer with pre-cleaned 50 ml sample containers. For the dust assay, larger portions of snow were filled into 500 ml con-tainers after removing them from the snow layer with a clean shovel. Finally, the mass of the snow column was determined by extracting a sample of known volume with an aluminium tube and weighing it *in-situ* on a simple electronic scale. After removing the remaining snow on the panel, the procedure was repeated in 10 cm intervals. By 20 July the snow cover had melted down to bare glacier ice. Therefore, cubic samples of darkened surface ice were extracted on the last two campaign dates (3 samples on 20 July and 4 samples on 25 August; c.f. Figure 3f). Four vertical cuts, delineating a square of an approximate edge length of 15 cm, were made with a battery-operated chain saw. Then a chisel was used to detach the sample block from the ice surface. To conserve the surface structure, the samples were packed in resealable mini-grip bags and then wrapped in shock-absorbing packing material. In addition, all samples were stored and transported in a polystyrene box containing dry ice as a cooling agent.

4.2. Albedo and spectral reflectance measurements

On all four campaign days a broadband albedometer (provided by the Institute for Atmospheric and Climate Science at the ETH Zürich) was installed on the glacier surface to measure incoming and outgoing radiation, from which the albedo can be derived. The two sensors (Kipp & Zonen, CM6B), facing the zenith and the glacier surface, respectively, continuously measured direct and diffuse radiation in the VIS and near infrared (NIR) wavelengths (λ = 305-2800 nm) from 11:30 am to 1:15 pm coordinated universal time (UTC). For the complete duration of the measurements, low cloud cover conditions of less than estimated 10% were met. Considering the inhomogeneous cryoconite distribution on the glacier surface, great care was taken to select a suitable instrument position to guarantee best possible representativeness of surface structure and debris cover.

Complementary, on 25 August a portable Spectrometer (FieldSpec3®) from the Department of Geography at the University of Zürich was used for spectrally resolved radiance measurements. Data

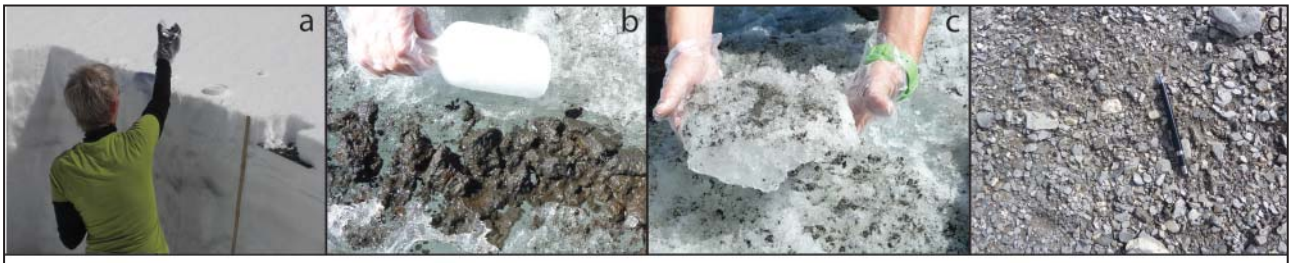

e

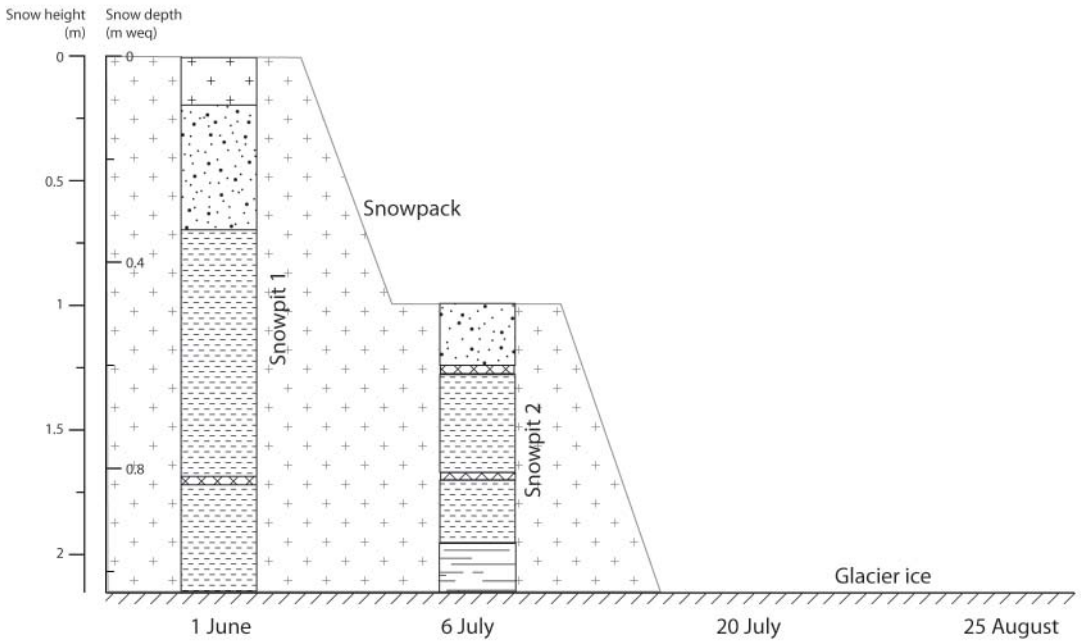

f

Date	1 June	6 July	20 July	25 August	Total
Snow samples	21	11			32
Samples of PM		4	5	6	15
Ice samples			3	4	7
LLR sample				1	1
Broadband albedo	X	X	X	X	
Spectral reflectance				18	18

Figure 3: Sample types and sampling situation during the fieldwork. In the upper panel, pictures illustrate the different sample types: snow samples from the snowpit (a), random samples of PM (b), ice samples (c) and sample of LLR (d). The lower panel (e) depicts the conditions found on Plaine Morte glacier during the four days of fieldwork (snow cover vs. bare glacier ice). For a detailed legend on the schematic depiction of the snowpit stratification see Figure 7. The table below (f) lists the type and amount of samples (measurements) taken on each of the fieldwork dates.

were collected in the in the wavelength range from ~350 to 2500 nm with a resolution of 3 nm in VIS (~390-750 nm) and 10 nm in NIR (800-2500 nm), respectively. A total of 18 targets was measured with variable sensor height to represent the manifold surface structures of the glacier surface. Of each target 30 individual measurements were taken and averaged, accompanied by 10 reference measurements over virtually perfectly reflecting Spectralon® material from VIS to NIR spectrum. For more details on the measurement procedure and data processing see Takeuchi (2009).

4.3. Sample extraction and preparation

During the field campaigns on Plaine Morte glacier, a total of 32 snowpit samples, 10 samples of PM, 7 cubes of surface ice and 1 sample of LLR and meltwater, respectively, were collected (c.f. Figure 3f) and transferred to a coldroom (-20°C) located at the Paul Scherrer Institute (PSI) in Villigen, Switzerland. At any time during the transport and the storage phase, the samples were kept in frozen condition to prevent chemical alteration. All treatment steps were performed with pre-cleaned tools and containers. Cleaning involved thorough rinsing with ultra-pure water (18.2 MΩ cm). Tools and containers for dust analysis were rinsed at least three times and then dried in a laminar flow box. Polyethylene sample containers for chemical analyses were soaked for five days, changing the ultra-pure water daily. The chain and blade of the battery operated chain saw were cleaned by flushing with pure gasoline.

The three main sample types (snow, PM and ice samples) were collected for different purposes and were therefore treated differently during the biogeochemical analyses (c.f. Table 2). Due to large temporal and spatial heterogeneity of dust and cryoconite deposits a characterisation of typical average samples was neither reasonable nor feasible in the course of this study. Nevertheless, the locations for ice sample extractions were chosen carefully to guarantee best possible representativeness of the quantitative analyses performed on these samples. In contrast, the samples of PM were collected with no attempt to obtain truly representative material because their purpose was to study the qualitative characteristics of different types of cryoconite, rather than determine the typical average composition of Plaine Morte cryoconite. Therefore it was not possible to relate the findings to a specific surface area and to study their effect on the albedo of the glacier. Insofar, results from samples of PM were of minor importance to the outcome of this study. Thus, focus was put on the ice samples, and results from PM samples were only discussed for illustrative purposes in interesting cases.

Table 2: List of all sample types and the methods applied to them. Brackets mark where not all samples could be processed due to insufficient sample amount.

Method	*Parameter*	*Snow samples*	*Samples of PM*	*Ice samples*	*LLR sample*	*Water sample*
IC	*Major ions*	*X*				*X*
IR-MS	*Stable isotopes*	*X*				
XRD	*Mineralogy*	*X*	*X*	*(X)*	*X*	*X*
ICP-MS	*Trace elements*	*X*		*X*		
LOI	*Organic fraction*		*(X)*	*(X)*	*X*	
Microscopy	*Biogenic matter*	*X*	*X*	*X*	*X*	*X*
OC/EC analysis	*Elemental carbon*	*X*		*X*		

The cubes of surface ice were portioned in the cold-room using a bandsaw equipped with a stainless steel blade. For each of the analytical methods an ice segment of the uppermost 2.5 cm (enriched in dust load) was cut and thereafter stored in appropriate, pre-cleaned containers and kept frozen until analysis. To be able to calculate the surface related debris load, the surface area of each segment was measured and noted.

4.4. Standard snowpit analyses

In the Alps, variations in stable isotope ratios directly reflect temperature changes. The seasonal pattern of ionic species is indirectly temperature driven by changes in source (e.g. enhanced biological activity) or transport mechanisms (c.f. section 2.3). With some restrictions, both methods can be applied to snowpit data, although melt water percolation can disturb the signals. The ionic composition of a snowpack is thereby more prone to melt and drainage effects than the stable isotope ratio. Depending on the solubility and thus the position of the ions within the ice lattice, some ionic species tend to be leached more easily than others (Eichler et al., 2001). Due to the incorporation of the stable isotopes into the ice lattice, the isotope ratios are preserved better and are only impaired by the formation of ice lenses caused by refreezing of melt water in lower layers (Ginot et al., 2010). Therefore, the stable isotopes are more suitable for seasonal layer identification.

4.4.1. Reconstruction of snowpack

The snowpack at Plaine Morte was stratified by individual snowfall and occasional melt events. In order to fully understand the chemical composition of the different layers, temporal information of these events was considered to be helpful. Since isotopic ratios only provide a seasonal signal with low temporal resolution, weather records or reconstructions are needed to assign the corresponding snowfall events to the individual layers. In the absence of continuous meteorological data from an AWS, reconstructions of precipitation events were required. Due to its position on the dividing ridge between the two climate regimes of dry southern and wetter northern Alpine climate, the weather conditions at Plaine Morte could be potentially influenced from both climate regimes. The precipitation pattern from Montana and Lenk were poorly correlated, which illustrated the need to determine the dominant source of air mass advection for the special case of the Plaine Morte glacier. Since the glacier itself is shielded by ridges of more than 2800 m height to the west, south and east, the north-oriented notch, hosting the Raetzli glacier tongue, might be an important inlet for air masses approaching from the north. Therefore, precipitation amounts were calculated multiplying the precipitation data from the station at Lenk (1058 m a.s.l.) by a factor of 1.8, which was needed to obtain a cumulative snow depth of 1.28 m weq measured on 1 June. Unfortunately the gauging station at Lenk did not provide temperature data. Therefore, daytime mean temperatures were derived from the station records of Montana, using the moist adiabatic laps rate of 0.5°C per 100 m (Roedel, 1994). Snow fall events were defined to be periods of one or more days precipitation and a mean temperature below freezing point, and were considered to have finished when these conditions were not met for more than four days in a row. The contribution of each snowfall event to the total snowpack (in m weq) was calculated as the sum of precipitation over the entire event.

4.4.2. Ion chromatography (IC)

IC was only performed on snow samples of the snowpits from 1 June and 6 July. The discussion of ionic composition of the samples was therefore restricted to the snowpit samples. The ionic pattern within the snowpack provides information on transport mechanisms and deposition history of PM or aerosols during the accumulation season,

containing an indication on its sources.

Prior to IC, the samples were flushed with pure, inert molecular nitrogen gas (N_2) before melting, to minimize the interaction of the sample liquid with contaminating laboratory air. After extracting an aliquot of 1 ml from the sample for the purpose of stable isotope measurements, the chromatography was performed on a fully automated ion chromatograph (850 Professional IC, Metrohm AG) at the PSI. The determination was restricted to major inorganic soluble ions (cations: NH_4^+, Na^+, K^+, Mg^{2+} and Ca^{2+}; and anions: Cl^-, NO_3^- and SO_4^{2-}). Full names of these ionic species were introduced in section 2.4 and can be looked up in the list of chemical denotations (p. X). Some organic anions (formate, acetate and methane-sulphonic acid) along with fluoride had to be excluded from the analysis, since their signal was disturbed by unidentified species. Additionally, oxalate was not included due to its very low concentrations, which could not significantly be distinguished from blank values.

All snowpit and six surface samples were analysed without dilution or decantation, but the surface samples were centrifuged for a complete sedimentation of the particles in suspension. To ensure the reliability of the measurement device, method blanks (ultrapure water) and standard solutions were measured regularly. For comparability reasons among different ionic species, the measured concentrations in parts per billion (ppb) by volume were converted to micro equivalent (µeq) per litre. Blank values did not show systematic contamination and were mostly below the detection limit. Therefore no blank correction was performed. Measurement results below the detection limit were replaced by the value corresponding to half the detection limit of the ion in question. The ionic concentrations of snowpit 1 were log-normally distributed and correlation among ions was tested using the one tailed Pearson correlation. Outliers, which strongly dampened existing correlations or conversely suggested a non-existing correlation, were removed. Additionally, cumulative fluxes of all ions were calculated for the two snowpits, to identify temporal changes in the ionic budget between snowpits 1 and 2.

4.4.3. Isotope ratio mass spectrometry (IR-MS)

Stable isotope ratios can be a useful tool to identify seasonal layers in a snowpack or ice core. In the Alps, the ratio of heavy (^{18}O) to light (^{16}O) stable oxygen isotope in water vapour and precipitation is strongly temperature dependent. The ratio is usually normalized to a standard (Vienna Standard Mean Ocean Water (VSMOW)) and is commonly referred to as the $\delta^{18}O$ signal. The $\delta^{18}O$ ratio, as defined by Dansgaard (1964), can be calculated as follows:

$$\delta^{18}O = \frac{\left(\frac{^{18}O}{^{16}O}\right)_{sample}}{\left(\frac{^{18}O}{^{16}O}\right)_{standard}} - 1 * 1000‰ \qquad (4.1)$$

Since oxygen isotopes, as part of the water molecule, are incorporated into the ice lattice of snowflakes, temperature information is preserved in snowpacks. In this study, the $\delta^{18}O$ signal was used to identify the overlap of the two snowpits from 1 June and 6 July, after converting snow depths measured into m weq, using the density profile. This offered the opportunity to compare the chemical composition of the snowpits, which reveals chemical alterations during longer ablation episodes.

Aliquots of the IC samples were filled into glass vials, sealed and refrozen until analysis. Analysis was performed by an automated IR-MS (Delta Plus XP, Finnigan MAT) at the PSI, which determines the ratio of stable oxygen isotopes in water molecules. Two in-house standards were measured regularly to ensure the reliability of the measurements. The trend observed in the standard measurements was used to correct the results. For more details on the instrument, measurement procedure and data evaluation see Ciric (2009).

4.5. Mineral dust analyses

Mineral dust analysis was performed to determine the predominant mineral dust source on Plaine Morte glacier. Therefore bulk mineralogy and trace element analysis were performed on snow and ice samples to identify dust input sources. Quantitative determination of the mineralogy was moreover a substantial part of the cryoconite composition analysis, allowing for a comparison between bulk mineralogy of LLR and cryoconite.

4.5.1. X-ray diffraction (XRD)

XRD is a standard non-destructive method to analyse the bulk mineralogy of soil and rock samples (Wenk and Bulakh, 2004). Minerals produce characteristic diffraction patterns due to their lattice spacing. Samples are exposed to X-rays from a range of different angles to produce the composite pattern of all minerals contained in the sample. Peak intensities of diffracted rays can be used to quantify the relative mineral abundance in the sample. For more details see Wenk and Bulakh (2004).

Before the samples could be prepared for XRD analysis, aliquots of sample material for other biogeochemical analyses (algae and partially trace elements and EC) had to be extracted from the 500 ml containers with a clean spatula. In a first step, all samples were melted and filtered through cellulose ester filters of 0.45 µm pore size (HAWP 50 mm diameter, Millipore) using a vacuum pump. The filters with the dust deposits were then dried in a laminar flow box and transferred to the Geological Institute of the University of Bern in plastic Petri-dishes. In a second step, different preparation modes were chosen according to the weight of the dried sample. Filters with a dust load in the range of micrograms did not need further preparations, since the filters could be directly mounted on the sample holder with an aluminium platelet. Samples with more than 3 grams of material were suitable for quantitative analysis. They were first grinded to very fine powder in a stone mill equipped with a wolfram mallet. Then lithium fluoride (LiF) was added to the powder at a mixing ratio of 10% by weight. The powder was then grinded in an agate mortar for ten minutes to optimally mix sample powder and LiF, which serves as internal standard. As a final step, the powder was pressed into the sample holder to form two pills with a smooth surface and disoriented minerals. The remaining samples of weights in the order of 1-2 g were grinded in the agate mortar. The coarser powder was then mixed with some droplets of ethanol and pipetted onto a silicon platelet. These three variants of sample preparation were necessary to assure the best results for each of the sample groups, but unfortunately limited the comparability of the evaluations.

XRD analysis was performed with an automated X-ray diffractometer of type X'Pert PRO (PANalytical) operated at 40 kV and 40 mA, covering an angle range of 5 to 75°. To optimise the result, the samples were rotated continuously during the measurement. Quantitative determination of bulk mineralogy comprises the relative abundance of quartz, calcite, dolomite, kali-feldspars and plagioclase and was performed on two analogue sample pills from the same sample material representing two control runs. The evaluation program (X'Pert Quantify) calculated the error of each measurement based on the standard deviation. For the qualitative analysis the software "High Score Plus" was used to generate an automated best-fit mineralogical composition for each of the sample diffraction patterns with a search-match algorithm.

4.5.2. Inductively coupled plasma mass spectrometry (ICP-MS)

The trace elemental analysis, was performed by L. Tobler from the Analytical Chemistry Group at the PSI, using a sector field ICP-MS (ELEMENT 2, Thermo Scientific). The following elements were of importance to characterise the dust: iron (Fe), aluminium (Al), calcium (Ca), magnesium (Mg), europium (Eu), neodymium (Nd), samarium (Sm), ytterbium (Yb), lanthanum (La), cerium (Ce), praseodymium (Pr). For a complete list of all detected trace elements and RRE, see list of chemical denotations (p. X). The snow, cryoconite and ice samples had to be treated differently during the preparation procedure. For the analysis of the snow samples, the residuals of the IC analysis were reused, which had been stored frozen after the initial analysis. The samples of PM had to be diluted with ultrapure water at a weight proportion of factor 20, while the ice samples did not require any initial preparation steps. For this study in particular, insoluble particles were of interest. Therefore all samples were acidified with ultrapure 70% nitric acid (HNO_3) to 0.2 molar for seven days, to partially dissolve the particles. Then the samples were refrozen until analysis. The correct procedure for particle analysis would include a complete digestion of the PM (Kilbride et al., 2006), but since this method had not been practiced so far at the PSI, acidification was chosen as a simple alternative approach, although it remains unclear how much of the particles can be dissolved in this manner. To avoid damage to the instrument, samples with visible sediment were centrifuged prior to analysis. These samples showed particularly high concentrations of all measured trace elements and therefore had to be strongly diluted with ultrapure water (factor 400). Generally, the precision of the instrument is in the range of 5% for all elements measured, but due to several dilution steps, errors might have increased for certain samples. To verify the potential presence of ash input from Eyjafjalla, the chemical footprint of the darkened horizon was compared to that observed in ash from Hekla (Moune et al., 2006; c.f. section 2.4). Both chemical footprints were normalized to the mean upper continental crust composition (Taylor and McLennan, 1995). Additionally, the chemical signal was compared to that found in Jungfraujoch snow after the overpass of the Eyjafjalla ash plume in May 2010, using enrichment factors (Bukowiecki et al., 2011; Tobler et al., 2011).

4.6. Analyses of potential darkening agents

Cryoconite was observed to be substantially darker than the surrounding LLR. Therefore cryoconite was assumed to contain additional darkening agents. With this respect EC and organic matter were considered to be the most likely absorbers. Cryoconite samples were therefore ignited to determine the organic matter and the EC content, respectively. Additionally, living microorganisms and biogenic matter were qualitatively assessed with different microscopic techniques.

4.6.1. Loss on ignition (LOI)

LOI is a commonly used semi-quantitative method to estimate the organic fraction in soil or sediment samples. This method is based on the fact that organic matter is oxidised to carbon dioxide (CO_2) at lower temperatures than most inorganic soil components. Therefore the weight loss during the combustion procedure at appropriate temperatures can be attributed to the organic content of the sample (Heiri et al., 2001). The organic fraction determined by the LOI method includes both (decomposing) biogenic matter (e.g. humic substances, spores or pollen) and living organisms.

Firstly, samples and porcelain crucibles were predried over-night at 50°C to minimize the free water content. Secondly, the crucibles were dried at 120°C for two hours and then cooled to weight-constancy in a desiccator together with the samples. Thirdly, a few grams of sample material were carefully

weighed into the crucibles at a precision of micrograms and then combusted at 430°C for two hours. Finally, the weight of the combusted samples was determined after cooling the samples over-night in a desiccator. The percentage weight of organic matter (OM) was calculated as follows:

$$OM = \frac{TW - IW}{TW - CW} * 100\% \qquad (4.2)$$

Where TW is the total weight of sample and crucible after drying, IW is the weight of the ignited sample and CW stands for the weight of the empty crucible.

4.6.2. Microscopic assay of biogenic matter and microorganisms

For the microscopic analysis of biogenic matter and microorganisms in the snow pack, snow samples were melted and filtered through polytetrafluoroethylene (PTFE) filters (JHWP 0.2 µm, Millipore) using a vacuum pump. The cryoconite and ice samples were filtered in the same manner, except for the processed sample amount. Due to the heavy particulate load only small sample aliquots of 100-1000 µl were filtered. The filters were then mounted on slides and fixed with a solution containing equal proportions of glycerol, formalin and ultra-pure water. To seal the preparations, Canada balm was applied around the edges of the cover slip. To prevent contamination the filtering procedure was accomplished in a laminar-flow-box, the work space was cleaned regularly with ethanol and sterile gloves were worn at all times. This procedure was chosen based on personal instructions by P. Santibáñez from the Montana State University, USA (c.f. Santibáñez et al., 2008).

The quantification of algal cells and bacteria was considered, since cyanobacteria and certain algal species were reported to have considerable direct and indirect effects on the albedo of snow and ice (Takeuchi, 2002a; Anesio et al., 2009; Wientjes et al., 2011; c.f. section 1.1). However, the identification of different algal species and bacteria proved to be difficult, firstly due to a lack of expertise and secondly due to the optical and physical thickness of most cryoconite granules. Several approaches and techniques were tested during the course of this study, but none of these allowed reliably identifying and quantifying algae and bacteria. As a first step, auto fluorescence peak intensities were used to distinguish algal cells from bacteria on a confocal epi-fluorescence microscope. Indeed, the characteristic intensity peaks at wavelengths of 645 nm and 678 nm, assigned to bacteria and algae, respectively (Langford et al., 2010), could be observed. However, cell counting was impossible due to the thickness of the granules (c.f. Figure 4a). The second approach to quantify algal cells involved staining of nuclei with 4‘ ,6-diamidino-5-phenylindole (DAPI) stain. The tests revealed that stain residuals could not be properly removed from the sample without losing

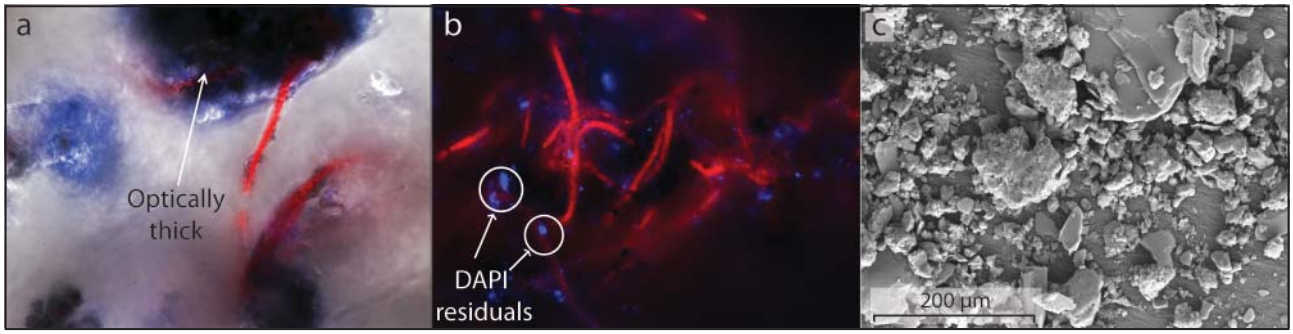

Figure 4: Pictures of different method tests, showing epi-fluorescence microscope images with optically thick granules (a), with DAPI residual disturbance (b), and a SEM image (c) with granules and mineral dust particles.

part of the sample material. Therefore the generated nuclei fluorescence was masked by the interfering signal from these stain residuals (c.f. Figure 4b). Consequently, focus was shifted from individual cells to the formation of cryoconite granules as a proxy for biological activity. As recently suggested by Takeuchi (2009), cryoconite granules were presumed to reduce the albedo of glaciers more efficiently than algal cells and bacteria themselves, which justifies the emphasis chosen for this study.

Cryoconite granules were classified into three categories and counted under a digital light microscope (Dino-Lite AM423). The associated software allowed elementary distance measurements on the captured scenes. Thus, in addition to simple counting, the granules approximate projected two-dimensional area was determined on all ice samples. Figure 5 shows the identified and quantified classes: black opaque granules (a), thick brown granules (b) and loose networks (c), which largely consisted of filamentous cyanobacteria and particles also including single filaments. The determination of the projected granule area (particularly in the case of loose network structures) was highly approximative. Since granule formation seems to be dominated by biological activity (Langford et al., 2010), this approach served as simple means to assess the contribution of algae and bacteria to surface darkening. Efforts were made to improve understanding of the processes of particle aggregation and granule formation. Scanning electron microscopy (SEM) images were produced by R. Bruetsch from the Nuclear Energy and Safety Department at the PSI, to identify the structure of gluing substances within the

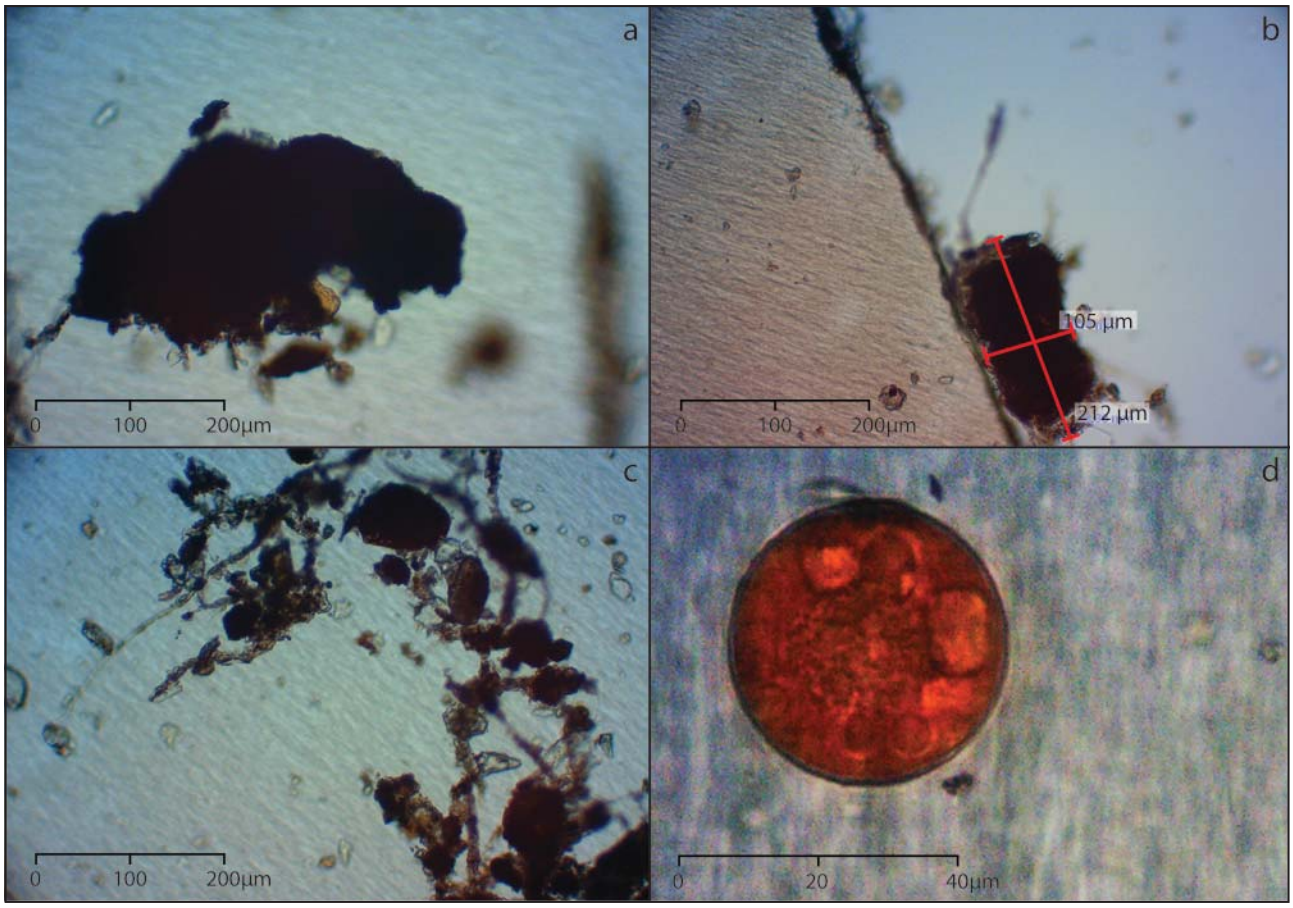

Figure 5: Examples of the different granule types: black opaque granule (a), brown thick granule with measurement bars in red (b), loose network structure (c) and an algal cell of the species Chlamydomonas nivalis (d). Note the difference in scale for (d).

granules (c.f. Figure 4c). Since EPS are important to granule formation processes (c.f. section 1.1), their investigation by SEM was considered. However, EPS are extremely labile and consequently cannot be exposed to electron beams without inducing evaporation with the current instrumental settings at the geographical laboratories of the University of Berne (personal communication C. Kamenik, University of Berne). Therefore labour-intensive preparation steps would have been required for this kind of analysis (Hand et al., 2010), which were beyond the scope of this study.

Chlamydomonas nivalis (c.f. Figure 5d) was counted in all snow and ice samples using a simple light microscope. This snow algae species is easy to identify due to its red colour caused by carotenoids (Thomas and Duval, 1995). Thomas and Duval (1995) described the life cycle of this snow algae species as follows: during winter time, pigmented cells of *Chlamydomonas nivalis* rest in frozen soil below the snowpack. As soon as snow melt causes water logging of the remaining snowpack, flagellated stages mount to the snow surface. There, the flagellated stages form red spores, inducing snow staining. It remains unclear, whether the resting stages of *Chlamydomonas nivalis* survive in cryoconite deposits, or whether staining on snow covered glaciers occurs by wind transport of algal cells.

In addition, a simple qualitative microscopic investigation of all snow samples was accomplished, assessing the relative abundance of microorganisms (algae/bacteria), pollen and (mould) fungal spores and hyphae. These investigations were based on light microscopy images of snow biota from different authors (Müller et al., 1998; Uetake et al., 2006; Elster et al., 2007; Santibáñez et al., 2008; Leya et al., 2009). For non-metric data (cell numbers and network area), the square root was used to obtain a normal distribution. Both granule number data, however, was log-normally distributed.

4.6.3. Thermo-optical OC/EC analysis

Soot can be determined by different methods (e.g. incandescence and thermo-optical methods), which generally yield different results (Kaspari et al., 2009). Originally, the analysis of carbonaceous particles from soot was planned on a single particle soot photometer (SP2), which is designed to measure the mass of strongly absorbing BC particles and determine their size distribution in aerosols, independent of particle morphology or potential coating. However, the application of this analysis method to liquid samples from snow or ice so far suffers from undetermined particle loss in the nebulizer and a low level of understanding for the corresponding processes (Kaspari et al. 2011; personal communication I. Wendl, PSI). Though, the nature and extent of this artefact are currently being studied by different research groups at the PSI (M. Laborde, M. Gysel and I. Wendl; studies in progress). Instead a thermo-optical OC/EC analyser (RT 3080, Sunset Laboratory Inc.) at the Department of Chemistry and Biochemistry at the University of Bern was used to determine both the OC and EC content. In contrast to the incandescence method, soot is thereby not defined by its absorption behaviour, but by its incineration temperature. Additionally, no information on the particle level (size distribution or number concentration) can be obtained. This results in a slightly reduced suitability for albedo considerations (c.f. section 2.5). The great advantage however, is the simultaneous determination of OC and EC.

Ice and snow samples were transferred to the Department of Chemistry and Biochemistry of the University of Bern in frozen condition. Prior to the analysis, the samples were melted at room temperature and sonicated for 15 minutes to loosen particle aggregates and to prevent particle loss to the vial walls. Due to the extremely high particle concentrations in ice samples and the relatively low upper limit of detection (around 100 µg), sample aliquots

of 50-200 µl were extracted. In contrast, the relatively clean snow samples had to be concentrated to reach the lower absolute detection limit of the instrument, which lies around 1 µg accounting for the variable instrumental error of up to ± 0.9 µg (personal communication Y. Zhang, University of Berne). This procedure required three to five samples representing the uppermost 30 to 50 cm of the snowpit, which consequently reduced the resolution of the EC profile within the snowpack. To obtain homogeneous particle distribution on the filter spot, the sample aliquots were diluted with ultra-pure water prior to filtration through pre-baked (6 h at 850°C) quartz fibre filters (2500QAO-UP, Pall). Then, the filters were acidified with three drops of 0.2 molar hydrochloric acid (HCl) for 2 h, to remove all carbonate from calcite minerals. For thermo-optical analysis, several methods exist, differing in their temperature and gas flow protocols. Here the NIOSH 5040 method was used, which is a standard two-step temperature procedure including a helium stage for OC combustion and a helium-oxygen stage for EC combustion (Aamaas et al., 2011). The thermo-optical procedure was originally designed for aerosol analysis. However, the adaption to the analysis of particles from ice samples seems to be less problematic than in the case of incandescence measurements. For more details on the instrument and method properties for liquid sample analysis see Aamaas et al. (2011). To assure instrument reliability, sucrose ($C_{12}H_{22}O_{11}$) was regularly measured as an OC-standard. The EC and OC content of the snow samples were determined in µg C per litre, which corresponds to the mixing ratio expressed as ppb by weight. For concentrations below the detection limit (ranging from 8 to 12 ppb), values of half the respective detection limit were inserted. To assess the spatial distribution of EC, the results of the ice samples were converted to µg EC/cm^2 of glacier surface. Since EC concentrations were log-normally distributed, Pearson correlation was calculated using the logarithmic results.

4.7. Data processing of albedo measurements

The field measurements of broadband albedo and spectrally resolved radiance were treated differently to correct for the grain growth- and zenith angle-induced albedo reduction, which was necessary in order to isolate the effect of impurities.

4.7.1. Broadband albedo

Gardner and Sharp (2010) published a theoretically based parameterization for snow/ice-albedo modelling, accounting for snow metamorphosis, changes in zenith angle, cloud optical thickness and light-absorbing carbon in snow. Using this model, the albedo change between the first two measurements on 1 June and 6 July, when the glacier was still snow covered, could be simulated. The equations below are based on the concept of specific surface area ($\hat{S}$), which is inversely proportional to the effective radius (r_e) of the snow grains and the density of ice (ρ_i; 4.3). This approach assumes the albedo of clean snow ($\alpha_{\hat{S}}$) to be directly determined by the specific surface area of the snow crystals (4.4). When the concentration of light-absorbing carbon (c) in parts per million (ppm) by weight is known, the resulting impurity induced change in albedo ($\delta\alpha_c$) can be computed (4.5). The alteration of albedo due to changes in solar zenith angle ($\delta\alpha_{\theta z}$; 4.7) is amplified by the occurrence of impurities and thus includes both the clean condition ($\alpha_{\hat{S}}$) and the contaminated condition (α_c; 4.6). The overall broadband albedo (α) is then calculated by summing all contributing components (4.8):

$$r_e = \frac{3}{\rho_i \hat{S}} \quad (4.3)$$

$$\alpha_{\hat{S}} = 1.48 - \hat{S}^{-0.07} \quad (4.4)$$

$$\delta\alpha_c = \max\left(0.04 - \alpha_{\hat{S}}, \frac{-c^{0.55}}{0.16 + 0.6\hat{S}^{0.5} + 1.8c^{0.6}\hat{S}^{-0.25}}\right) \quad (4.5)$$

$$\alpha_c = \alpha_{\hat{S}} + \delta\alpha_c \quad (4.6)$$

$$\delta\alpha_{\theta z} = 0.53\alpha_{\hat{S}}(1 - \alpha_c)(1 - \cos\theta_z)^{1.2} \quad (4.7)$$

$$\alpha = \alpha_{\hat{S}} + \delta\alpha_{\theta z} + \delta\alpha_c \quad (4.8)$$

For simplicity reasons, Gardner and Sharp (2010) assume crystals to be spheres with an equivalent surface area. Due to measurement constraints, the mean grain radius instead of the effective radius was determined in this study. Since mean grain size had not been measured during the field campaigns itself, it had to be reconstructed from measurements in the coldroom, using a grain growth model developed by Stephenson (1967) and promoted by Marshall and Oglesby (1994) for implementation in global climate models:

$$D^2 - D_0^2 = At\, e^{(-\frac{B}{T})} \quad (4.9)$$

The parameters are as follows: D_0 denotes the initial grain diameter, while D describes the grain diameter at time (t). T is temperature in Kelvin and A and B are constants, which were calculated from a graph in Marshall and Oglesby (1994).

The albedometer was installed parallel to the approximately horizontal glacier surface and operated for several hours around noon. This meant data could be easily corrected for the solar zenith angle of that particular day and location. Clouds affect the surface albedo by modifying the spectral distribution of solar irradiance and the ratio of direct to diffuse radiation (Gardner and Sharp, 2010). Since low cloud cover was observed during the measurement period, cloud induced albedo changes were neglected. The uppermost snow samples of the two snowpits were analysed for their EC content (c.f. section 4.5.3) to obtain concentrations at the surface during the albedo measurements. With the given concentrations of EC, the theoretical albedo was then calculated using the equations 4.3-4.8.

4.7.2. Spectral reflectance

Radiance data was transformed to reflectance by dividing the target values by the corresponding reference measurements. Since low cloud cover conditions were met on the corresponding campaign date (25 August), no correction for diffuse radiation had to be performed. The influence of solar zenith angle does not need to be corrected for, because this effect is levelled out by the radiance to reflectance transformation (personal communication A. Hueni, University of Zürich). In addition, the complex bi-directional reflectance behaviour (expressed by the bi-directional reflectance distribution function BRDF) of snow or ice might have a relevant impact on the radiance measurements. According to Oerlemans (2010), the large aperture angle of common radiation sensors minimises the effect of BRDF of ice surfaces. Since the glacier was snow-free on the date of spectral reflectance measurements, BRDF was neglected. The original project plan included spectral measurements of the ice samples in frozen condition, to reduce and quantify the effect of liquid water. Due to persisting low stratus conditions at the PSI and limited availability of the spectrometer device, this procedure could not be performed in sunlight. Tests with alternative sources of radiation (ordinary 120 watt halogen light bulb and VIS-lamp with known spectrum in the VIS wavelengths) showed unidentified irregularities. Unfortunately the obtained results could therefore not be included, resulting in unquantifiable influence from liquid water content.

5. Results and interpretations

5.1. Results of snowpack investigation

5.1.1. Reconstruction of snowpack formation

On the first day of fieldwork (1 June) a total snowpack height of 2.6 m was measured. Assuming constant density from the lowest sampling depth to the ice surface, the total snow height corresponded to 1.28 m weq. The reconstructed formation of the snowpack is visualized in Figure 6, along with the meteorological setting during the accumulation season in 2009/2010. Mean daily temperatures along with snowfall events (c.f. section 4.3.1.) and the cumulative snowpack height are shown. Figure 6 illustrates that on Plaine Morte winter temperatures (daily means) were well below zero degrees from mid-October to the end of May. This accumulation season was only interrupted by two periods with temperatures above freezing point at the end of April and May; with durations of 8 and 9 days, respectively and occasional short warmer episodes in October and November. Just prior to the first day of fieldwork some melting occurred followed by two days of snow fall. The ice lens observed at a depth of 0.82 m weq was most probably attributable to the melt period in November. This would imply that no vertical percolation or drainage of meltwater had taken place until 1 June. Figure 7 (left) illustrates the stratigraphy of the snowpack on 1 June and 6 July, which was governed by snow metamorphosis, sequential episodes of accumulation, melt and refreezing processes and amplified by dust depositions of local or remote origin. The darker layer at a depth of 0.1-0.35 m weq was assumed to be caused by volcanic ash deposited after the eruptions of Eyjafjalla. No yellowish horizons indicating Saharan dust input were observed within the snowpack. This stratification and the corresponding processes were mirrored in the chemical composition of the snowpack, and could thus be identified by means of chemical analyses.

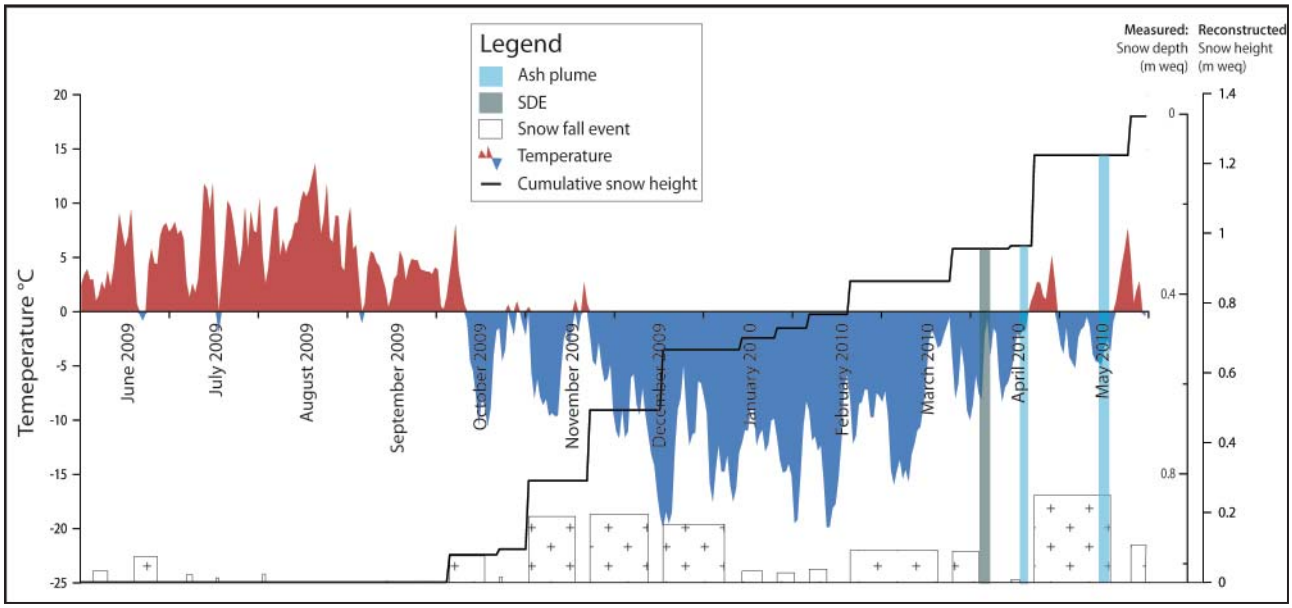

Figure 6: Snowpack reconstruction: Reconstructed temperature and solid precipitation data for Plaine Morte glacier in the period from June 2009 to end of May 2010, with the resulting snow accumulation. The red (and blue) curve represents mean positive (negative) daytime temperatures, derived from temperature records from the Montana station. The columns at the bottom mark snowfall events with their corresponding duration and snow height. The accumulative snowpack height is denoted by the black line. Additionally the temporal occurrence of the Eyjafjalla ash plume intrusions and the strongest SDE recorded on Jungfraujoch (c.f. section 5.1.3) are marked by the blue and green bars, respectively

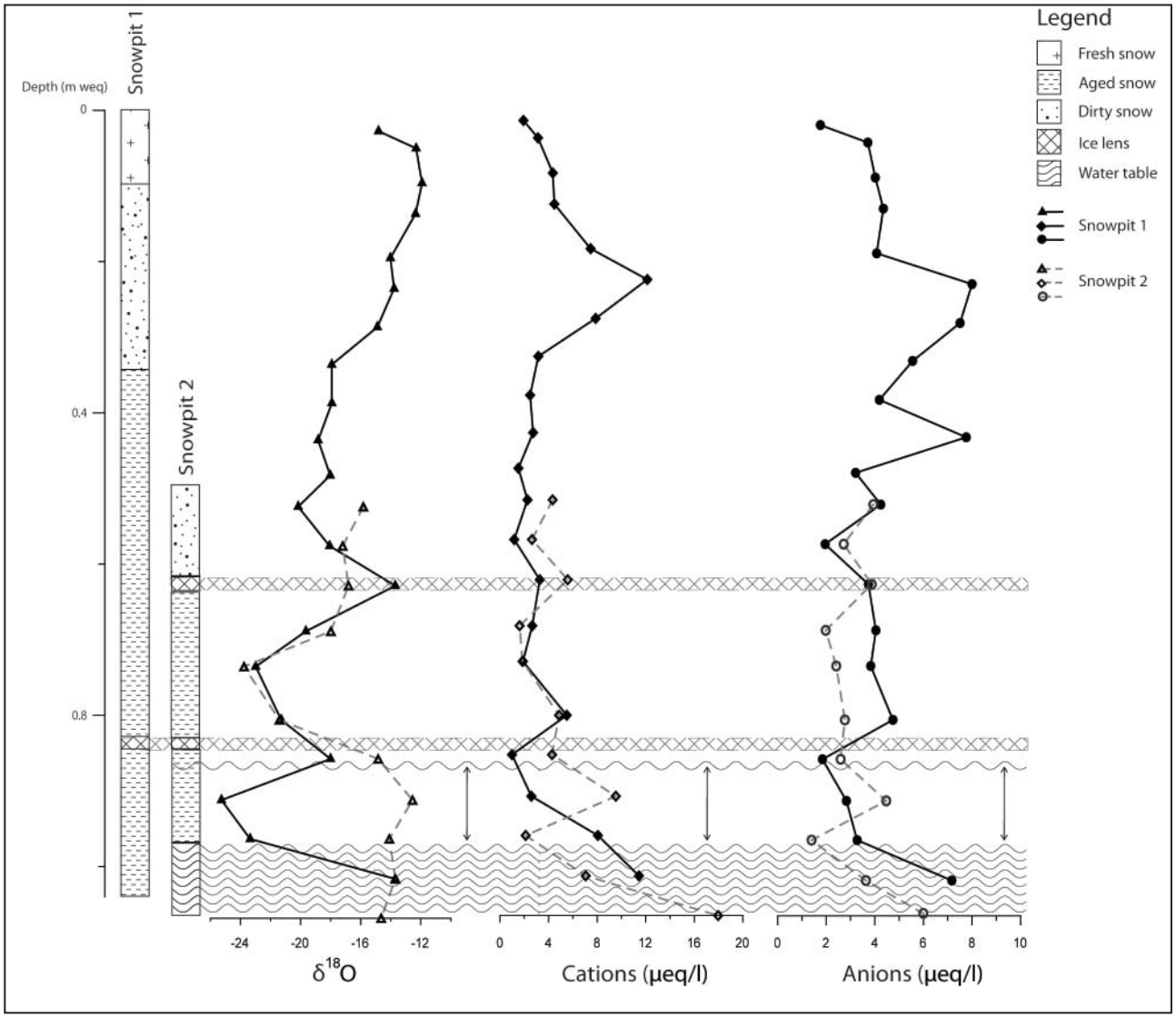

Figure 7: Comparison of the two snowpits on 1 June and 6 July, with their isotopic $\delta^{18}O$ ratio, the sum of cations and the sum of anions (in µeq/l) within the snow profile. On the left side, a schematic drawing of the snowpack stratigraphy is shown. The meshed bars depict ice lenses and the waved lines symbolise the water table found on 6 July, with the arrows indicating possible changes in water table height.

5.1.2. General characterisation of the snowpack on 1 June

On 1 June a gradual progression between winter and spring snow was found, reflected in the stable oxygen isotopic ratio with values down to -25‰ in the bottom layers and values around -15‰ in the upper layers, respectively. The transition between winter and spring was located at a depth of 0.35 m weq and corresponded to April snow. The mean $\delta^{18}O$ value of the snowpack amounted to -17.05‰. The peaks in the lower part of snowpit 1 (around 0.65 and 0.85 m weq) could be partly explained by refreezing of percolating meltwater, since an ice lens was observed at a depth of 0.82 m weq. Figure 7 illustrates the overlap of the two $\delta^{18}O$ profiles from 1 June and 6 July. Obviously the original isotopic ratio of snowpit 2 had been perturbed in the lowest part between 0.85 and 1.04 m weq. This perturbation was most probably caused by water logging in that part of the snowpit. Melting spring and early summer snow had percolated through the snowpack to form a water table on the impermeable ice surface, still carrying the isotopic footprint of milder temperatures. Therefore, these water logged

layers were characterised by higher $\delta^{18}O$ values (>-15‰) than observed in the corresponding layers of snowpit 1. Nevertheless, the cross-matching of the depth profiles seemed to be accurate, since the ice lenses from snowpit 1 and 2 overlap. The bottoms of the snowpits did not reach the same depths, since on 1 June sampling was not performed down to the glacier surface due to practical constraints.

Anion and cation concentrations showed some similarities between 0.54 and 0.82 m weq, but no obvious agreement was found (c.f. Figure 7, right). This confirms the meltwater percolation features observed in the isotopic profile. Some species showed elution symptoms or had accumulated in the ice lenses (refreezing of percolating meltwater). In snowpit 2 the samples from layers below 0.85 m weq showed distinct relocation patterns and pronounced cation excess. Changes in water table height and dissolution of mineral dust deposits might have resulted in these irregularities.

Significant decrease in the overall ion inventory was observed in the snowpack between 1 June and 6 July. With a loss of more than 50%, ions related to secondary aerosols (SO_4^{2-}, NO_3^- and NH_4^+) were most affected. All other ion concentrations decreased as well, with the exception of K^+, which showed a remarkable increase of more than 50%. The ionic species were characterised by different elution and relocation behaviour. For Mg^{2+} and Na^+ a minor reduction of the total abundance was observed. While Na^+ showed signs of relocation in the concentration profile, little change was ascertainable for Mg^{2+}. Little change was also observed for SO_4^{2-}, NO_3^- and Ca^{2+} concentration profiles, however, these species were subject to substantial loss. Further, Cl^- and NH_4^+ both featured notable relocation patterns and strong loss. Except for Cl^- all ions with strong elution symptoms (SO_4^{2-}, NO_3^-, NH_4^+ and Ca^{2+}) were enriched in the meltwater sample. The ionic budget of the snowpits showed some remarkable features. The sum of cations was very well balanced with the sum of anions (91.0 versus 91.8 µeq/l) in the snowpack on 1 June, although neither the hydrogen-cation (H^+) nor the bicarbonate-anion (HCO_3^-) was included in the analysis. The individual snow layers and the snowpit on 6 July, however, exhibited remarkable systematic cation or anion excess. Samples with low ion concentrations were generally characterised by anion excess, while the few samples with high total ionic load tended towards cation excess. For this specific behaviour no reasonable explanation was found, but apparently cations and anions were not evenly affected by the elution processes. While cations accumulated (mainly in the waterlogged part and in ice lenses), anion concentrations were generally reduced between snowpit 1 and 2. Thus, ionic and isotopic patterns were strongly altered during the ablation processes in the period from 1 June to 6 July, while the signals still seemed to be relatively intact in snowpit 1 on 1 June.

5.1.3. Impurities in snowpack

Ionic composition

For the investigation of impurities within the snowpack, only the intact signals from the early melting season (1 June) were considered. Figure 8 displays the ionic concentration profile of the snowpack on 1 June. In general, ionic concentrations fluctuated in a limited range of values, showing no extremes. Most obvious were the collective peaks at a depth of 0.2-0.35 m weq and in the bottom layer, where all ionic species showed increased concentrations. Ca^{2+}, K^+ and Mg^{2+} were characterised by a similar fluctuation pattern, which was independent of seasonality. Analogous characteristics were found for the species Na^+ and Cl^-. No pronounced seasonal pattern was found, except for NH_4^+, which showed consistently low concentrations in the lower part of the snowpack, representing winter snow and increasing concentrations in the upper 0.3 m weq of the snow profile, which represented spring snow.

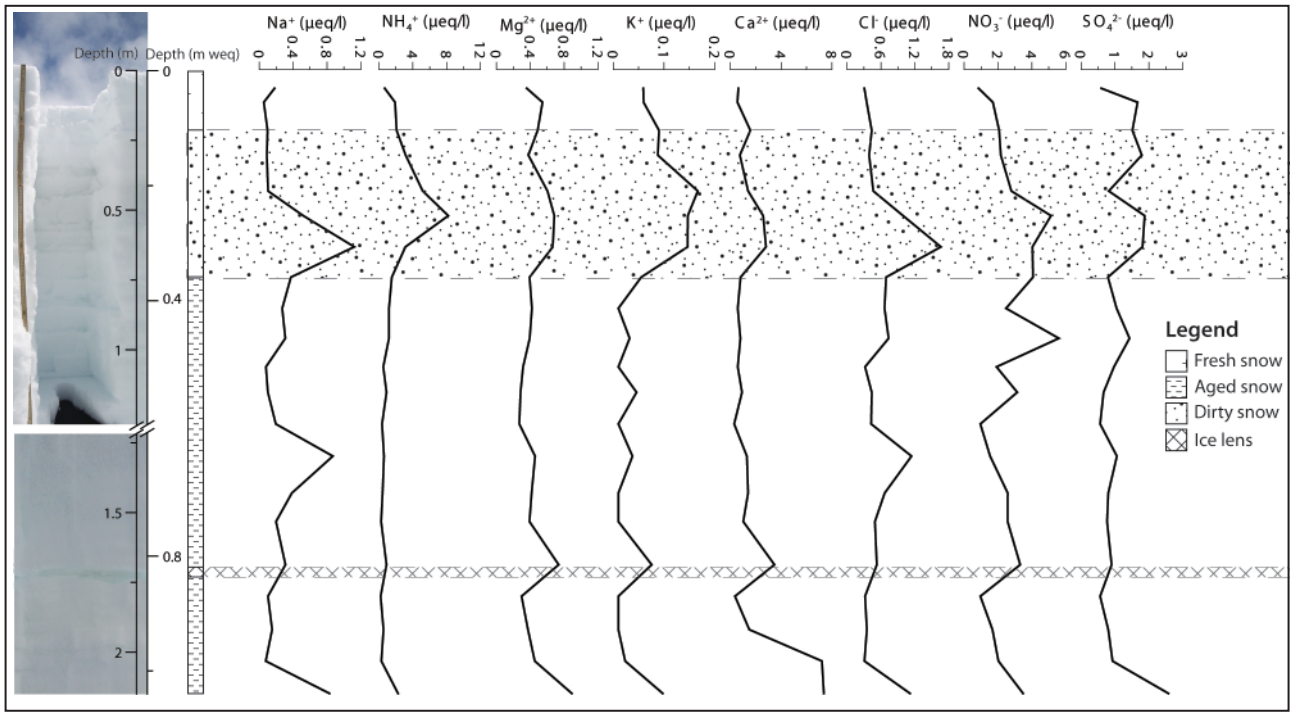

Figure 8: Concentrations of all ionic species (in µeq/l) within the snowpack on 1 June, with a picture of the snowpit and a schematic drawing of the snowpack stratification. The dotted and the meshed bar denote the observed darkened horizon and ice lens, respectively.

SO_4^{2-} and NO_3^- fluctuations seemed to be rather irregular compared with the other species. The ice lens at a depth of 0.82 m weq showed increased concentrations for most species, and was most pronounced for Ca^{2+}, K^+ and Mg^{2+}.

Correlations between the different ionic species are shown in Figure 9. The most striking feature of the ionic composition was the strong correlation between Na^+ and Cl^- (R = 0.92), combined with the characteristic sea salt Cl^- to Na^+ ratio of 1.16 (c.f. section 2.4). Further, Ca^{2+} and Mg^{2+} as well as Mg^{2+} and K^+ showed good correlation, as expected for their common source in mineral dust. In this case, K^+ was also highly correlated with NH_4^+. The secondary aerosol species SO_4^{2-}, NH_4^+ and NO_3^-) were relatively well correlated among each other. Additionally, SO_4^{2-} was partly associated with mineral dust (Mg^{2+}), which indicates internal mixing of dust and secondary aerosols during long-range transport. Mg^{2+} was significantly correlated (on the 1% confidence level) with all other ionic species.

Mineral dust

ICP-MS results showed that the elements Fe, Mg and Al were well correlated among each other (R = 0.86-0.91) and generally strongly enriched on the glacier surface (factor >100), which is reasonable, since all three elements are common constituents of rock forming minerals. Figure 10 depicts typical XRD peak-patterns of snow samples from the snowpack on 1 June, illustrating generally low peak intensities and strong disturbance from the filter and aluminium platelet. The 2 theta peaks at 9° and 26.5° most probably correspond to mica and quartz, respectively. Unfortunately these were the only two minerals which could be identified in the snowpack.

Due to the lack of a suitable tracer, SDE records from the aerosol monitoring station at Jungfraujoch, were used to locate potential Saharan dust deposits within the snowpack (data kindly provided by Meteo Schweiz). The only noteworthy SDE in the accumulation season 2009/2010 was recorded on 7 and 8 April 2010, just prior to the occurrence of

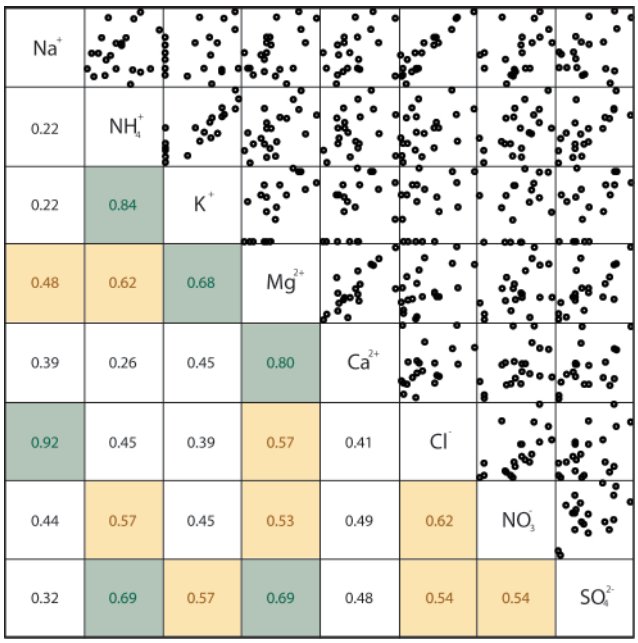

Figure 9: Correlation matrix for major ions in snowpit 1, including scatter plots for all pairs of ionic species in the upper right corner. Green (yellow) correlation coefficients (R) are significant at the 0.1% (1%) confidence level, assuming the data to be log-normally distributed.

the first Eyjafjalla ash intrusion into the atmosphere over Switzerland. According to the reconstruction of the snowpack, corresponding deposits of the SDE and volcanic ash should be located between 0.35-0.4 m weq and 0.1-0.35 m weq, respectively. With durations of 8 to 9 h and comparatively low particulate numbers the recorded SDE did not seem to be an outstanding dust event, which was reflected in low Fe, Mg and Ca concentrations. In addition, no typical yellowish colouration of snow horizons was observed within the snowpack and XRD results were ambiguous for the layer in question. In contrast, for the darkened horizon at a depth of 0.1-0.35 m weq, the presence of mica, quartz and high Fe, Mg and Ca concentrations were found. Figure 11 illustrates the snowpack on 1 June with its stratigraphy and dust horizons and selected mineral dust indicators (Al, Fe, quartz and mica).

Additionally, the elemental composition showed an enrichment of REE and Fe (factor 18-23 for La, Pr, Ce, Nd and Sm, factor 10-11 for Fe, Eu and Yb) in the layer from 0.1-0.35 m weq (c.f. Figure 12a and section 2.4). A similar enrichment was observed in the bottom layer of the snowpack. Figure 12b shows the REE composition of Plaine Morte snow from the dust horizon compared to the mean composition of Hekla ash (c.f. section 2.4), both normalized to the mean upper continental crust composition. The concentrations of Eu and Yb seemed to be lower than expected for Icelandic volcanic ash. However, the pattern looked comparable, after a single extreme outlier regarding Yb concentrations in Hekla snow had been excluded.

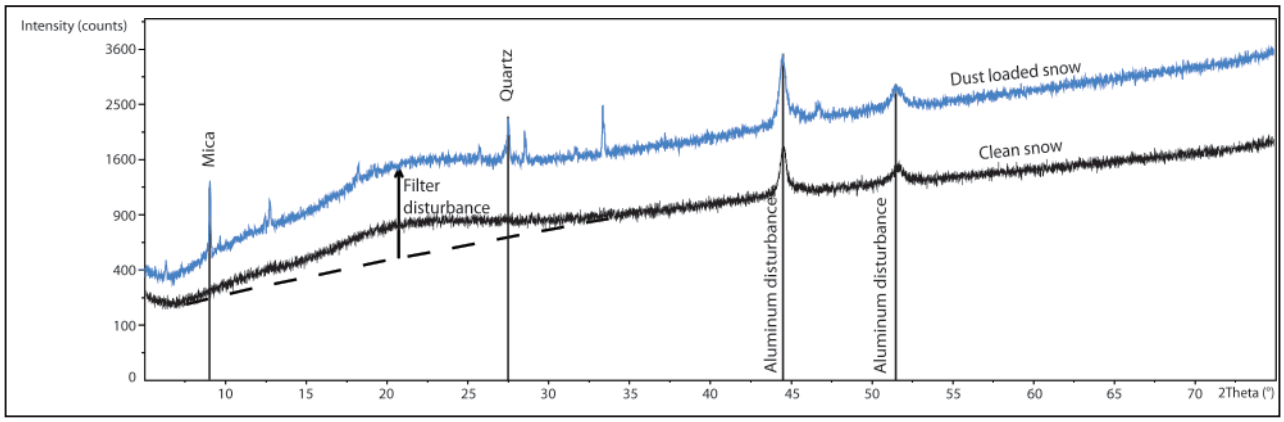

Figure 10: XRD peak-pattern of two snow samples representing clean snow (black) and dust loaded snow (blue). The only identifiable peaks, attributed to mica (at 9°) and quartz (at 27.5°), are marked. The arrow illustrates the high background signal caused by the filter disturbance. The aluminum peaks around 45° and 50° are caused by the gleaming aluminum platelet, which is part of the sample holder.

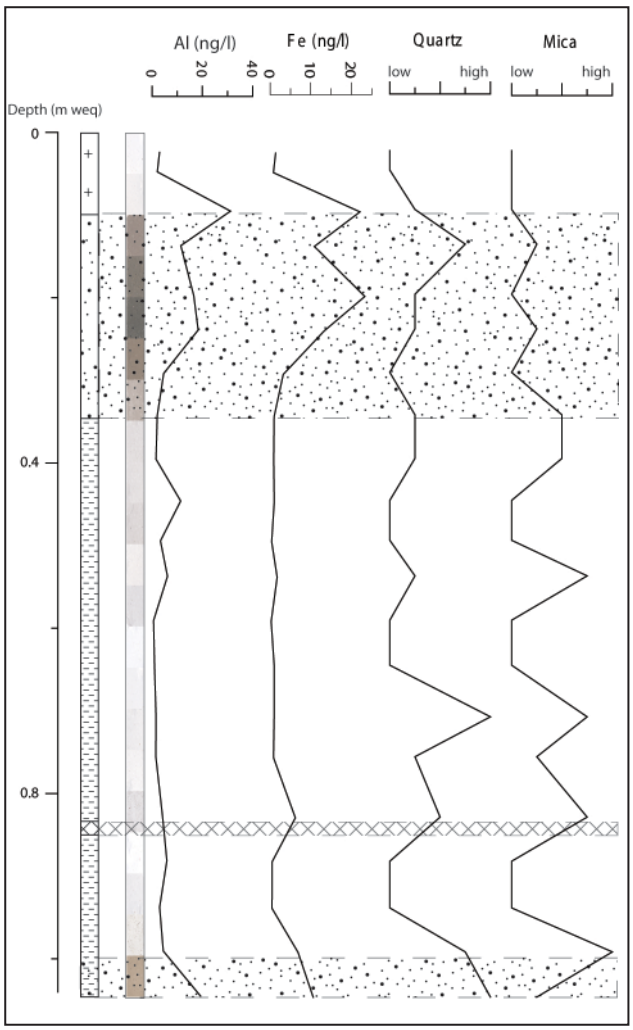

Figure 11: Indicators for mineral dust within snowpit 1. Next to the schematic snowpack stratigraphy, a picture of all snow sample filters is placed, illustrating the variance in dust load. The concentrations of the elements Al and Fe (in ng/l) as well as presence of mica and quartz (high/low) are drawn.

Biogenic matter and elemental carbon

The qualitative microscopic investigation of the snow samples from 1 June revealed varying amounts of biogenic matter. Pollen were strictly limited to the layer attributed to spring snow from a depth of 0.05-0.35 m weq. The same horizon was characterised by remarkable amounts of algae, bacteria, fungi and fragments of dead biogenic matter. In addition, large quantities of near-transparent micro-sized mineral particles were observed. Overlying this biota rich layer, a clean layer of fresh snow was found. Little organic matter (except for fungi) was also observed between 0.35 m weq and the bottom of the snowpit. However, this relatively clean bottom layer was interrupted by a horizon with increased amounts of microorganisms (0.75-0.8 m weq). The lowest layer of the snowpit was again characterised by a slightly higher assemblage of algae and bacteria. Throughout the entire snowpack, no cells or spores of the species *Chlamydomonas nivalis* could be identified and organic matter only appeared in non-aggregated form. Characteristically, EC was highly concentrated in the topmost layers of the snowpack, while the vast part of the snowpits was found to have EC concentrations below the detection limit. Notably, the highest concentrations were found in the layer from 0.15 to 0.25 m weq.

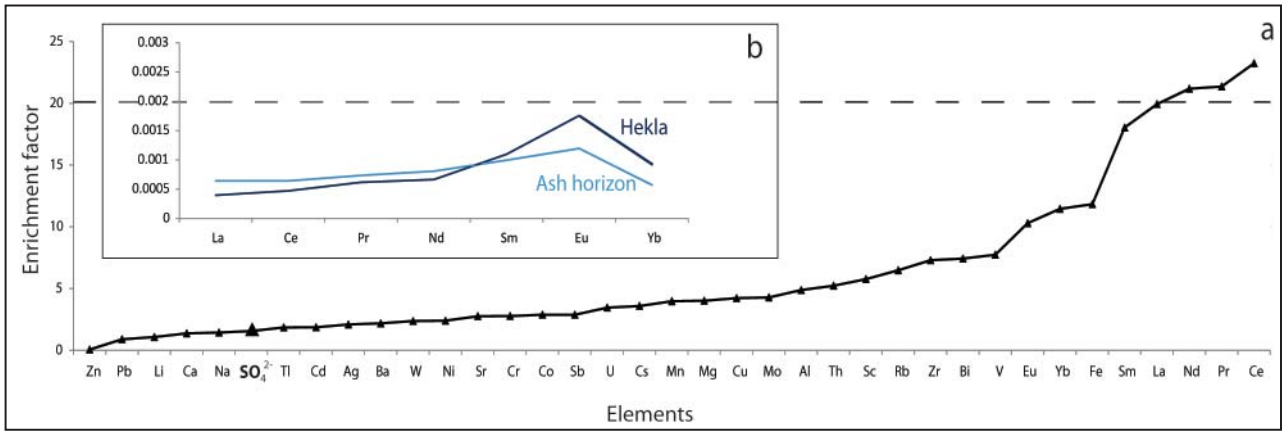

Figure 12: Trace element composition of the ash horizon: The lower graph (a) shows the enrichment factors of trace elements and SO_4^{2-} (highlighted) in the ash horizon (0.1-0.35 m weq) compared to the baseline. The dashed line marks the threshold (enrichment factor 20) observed in Jungfraujoch snow after the Eyjafjalla eruptions (Tobler et al. 2011). The graph in the upper left corner (b) shows the REE composition of the ash horizon in comparison to Hekla ash (c.f. section 2.4), both normalized to the upper continental crust.

Figure 13 displays the EC concentrations and amount of microorganisms, pollen and fungi (high/low) within the snowpack of 1 June and 6 July. Between the snowpack on 1 June and 6 July, remarkable changes in EC concentrations and organic matter appearance were observed. The surface samples showed EC concentrations of 25 ppb on 1 June and 84 ppb on 6 July. The EC inventory over the total snow profiles showed a strong increase of 88% between the two sampling dates from 1.2 to 2.2 µg/cm^2, indicating additional EC deposition of 1 µg/cm^2 with spring snow. While organic matter was exclusively present as single cells or pollen grains in snowpit 1, snowpit 2 showed substantial amounts of aggregated cells and dark coloured decomposing organic fragments (c.f. Figure 13).

5.2. Biogeochemical analysis of cryoconite

Visual inspection showed distinct heterogeneity of cryoconite distribution on the glacier surface. Figure 14 illustrates the surface darkening between 20 July (a) and 25 August (b) and some of the most common surface types observed, including uniformly dispersed dust (c), large-scale accumulations of cryoconite in shallow pools (d) and less frequently small cryoconite holes of a few cm width (e). Cryoconite holes were often associated with surface runoff and streams, and the stream beds were mostly covered by cryoconite clusters (c.f. Figure 14f). The ice samples showed rather large deviations in terms of total cryoconite load. Dry weight ranged from 22 g/m^2 to 423 g/m^2. The total dust accumulation was found to be largely depending on the

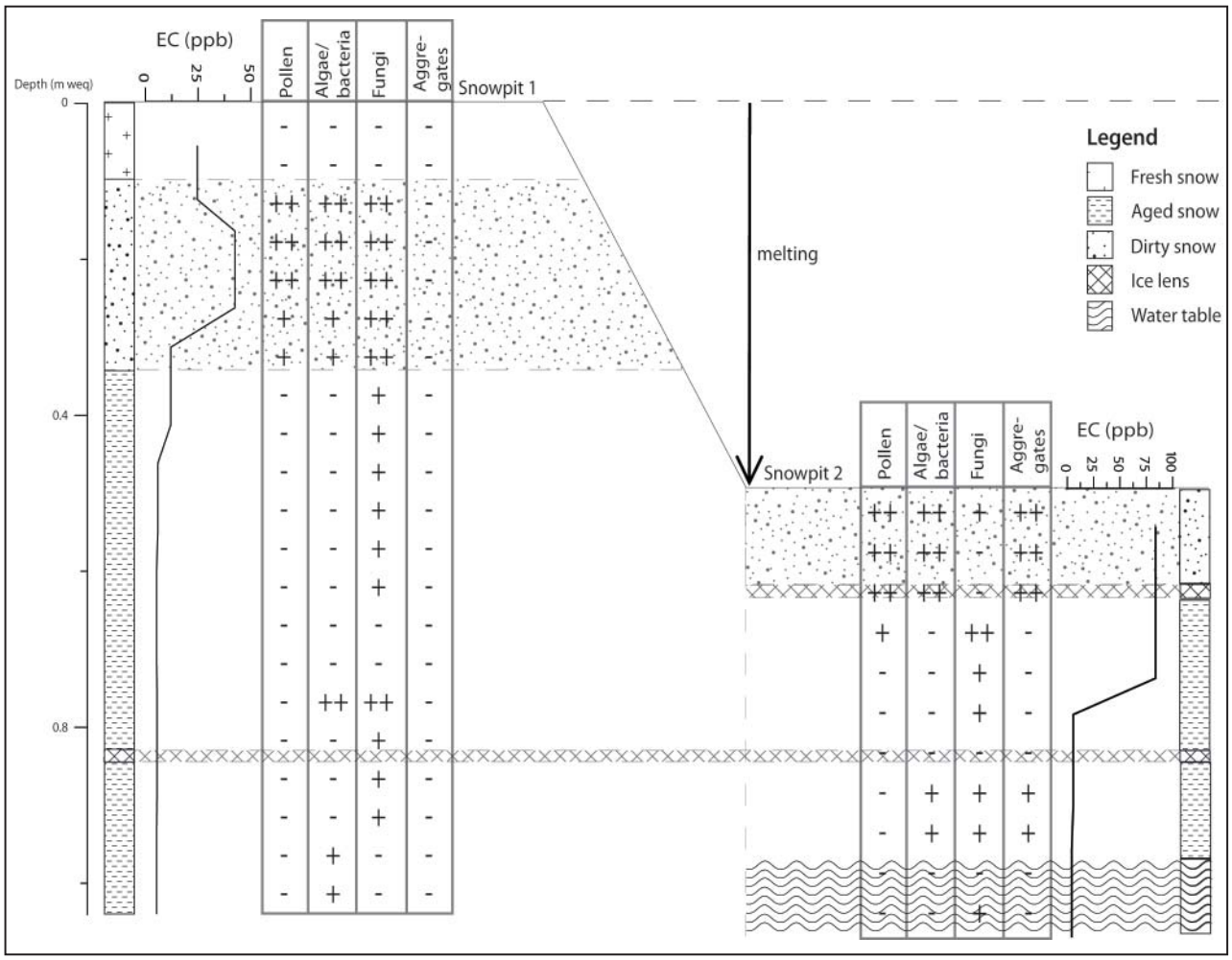

Figure 13: Stratification of the snowpack on 1 June and 6 July with EC concentrations (in ppb) and biogenic matter occurrence. The presence of different types of biogenic matter (pollen, algae/bacteria, fungi and aggregates) was marked with (++) for high load, (+) for medium load and (-) if little or no objects were found.

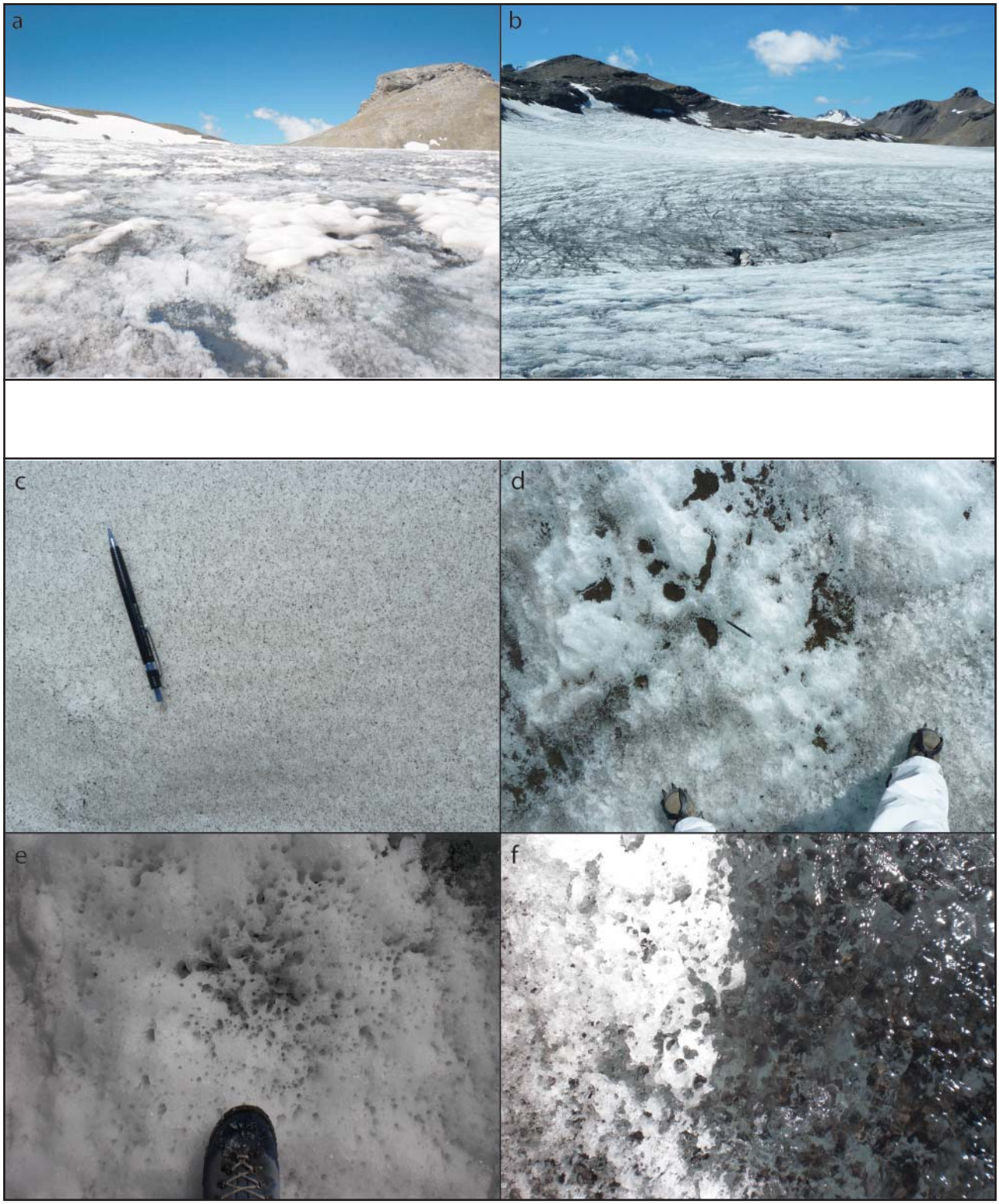

Figure 14: Pictures of surface darkening and different surface types. In the upper panel, pictures (a) and (b) illustrate the surface darkening observed on Plaine Morte glacier between 20 July (a) and 25 August (b). The lower panel shows pictures of different surface types, illustrating the heterogeneity of the cryoconite distribution on the glacier surface. Uniformly distributed dust (c) and shallow cryoconite pools (d) observed on 25 August, cryoconite holes (e) and flooded cryoconite holes (f) observed on 20 July.

extremely heterogeneous structure of the glacier surface. Therefore no increase in dust load could be observed for the time period between the two sampling dates (20 July and 25 August).

Mineral dust

Table 3 shows the mineral (a) and the overall (b) composition of ice samples and LLR. With regard to the albedo investigation, the total cryoconite load was determined in g per m^2 of ice surface. The comparison of the different ice samples (IS 1-7) revealed very similar bulk mineralogical composition. Largest deviations among cryoconite from different ice samples were observed for kali-feldspars and plagioclase. Dolomite was excluded from the table, since the concentrations detected were generally lower than the standard deviation (<0.1%). These similarities were supported by the surprisingly uniform relative abundances of rock forming elements (Fe, Al, Mg and Ca with correlation coefficients of R = 0.98-0.99) as detected by the trace element analysis and by almost identical peak-patterns of the diffraction signal (c.f. Figure 15, IS 1-7).

A comparison of LLR and ice sample peak-patterns revealed two distinct differences (c.f. Figure 15). Firstly, the baseline of the diffraction signal was shifted in comparison with the baselines of the ice samples. This most probably stems from a lower level of disturbance by organic matter and will be discussed below. Secondly, local bedrock was determined to be highly calcareous (41% calcite), while cryoconite on ice samples showed negligibly low calcite contribution (c.f. Table 3b). This discrepancy could be explained by gradual dissolution of $CaCO_3$ in water, thus reducing the relative calcite abundance in mineral dust deposited on snow and ice. Since samples were filtered immediately after melting, artefact dissolution of $CaCO_3$ during the laboratory procedure could be excluded. The differences observed in the peak-patterns of LLR and cryoconite seemed to be exclusively caused by these two effects. Thus, the ratios of different mineral components in ice

Table 3: Composition of cryoconite in ice samples (IS1-7) and of LLR. (a) shows the total mineral dust load (in g/m^2 of ice) and the relative contribution of quartz, calcite, plagioclase and kali-feldspars as determined by the XRD analysis (all in %). UF denotes the remaining unexplained fraction. In (b) the overall cryoconite composition is displayed with the total cryoconite load (in g (dry sample weight) per m^2 of ice) and the relative contribution of mineral dust, organic matter and EC (in %). TUF denotes the total unexplained fraction (in %), wich corresponds to UF exluding the fractions of organic matter and EC.

a	*IS1*	*IS2*	*IS3*	*IS4*	*IS5*	*IS6*	*IS7*	***LLR***
Mineral dust (g/m^2)	*49*	*-*	*-*	*42*	*195*	*166*	*90*	***-***
Quartz (%)	*33*	*-*	*-*	*33*	*35*	*34*	*33*	***26***
Calcite (%)	*0*	*-*	*-*	*0*	*0*	*0*	*0*	***41***
Kalifeldspar (%)	*1*	*-*	*-*	*2*	*3*	*3*	*3*	***0***
Plagioclase (%)	*5*	*-*	*-*	*5*	*7*	*6*	*5*	***3***
UF (%)	*61*	*100*	*100*	*59*	*54*	*57*	*59*	***30***

b	*IS1*	*IS2*	*IS3*	*IS4*	*IS5*	*IS6*	*IS7*	***LLR***
Cryoconite load (g/m^2)	*124*	*22*	*25*	*102*	*424*	*385*	*221*	***-***
Mineral dust (%)	*39*	*-*	*-*	*41*	*46*	*43*	*41*	***70***
Organic matter (%)	*6*	*-*	*7*	*8*	*9*	*9*	*9*	***1***
EC (%)	*0*	*2*	*1*	*1*	*1*	*1*	*1*	***-***
TUF (%)	*54*	*98*	*91*	*50*	*44*	*46*	*49*	***28***

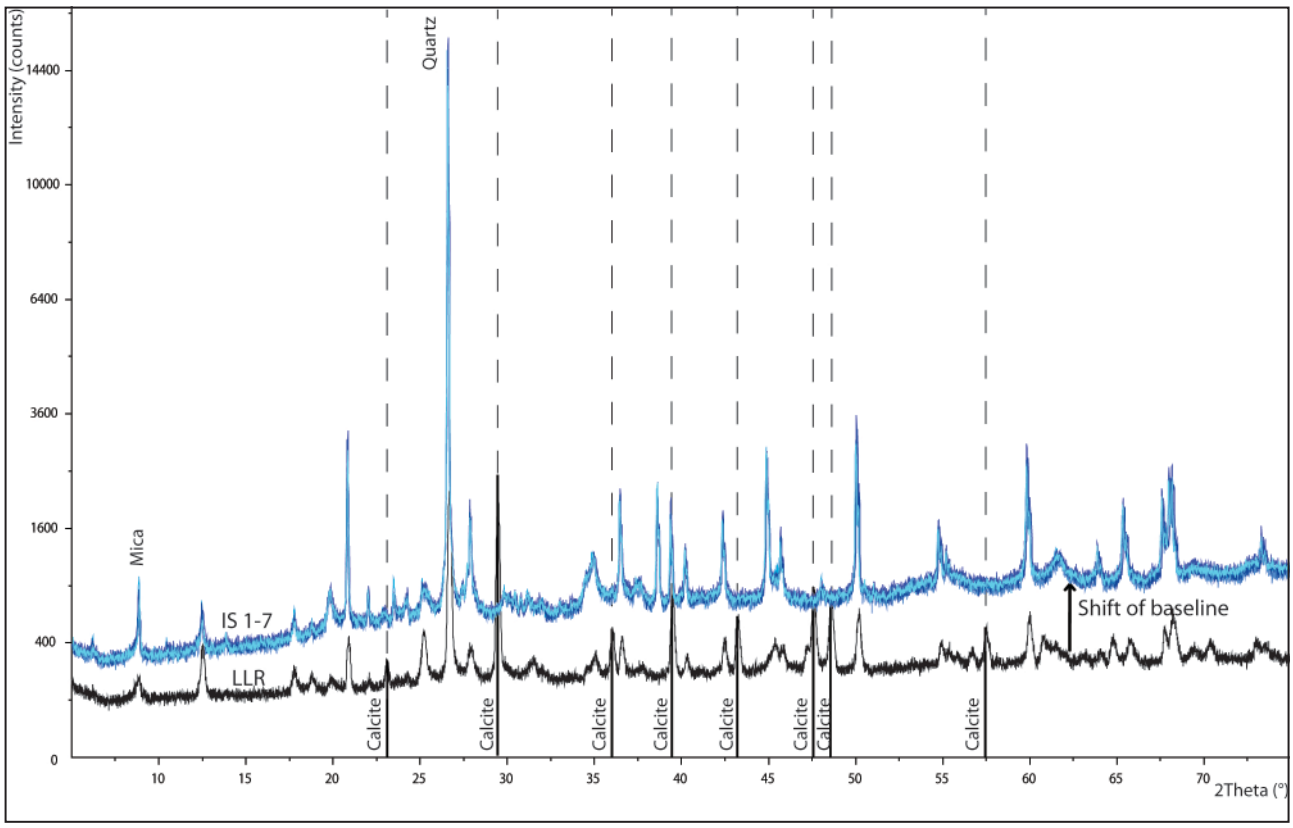

Figure 15: XRD peak-pattern of LLR (black pattern) compared to all ice samples (IS 1-7, patterns in different shades of blue). The vertical black lines show the positions of major calcite peaks, which are observed in LLR, but not in IS 1-7. The shift in baseline is marked with an arrow.

samples were consistent with the LLR composition except for the calcite content, indicating predominant dust input from local sources. Similar results were obtained for samples of PM. Calcite concentrations were very low (<1%), except for samples with visible fragments of shale. This illustrates the efficiency of calcite dissolution in the humid environment of the glacier surface for small particulate grain sizes.

Further, Table 3b illustrates that all samples showed varying contribution of unexplained fractions (UF) to the total cryoconite load. This unexplained fraction from the XRD analysis may include organic matter, different kinds of mica and clay minerals. The results from LOI showed that the organic content of LLR was below 2%, while cryoconite from ice samples showed values between 5-10% (c.f. Table 3a). The remaining total unexplained fraction (TUF) was again smallest for the LLR sample.

Biogenic matter and microorganisms

The red algae species *Chlamydomonas nivalis* was found in all ice samples and samples of PM. Concentrations ranged from 35 to 695 individuals per cm^2. In general, the number of *Chlamydomonas nivalis* cells increased with increasing dust load, but no significant correlation was observed. In some ice samples, protozoa and rotifers were found but not identified or counted. Black opaque granules were the most frequent granule class observed in the majority of all samples and reached a maximum concentration of roughly 57'000 granules per cm^2. Their mean diameter ranged from 55 µm to 140 µm. For the thick brown granules, comparable abundances were observed and mean diameters were found to range from 46 µm to 107 µm. For both granule types, no trend with respect to the total dust load could be observed. For details on the results from the microscopic analysis see Table 4. The occurrence

Table 4: Results of the microscopic assay for all ice samples (IS 1-7). Concentrations of Chlamydomonas nivalis and granule types are given in number of cells or granules per cm² of ice (a). (b) displays the cumulative area of granules and networks in mm² per cm² of ice and in (c) the mean diameter of black opaque and brown thick granules is shown (in µm).

a	IS1	IS2	IS3	IS4	IS5	IS6	IS7
Chlamydomonas nivalis	597	82	35	180	695	481	46
Black opaque granules	7082	6312	2229	2238	14042	56860	3742
Thick brown granules	6452	5551	557	2441	18011	54325	5902

b	IS1	IS2	IS3	IS4	IS5	IS6	IS7
Black opaque granules	382	208	240	28	163	782	36
Thick brown granules	287	222	23	31	191	782	44
Network	23	0	18	5	103	182	23

c	IS1	IS2	IS3	IS4	IS5	IS6	IS7
Black opaque granules	109	94	140	56	55	60	48
Thick brown granules	107	95	97	61	53	61	46

of the third granule type (loose networks) was not determined in terms of number concentration, since the nature of network structures demanded the specification in terms of area covered.

Elemental carbon

The EC load in ice samples ranged from 36 µg to 564 µg/cm² and the mean OC to EC ratio was 3.9. The relative contribution of EC to the total cryoconite mass is displayed in Table 3a. The total mass of EC seemed to be largely depending on the total cryoconite mass, since a high correlation of R = 0.93 (significant at the 1% confidence level) was found between total cryoconite load and EC concentrations. Only two samples deviated somewhat from this relation, while the five remaining samples showed perfect correlation (R=0.99, significant at the 0.1% confidence level). In contrast, between the measured EC load and the concentrations of black opaque cryoconite granules, no significant correlation could be found.

5.3. Broadband albedo and spectral reflectance

Broadband albedo

As can be seen in Figure 16, the albedo strongly decreased from 0.72 in early June to 0.16 in late August. The prominent albedo reduction within two weeks in July was attributed to a prolonged heat wave, causing melt of the entire snowpack and therefore the transition from snow cover to bare ice surface. However, these values contain natural albedo changes due to snow grain metamorphosis and solar zenith angle increase. Model calculations for clean snow (Gardner and Sharp, 2010) showed a slightly higher albedo for 1 June and substantially higher value for 6 July. The decrease in albedo attributed to grain growth (-0.04) was limited, only accounting for 18% of the total reduction observed, while changes in zenith angle were negligible during that period. The albedo-relevant EC concentrations in the topmost layers of the snowpack on 1 June and 6 July were 25 and 84 ppb, respectively.

For 1 June, 19% of the discrepancy between calculation and measurement could be explained by EC induced albedo decline. On 6 July however, despite the higher concentration, the explanatory power of the EC concentration was limited to 16%.

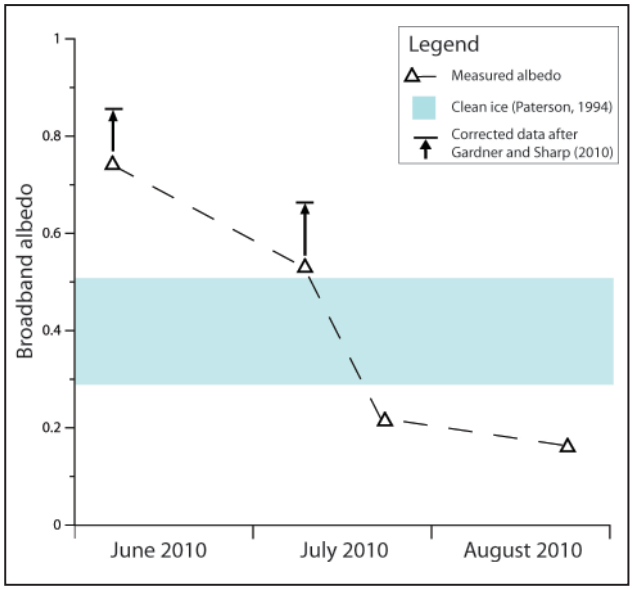

Figure 16: Measured and corrected broadband albedo on the four field campaign dates with model simulations for clean snow conditions for 1 June and 6 July (correction for grain size and zenith angle changes) after Gardner and Sharp (2010). For 20 July and 25 August no correction could be made. Therefore the reference range for clean ice (Paterson 1994) is displayed (blue bar).

Spectral reflectance

For comparability reasons, on 25 August broadband albedo and spectral reflectance were measured at the same spot. The integral of spectral reflectance (0.14) compared well with the broadband albedo of that specific surface type (0.16). Figure 17 depicts the spectral reflectance patterns of selected surface types, illustrating the heterogeneity of the glacier surface and its reflection properties. For samples with high dust load and/or high liquid water content, a flattening of the reflectance curve was observed in VIS and the lower range of NIR wavelengths (390-1000 nm). All ice surfaces showed characteristic drops in reflectance around λ = 800 nm and λ = 1050 nm. Measurements over the water surface of little clear supra-glacial streams (Figure 17d) showed a major reflectance reduction in wavelengths below 1200 nm, but still exhibited the typical ice absorption bands in NIR. Band ratios of spectral ranges in VIS wavelengths showed high proportions of the blue spectrum for clean ice surfaces, reflecting the bluish colour of temperate glacier ice. In contrast, cryoconite covered surfaces show comparatively low blue to red ratios. No distinct patterns of absorption were observed in wave length bands of 400-600 nm and 670-680 nm, even for cryoconite surfaces with distinct reddish colour cast (Figure 17f).

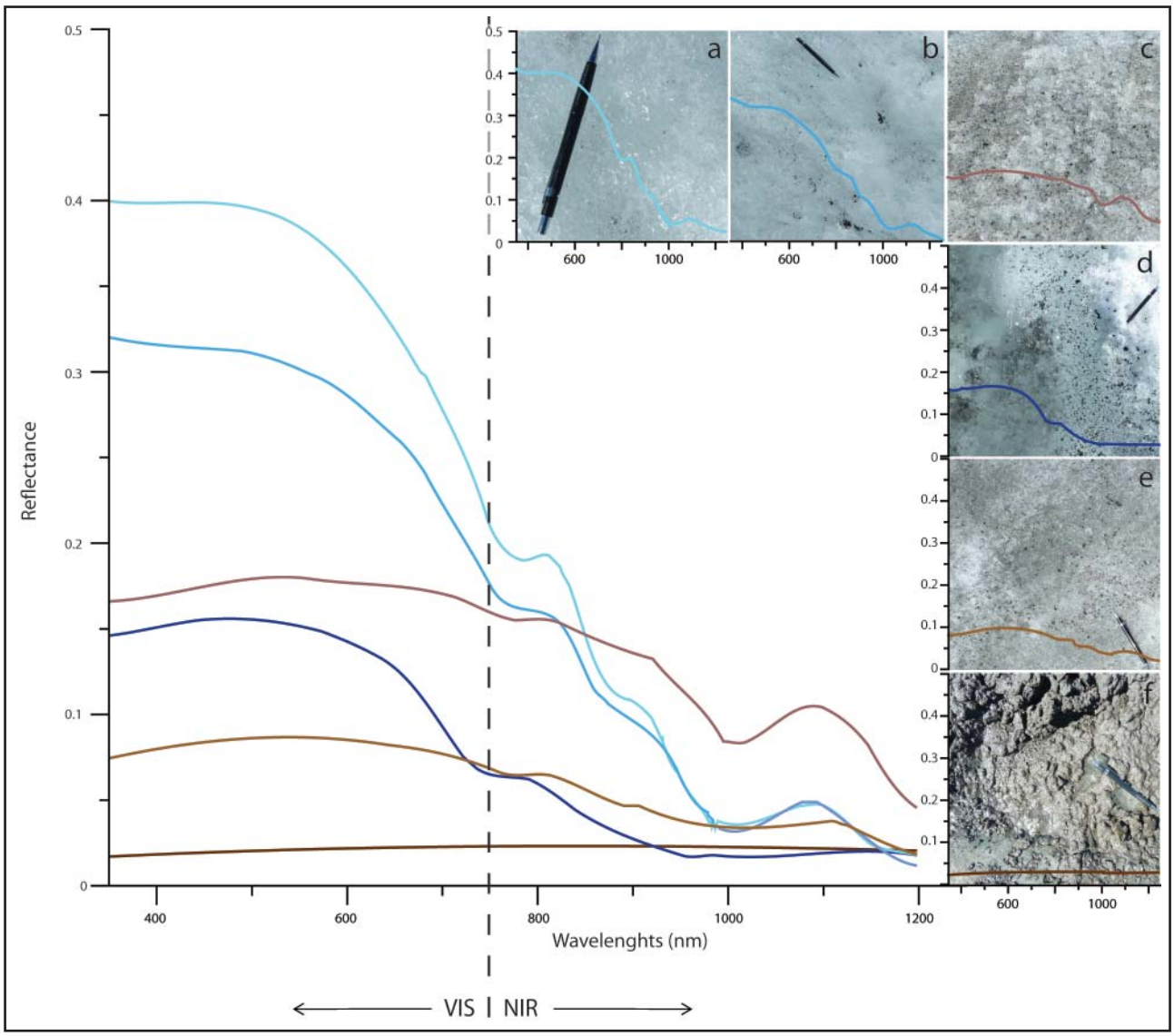

Figure 17: Spectral reflectance patterns in VIS and NIR of selected ice surface types with varying cryoconite load. The pictures on the right side show the targets with the corresponding reflectance pattern for identification.

6. Discussion

6.1. Snowpack investigation

6.1.1. Snowpack characterisation

According to the snow accumulation reconstruction from meteorological records (2009/2010) on Plaine Morte, the cumulative precipitation during the accumulation season from October to April amounted to 0.92 m weq. This finding is in contrast with mass-balance measurements by the Glaciology Department of the Geographical Institute at the University of Fribourg. Investigations by the glaciological team revealed that the location chosen for this study is characterised by comparatively low winter accumulation and consequently relatively high overall mass loss. Winter accumulation for the site was measured to be 3.18 m snow in early April, corresponding to 1.37 m weq assuming a mean density of 0.4 g/cm^3 (data kindly provided by M. Huss, University of Fribourg). This is roughly 0.3 m weq more than found by the reconstructions of the snowpack in this study. These were based on the assumption of north-dominated weather conditions and designed to match the snow depth measured on 1 June. The two measurements were taken at a horizontal distance of roughly 500 m, which is sufficient to explain the observed difference due to heterogeneous snow accumulation on the glacier surface. With the precipitation record from Lenk and the derived extrapolation factor of 1.8, a slightly higher annual precipitation rate was yielded (2200 mm) than the climatic mean of 2000 mm suggested by both records from the period 1971-1990 (after Atlas der Schweiz, 2.0) and data from Spreafico and Weingartner (2005). These inconsistencies might be rooted in different sources of uncertainties. Firstly, snow drifts might cause inhomogeneous accumulation patterns across the glacier surface and alter the total accumulation rate. However, from an orographic point of view, the plateau does not seem to be destined to accumulate large scale snow drifts. Therefore wind induced additional snow input is not a reasonable explanation. Secondly, the precipitation rate during the accumulation season 2009/2010 might have been slightly above-average. Unfortunately no longer time series of mass-balance measurements for Plaine Morte glacier exist. However, precipitation records from Lenk indicate that precipitation rates of that particular year were in the range of the mean value of the past decade. Thirdly, some meltwater drainage might have reduced the total water column height between April and June 2010, but the intact snow profile did not support this presumption. Fourthly, artificial snow production or other activities of the tourist industry might influence the snowpack locally. Finally and most likely, the hypothesis of north-dominated weather conditions might not meet the complexity of Alpine climatology, allowing seasonally variable influences from either side of the ridge. Thus the attempt to date the different snowpit horizons and to attribute them to individual snowfall or melt events proved to be complex with the available data. Therefore resulting localisations of dust events are rough approximations and have to be interpreted carefully.

Stable isotope ratio

The isotopic ratio observed in the snowpack at Plaine Morte clearly showed seasonal fluctuations and the pattern was preserved well enough to find the overlap of the profiles from the two snowpits. However, the mean $\delta^{18}O$ value of -17.3‰ within the snowpack substantially deviated from the theoretical $\delta^{18}O$/altitude relationship proposed by Schotterer et al. (1997). From measurements at different high Alpine sites this study derived a height gradient of 0.2‰ per 100 m (Schotterer et al., 1997), which results in a theoretical annual mean of -14.6‰ for Plaine Morte. This rather large offset can be explained by the fact that the Plaine Morte snowpack

only preserves the autumn/winter/spring signal. An ice core record from Plaine Morte glacier revealed that the seasonal signal is not preserved on longer time scales. The corresponding study found an extraordinarily high $\delta^{18}O$ mean of -13.3‰ and no regular fluctuations, indicating post-depositional effects (Schotterer et al., 2004). The seasonal pattern observed in the snowpack, however, was also reflected in the presence of biogenic matter, EC and NH_4^+ concentrations within the snowpack. High concentrations were limited to the uppermost 0.35 m weq of the snow profile, where the isotopic ratio was >-15‰. This threshold was suggested to represent the transition to summer precipitation on roughly 4000 m high Fiescherhorn (Schwikowski et al., 1999). On Plaine Morte glacier this same threshold seemed to mirror the transition to spring temperatures with enhanced vertical mixing and resulting influence from more polluted air masses.

Ionic composition

On Plaine Morte glacier, features of an intact ionic pattern (as described in section 2.4) could be observed in the snowpack sampled on 1 June, except for distinct Ca^{2+} dust peaks and the seasonality of NO_3^- and SO_4^{2-}, but due to its relatively low elevation, ions were subject to strong leaching processes after the onset of the ablation season. This was clearly illustrated by the severely perturbed ionic signals in snowpit 2 and increased concentrations of NH_4^+, NO_3^-, SO_4^{2-} and Ca^{2+} in meltwater. Therefore, in the present study only the intact ionic patterns of snowpit 1 were further investigated to identify single dust input events. The ion concentrations of the snow samples compared quite well with the elemental concentrations of Ca and Mg, analysed with ICP-MS. Interestingly, no systematic difference was found, although acidification prior to ICP-MS analysis was expected to dissolve some of the particles contained in the samples and therefore cause increased values compared to the ion concentrations. The mean ionic concentrations were compared with background values (winter means) from Colle Gnifetti (data kindly provided by M. Schwikowski, PSI), which with its altitude of 4450 m a.s.l. represents clean air conditions (Wagenbach et al., 1988). Due to its lower altitude and therefore increased PBL influence, the snowpack at Plaine Morte showed a tendency towards higher means (except for NH_4^+ and Mg^{2+}), but the deviation was inconsistent, varying from a factor of 0.8 for Mg^{2+} to 4.3 for Cl^-. These observations, along with the low fluctuation range, might again be caused by the fact that on Plaine Morte no summer snow was analysed. Since Na^+ and Cl^- could be attributed to sea spray as dominant source and sea salt is near-transparent (Warren and Wiscombe, 1980), these two species are irrelevant to impurity source identification and albedo changes. Therefore they were excluded from further interpretations. The ice lens found at a depth of 0.82 m weq was nicely reflected in peaking isotope ratio and increased ionic concentrations. Additionally the overlying snow layers showed enhanced biological activity, illustrating that algal growth is triggered by higher temperatures and subsequent meltwater formation (Uetake et al., 2010).

6.1.2. Identification of dust events

Figure 18 illustrates the snowpack on Plaine Morte glacier (1 June) showing visible stratification with several dark coloured layers. These layers were presumed to represent periods of increased dust input, either from a local dust source (not probable, since most of the surrounding peaks were still snow covered) or from long-range transport. In addition to Saharan dust, for this particular year, ash deposits from the volcanic eruptions of the Icelandic volcano Eyjafjalla were expected. The purpose of analysing the snowpit samples for their dust content was to qualitatively investigate the relative contribution of different dust sources to the total dust accumulation on the surface of Plaine Morte glacier.

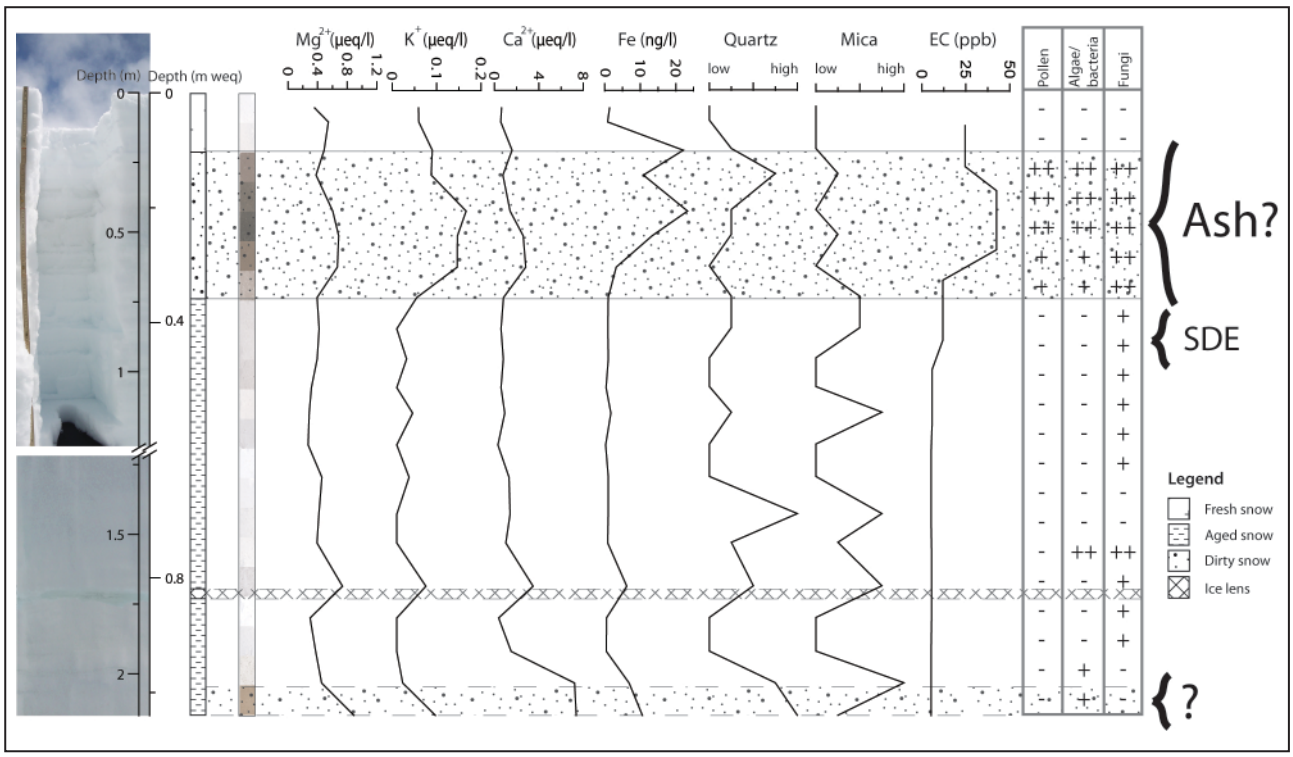

Figure 18: Snowpit stratigraphy with different dust markers, impurities and dust horizons. Snowpit 1 is shown with a photograph and a schematic drawing of the different snow layers. Pictures of the dust loaded filters illustrate the dust horizons. Concentration profiles of mineral dust marker ions (Mg^{2+}, K^{+} and Ca^{2+} in µeq/l) and the trace element Fe (in ng/l) as well as presence of mica and quartz (high/low) are shown. Additionally EC concentrations and the occurrence of different species of organic matter are depicted, where (++), (+) and (-) denote high, medium and low occurrence, respectively. The deposition horizon of Eyjafjalla ash and the location of the strongest observed SDE within the study period are marked. The enrichment of dust markers in the bottom layer of the snowpack at 1 June remained unclear (?).

SDE

The generally rather low fluctuations of the dust marker ions indicate no interferences from strong SDE or other remarkable dust inputs (c.f. section 2.4). Indeed, no major SDE was observed in the accumulation season 2009/2010, except for a moderately particle rich event on 7 and 8 April, recorded on Jungfraujoch (data kindly provided by M. Collaud-Coen, Meteo Schweiz). Correspondingly, the snowpack did not show pronounced Saharan dust layers. These findings suggest only a minor contribution of Saharan dust to the total cryoconite accumulation during that particular year. From this perspective the effect of SDE on the albedo of Plaine Morte glacier seemed to be limited, especially since neither quartz, mica or Ca^{2+}, nor light-absorbing iron oxides (Fe record) were enriched in the corresponding layer (0.35-0.4 m weq).

Volcanic ash

In the vicinity of Jungfraujoch, EMPA (2010), Bukowiecki et al. (2011) and Tobler et al. (2011) reported chemically distinct ash signals in aerosols and snow cover after the overpass of the Eyjafjalla ash plume. Most peculiar was the enrichment of REE, SO_4^{2-} and titanium (Ti), indicating Icelandic volcanic origin. A very similar signal was found in the darkened horizon (0.1-0.35 m weq) in the snowpack at Plaine Morte. However the enrichment factors were generally lower than reported by Bukowiecki et al. (2011) and the Ti enrichment could not be verified, since it had not been determined. This was most pronounced for SO_4^{2-}, which did not show a distinct peak in the ash horizon resulting in minor deviation from the baseline concentrations. Although SO_4^{2-} was previously found to be extremely prone to elution (Eichler et al., 2001), leaching of larger amounts

of SO_4^{2-} is not probable, since no distinct melt features were observed in the snowpack of 1 June. Consequently, the signal was most probably attenuated by atmospheric processes. Indeed, model simulations by EMPA (2010) revealed that Plaine Morte glacier was only situated at the perimeter of a low density tail of the ash cloud. Additionally, the same study reported spatially restricted down-mixing of ash particles into the PBL. Therefore ash inputs on Plaine Morte might have been limited, although the filtered snow samples showed substantial particulate load (c.f. Figure 18). The nature and origin of the second observed REE enrichment horizon at the bottom of the snowpack remained unclear.

Biogenic and elemental carbon deposits

The stronger input from polluted air masses, due to the onset of convective systems and resulting vertical mixing of air masses coincided with the Eyjafjalla ash plume intrusions into the atmosphere over Switzerland (April/May). Therefore, the ash horizon not only showed increased ion concentrations and the typical REE footprint, but also large amounts of organic matter and enhanced EC concentrations (c.f. Figure 18). Thus the signal of the Eyjafjalla ash deposits might be superimposed by this seasonal signal. Additionally, the clean fresh surface of the snowpack on 1 June indicates that accumulation of biogenic matter and EC predominantly occurred by dry deposition at the end of May and illustrates the possibility for clean conditions during the summer months.

6.1.3. Budget of impurities in snow

The comparison of the snowpack at different stages of the ablation process might potentially reveal the mechanisms behind particle enrichment at the glacier surface. Therefore the concentrations of all measured parameters were balanced with the concentrations found on ice samples at the end of the ablation season.

Ion budget

The vast alterations of the ionic composition between the two snowpit sampling dates were compared to elution sequences in ice cores affected by meltwater percolation. However, no similarities between these sequences and the observed elution patterns could be found. Both Eichler et al. (2001) and Ginot et al. (2010) investigated ice core sections at several meters depth. Therefore they were investigating a near-closed system (apart from percolating meltwater). The snowpack at Plaine Morte in contrast, might additionally have been exposed to several post-depositional processes not related to percolation of water. On the one hand, exchange with the atmosphere continues during the ablation season via dry deposition and re-release of certain ionic species to the atmosphere. On the other hand dust deposits on the ice surface potentially release additional ions to the water table forming at the bottom of the snowpack during the summer months. Metabolism by organisms of the cryosphere might further alter the ionic signals by nutrient sequestration from the atmosphere (Anesio et al., 2009) or alternatively from dust deposits (Thomas and Duval, 1995), but these processes have been scarcely documented so far (Priscu et al., 2005). The elution sequence of Li et al. (2006) was most likely to fit observations at Plaine Morte, since this author focussed on elution within the upper part of the snowpack. However, discrepancies were found especially for the elution susceptibility of NH_4^+ and NO_3^-. Although reported to be comparatively persistent elsewhere (Eichler et al., 2001; Li et al., 2006; Ginot et al., 2010), large loss of these ionic species was observed from 1 June to 6 July. This effect might be of great interest regarding microbial activities including nitrogen sequestration from the atmosphere or from nutrients within the snowpack (Anesio et al., 2009; Uetake et al., 2010). Ionic concentrations might thus provide important information on biological activity on the glacier surface. However, these interrelations need

further investigations, which are beyond the scope of this study. Additionally, the formation of a water table induced drainage of meltwater from the glacier surface, removing large portions of the total ion load. K^+ was the only species with increasing cumulative flux from snowpit 1 to snowpit 2; all other ionic species experienced more drainage than additional deposition or dissolution. The strongly increased concentrations found for K^+, Mg^{2+} and Ca^{2+} in the water logged layer lead to a pronounced cation-excess. This was explained by dissolution of multi-annual dust layers on the ice surface beneath the snowpack. Similar effects had been reported within cryoconite holes by Bagshaw et al. (2007). Considering the variety of secondary processes influencing solute ionic snowpack concentrations, balancing of ionic species was not informative regarding the accumulation of dust.

Minerals and trace elements

Unfortunately, trace elements and minerals were not suitable for budgeting dust inputs either. In the case of trace element analysis, this was due to the high instrument sensitivity combined with the extraordinarily high concentrations in ice samples. Conversely, for mineralogy analysis, particulate concentrations in the snow samples were too low. Snow samples were filtered through cellulose ester filters to avoid signal disturbances by the filter material. Nevertheless, the obtained results showed relatively high background signals from the filter itself and from the aluminium platelet of the sample holder. These disturbances resulted in systematic shifts of the peak-patterns, which complicated the identification of minerals. In addition, the low particle concentrations produced low intensity signals, which in many cases could not clearly be distinguished from the background signal. Formenti et al. (2010) found that XRD analyses on aerosol filters were limited to particle loads greater than 800 µg. Particle load had not been determined in the present study, but from visual judgement, all snowpit samples might have been well below this threshold. Thus, XRD analysis on snow samples was subject to large uncertainties and therefore restricted to qualitative statements about the presence of mica and quartz. Since both minerals might be present in most potential dust sources, these findings did not help to identify the source region of the dust horizons or allow quantification of the particles. Thus the budget of mineral dust inputs could not be derived from the measurements in this study. However, an average SDE deposition rate of 40-100 µg/cm^2 was found over Europe (Collaud-Coen et al., 2004). This yields a mean annual contribution of roughly 2% to the total dust mass per unit area. Implications of this budget for the albedo-relevance of Saharan dust are discussed in section 6.3.

Biogenic matter and microorganisms

No cell counting of microorganisms was performed, except for *Chlamydomonas nivalis*. Although the snowpack on 6 July was waterlogged and cryoconite was found to contain pigmented cells of *Chlamydomonas nivalis*, no flagellated stages or pigmented spores were observed in the meltwater or at the snowpack surface. Takeuchi (2009) reported occurrence of algal blooms just prior to the exposure of the bare ice surface. Therefore it can be assumed that the blooming stage of the life cycle described in section 4.5.2 had not yet been triggered on 6 July. For further investigations on algal and bacterial communities and their interrelation with cryoconite forming matter, the limi-ting factor for biological activity would be of great interest. Therefore cell counting would be needed, in combination with more detailed information on growth promoting factors such as the presence of meltwater, temperature and nutrient availability (Liu et al., 2007). In the surface layers of the snowpack, the amount of dark aggregated biogenic matter increased strongly from 1 June to 6 July, however no

granules in general and especially no granules with filamentous cyanobacteria were formed within this period. These observations are consistent with findings from Uetake et al. (2010), who classified cyanobacteria to be ice-specialists. Additionally, these findings indicate that the granule formation process might be a matter of longer time-scales than a single ablation season.

Elemental carbon budget

Within the snowpack, EC was strongly enriched at the surface. Overall, the layer attributed to spring snow ($\delta^{18}O$ <-15‰) contained roughly 75% of the total EC load found in the snowpack at 1 June. Thus, freshly deposited surface snow contained a substantial amount of EC, which implies wet deposition and scavenging. The latter deposition mechanism has been reported to be most efficient in removing BC from the atmosphere (Hadley et al., 2010; Aamaas et al., 2011). Largest concentrations, however, were observed in the ash horizon. This indicates that EC deposition primarily occurred after the PBL had expanded to higher altitudes. The bottom layers in contrast were characterised by EC concentrations below the detection limit, which results in values relatively close to the background level (ca. 4 ppb) detected at Col du Dôme (Legrand et al., 2007). The maximum contribution of local emissions is expected to be equal to the difference between the background concentration and detection limit. Overall this suggests predominant input by polluted air masses from the valleys and only minor local EC emissions. This was supported by the 88% increase of total EC load from 1 June to 6 July, evidently originating from more remote sources after the end of the snow sports season. Hinz et al. (2005) reported carbonaceous particles to be highly correlated with NO_3^- and SO_4^{2-} during anthropogenic source events. Unfortunately, proper source analysis by correlation with anthropogenic secondary aerosol species could not be performed due to differing and generally low sampling resolutions. Although the local EC input seemed to be limited on a glacier wide scale, stronger pollution in the vicinity of the tourist facilities cannot be excluded with the available data. Balancing the snow column EC load with the total amount of EC found on the glacier surface per unit area yields an enrichment factor of 15 to up to 200. This strong accumulation indicates increased deposition in summer (Lavanchy et al., 1999) and low drainage efficiency by meltwater, as previously reported by Doherty et al. (2010). However, leaching cannot definitely be excluded, since Conway et al. (1996) observed massive removal of hydrophilic BC (and to a lesser extent also of hydrophobic BC) from the snow surface within a few days after deposition. Assuming minimal EC loss, the observed enrichment indicates a residence time of decades to centuries on the surface of Plaine Morte glacier. This residence time estimate is strongly depending on the assumed period of negative mass balance for Plaine Morte. With the data available, this period cannot be determined more precisely. The remote sensing results from Paul et al. (2005) suggest a lift of ELA between 1985 and 1998. However, due to the poor temporal resolution and the potential bias caused by episodical snowfall events, these data do not help to clarify the issue.

6.2. Cryoconite composition

The biogeochemical composition of cryoconite found on ice samples is visualised in Figure 19. In general, differences in relative composition between ice samples were rather small. Largest deviations were found in total cryoconite load.

Mineral dust

Regardless of the contribution of local dust to the total cryoconite mass, the relative impact of local dust on the albedo of the glacier was expected to be comparatively low, since cryoconite appeared to be considerably darker than the surrounding

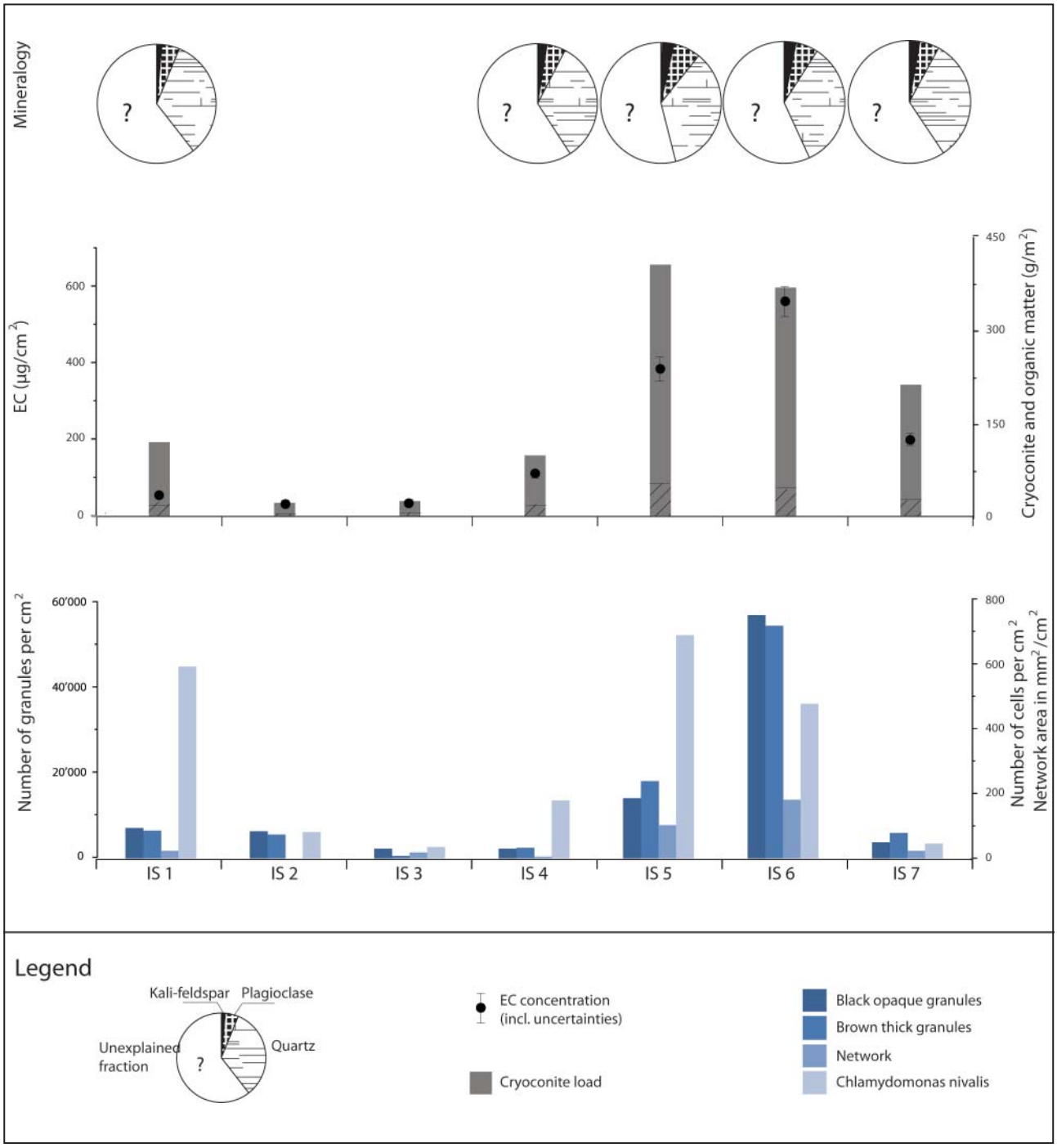

Figure 19: Biogeochemical composition of cryoconite from ice samples: the upper panel shows pie charts of the bulk mineralogy of all ice samples except for ice samples 2 and 3 (IS2, IS3), where the sample amount was insufficient for the quantitative XRD analysis. The middle panel shows the total cryoconite load with its organic fraction (in g/m² of ice, grey columns with shaded section) and EC concentrations (in µg/cm² of ice) for each ice sample (black dots). The whiskers depict the instrument error of the OC/EC analyser. Where invisible, the error was smaller than the symbol. The lower panel shows the concentrations of black opaque and thick brown granules and Chlamydomonas nivalis (in number of granules/cells per cm² of ice). The network area is given in mm² network area per cm² of ice.

bedrock. This implies an additional darkening agent within cryoconite matter. XRD and ICP-MS analyses revealed very similar mineralogy of cryoconite for all ice samples (c.f. Figure 19, upper panel) and in comparison to LLR (except for calcite content). Thus if other sources contribute to the mineralogy of cryoconite on Plaine Morte glacier, their relative contribution must either be negligibly small (volcanic ash), or they must show a bulk composition, which is not clearly distinguishable from local bedrock (Saharan dust). Predominance of local dust input seems to be reasonable, since at Plaine Morte the surrounding slopes mainly consist of physically weathered phyllite, which is free of snow cover during most of the summer season. Actually, SDE and ash from Eyjafjalla eruptions in that particular year only contributed minimally to the total dust accumulation. On Plaine Morte glacier, outcropping dust layers from the melting glacier ice might be a large contributing source for total annual dust accumulation, since seasonal dust layers were observed in the ice (c.f. title image, p. III) and annual mass-balance was estimated to be -1 m weq in 2010. The mean annual SDE input stated by Collaud-Coen et al. (2004) might add substantially to the annual local dust deposition in some years, however, it is most probably outweighed by the accumulation of outcropping dust layers.

Elemental carbon

Balancing of the snowpit concentrations revealed that EC is strongly enriched in cryoconite compared to the annual deposition rates and compared to the mean OC to EC ratio in Swiss soils (Cornelissen et al., 2005). Despite the remarkable enrichment factors the relative EC content within cryoconite was found to be rather small, ranging from 0.4 to 1.6%. However, this contribution can be expected to increase in future, due to its hydrophobic behaviour leading to aggregation and limited elution in the humid glacial environment (Doherty et al., 2010; Langford et al., 2010). In addition, multiannual accumulation of EC is favoured by its resistance against microbial decomposition (Laird et al., 2008) and against chemical weathering (Rose, 2001). EC correlated very well with the total cryoconite mass (c.f. Figure 19, middle panel). Therefore it is probable that EC along with other airborne dust is relatively evenly distributed over the glacier surface caused by internal mixing of aerosols (Hand et al., 2010). However, no significant correlation with the number of black opaque granules could be detected, which indicates that the formation of cryoconite granules is independent of EC concentrations. As suggested by Langford et al. (2010), biological activity might be more important for the aggregation of PM (EPS, cyanobacteria) than EC, since EC is included into the granules by the same processes as mineral dust. The dark colouration of the black opaque granules therefore seems to be co-determined by EC and partly decomposed organic matter (Takeuchi, 2002b; Anesio et al., 2009; Langford et al., 2010).

Organic matter

The organic fraction (c.f. Figure 19, middle panel) was found to be in the range of findings on Himalayan glaciers (Kohshima et al., 1993), but tended to be higher than in arctic cryoconite (Langford et al., 2010). The discrepancy between the organic content of LLR and cryoconite is explained by enhanced biological activity within cryoconite (Anesio et al., 2009), which in many high Alpine or polar glacial environments constitutes an isolated refugia of life (Bagshaw et al., 2007). Thereby, meltwater availability and absorption induced warming of meltwater ponds and cryoconite matter were reported to be the most important promoting factor for increased microbial activity on the glacier surface (Wharton et al., 1985). Therefore the comparatively high organic content of cryoconite reflects microbial activity, which was illustrated by the extraordinarily high number of algal and bacterial cells observed.

Cryoconite granules

Cryoconite granules showed two morphotypes: on the one hand, black clots, which were coated with or consisted of a very dark, opaque matter, on the other hand, looser aggregates with near transparent, mostly brownish glue-like matter (most probably EPS) holding the particles and microorganisms together. The mean diameter of all granules (104 µm) was low compared to the findings of Takeuchi et al. (2001) and Kohshima et al. (1993), who found diameters of 500-2000 µm and 200-3000 µm, respectively, or Langford et al. (2010), who reported mean aggregate sizes of 400-600 µm. Interestingly, ice sample 2 with its several cm deep but extremely narrow (<1 cm) cryoconite holes showed comparatively high numbers of granules, although its total cryoconite mass was low (c.f. Figure 19, lower panel). Additionally no loose networks were found, suggesting networks and aggregates to be in the initial stage of granule formation, since cryoconite hole formation is considered to require some time and granules can be assumed to be fully developed within the hole (Langford et al., 2010). Quantification of the granules revealed that in general, the amount and size of the granules were not significantly correlated with the total cryoconite load on Plaine Morte. Additionally, discrepancies of the visual structure of the debris (uniformly or aggregated matter) were not reflected in the granule amount, implying that the microbial community as an entity is not determining the structure of cryoconite, but rather its biological diversity. This was supported by the fact that the number as well as the area of granules did not correlate with the organic fraction of cryoconite. Therefore it is questionable, whether granule counting adds information on the living microbial community.

With the analytical methods used in this study, around 50 to 60% of the cryoconite matter could be identified. The remaining unexplained fraction is most probably dominated by clay minerals, since clay minerals are preferentially displaced by wind erosion and can thus be expected to enrich on the glacier surface and form a major constituent of cryoconite. This could substantially increase the relative contribution of the mineral dust fraction to the total cryoconite dry weight. However, contribution of other unidentified substances cannot be excluded. Due to the heterogeneity of cryoconite distribution on the glacier surface, representativeness of the samples is a major issue. On time scales of a single ablation season, changes in total dust accumulation seem to be comparatively small with respect to redistribution processes influencing the surface structure upon the glacier. Anyhow a reciprocal effect seems to link the distribution of cryoconite and the formation of cryoconite holes with the drainage system of Plaine Morte glacier. As observed elsewhere (Wharton et al., 1985), streams occurred frequently in conjunction with cryoconite holes and large aggregates of cryoconite matter. Radiation absorption of cryoconite matter and subsequent melt and depression formation can potentially influence the drainage system of the glacier by channelling meltwater. This implies additional cryoconite supply to the depression, causing additional absorption and melt and consequentially a deepening of the drainage system. Although no quantitative analysis of mineral dust input to the snowpack could be performed, visual observations indicated multi-annual cryoconite accumulation, as reported above for EC. This assumption was expressed before by Langford et al. (2010), stressing the particle retention potential of microorganisms and Hodson et al. (2010), stating gently sloping glaciers to be most affected by this process.

6.3. Effect on albedo

6.3.1. Modelled and measured albedo of snow surface

The comparison of measured broadband albedo and modelling outputs after Gardner and Sharp (2010) revealed some remarkable results. Figure 20 displays the relative contribution of EC, grain growth and the unexplained fraction to the albedo reduction, with respect to the albedo of clean snow/ice. Although EC surface concentrations and the absolute effect of EC increased from 1 June to 6 July, the explanatory power of EC induced albedo reduction decreased from 19 to 16% within this period. This indicates that the relative contribution of other impurities gained importance, which is remarkable, since BC is known to increase its effect on albedo during snow metamorphosis, peaking in maximum absorption on coarse grained old snow (Warren and Wiscombe, 1980). Microscopic images showed low concentration and high transparency of mineral dust and algal cells on 1 June. Therefore a relative contribution of 1% or less seems to be plausible. On 6 July increased amounts of slightly coloured cell-aggregates, pollen and other decomposing fragments of biogenic origin were observed, combined with relatively large numbers of mineral particles. This might account for the relatively large fraction of unexplained albedo reduction on 6 July. Most of this can probably be attributed to organic matter,

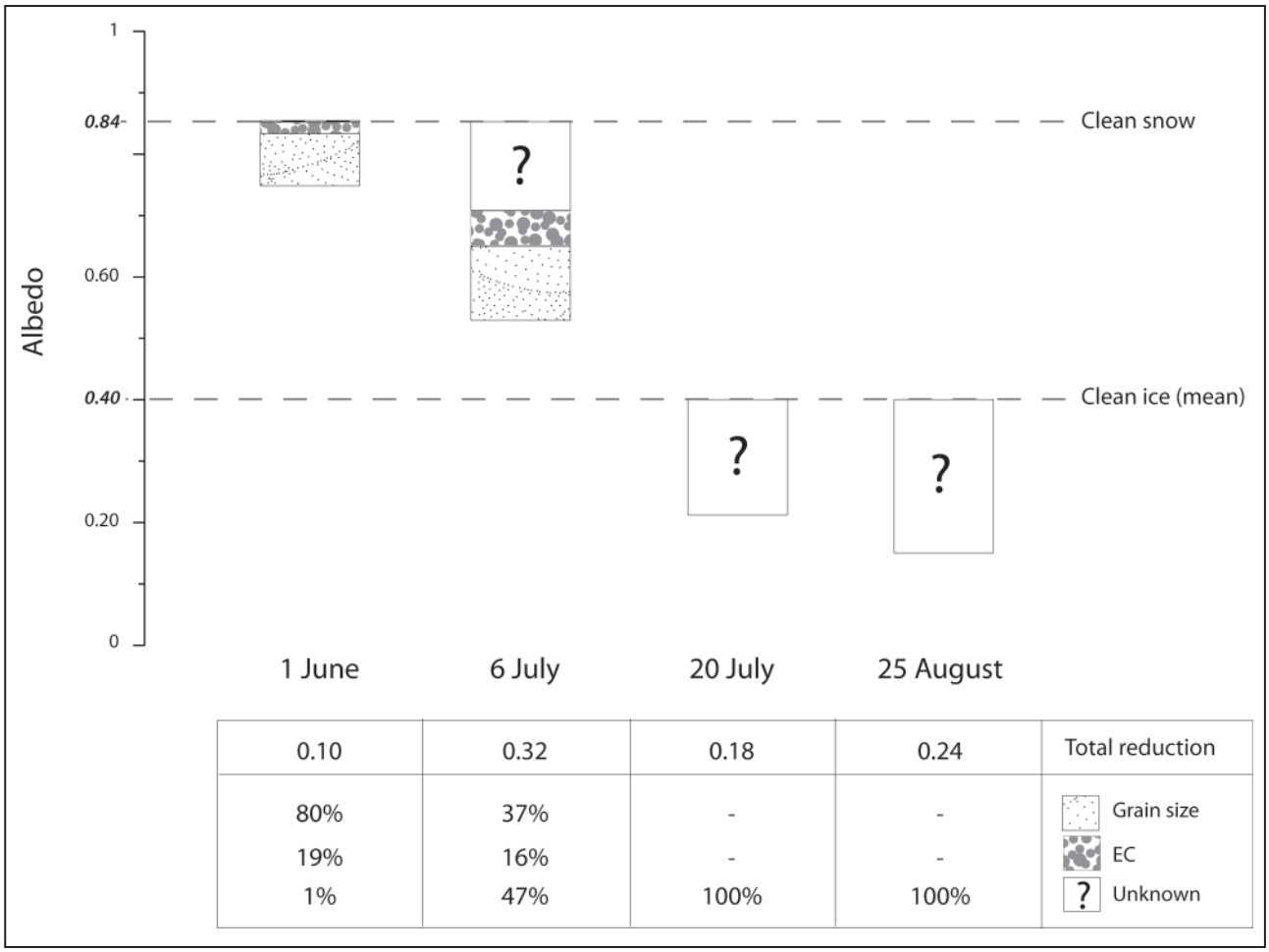

0.10	0.32	0.18	0.24	Total reduction
80%	37%	-	-	Grain size
19%	16%	-	-	EC
1%	47%	100%	100%	Unknown

Figure 20: Measured broadband albedo in comparison to reference values (0.84 for fresh snow with re = 50 µm, as modeled after Gardner and Sharp (2010) and a mean value of 0.40 for clean ice as reported by Paterson (1994)). The total albedo reduction compared to the reference value is displayed with its relative contribution of grain size changes, EC and the unknown fraction (see legend). Below the figure, the absolute reduction and its relative contributions (in %) are listed in a table.

since mineral dust absorption was reported to be at least factor 50 less effective than BC per unit mass, while brown OC can account for up to 40% of the total absorption (Doherty et al., 2010). This assumption was supported by Takeuchi (2009) who suggested organic matter to be more efficient absorber than mineral dust, and Gardner and Sharp (2010) who reported the efficiency of dust to be as low as factor 200 less than light-absorbing carbon.

During snow melt, the liquid water content can be significantly increased, affecting the albedo of the snowpack. The effect of liquid water content on the spectral reflectance of snow was investigated by Green et al. (2002), showing a shift in local ice absorption minima but no remarkable decrease in total reflection. Therefore the effect of liquid water content in snow was assumed to be insignificant, which is justified by the fact that the upper layers of the snowpack were far from being water saturated on both measurement days.

Marshall and Oglesby (1994) report the relative importance of snow grain size to be larger in the early melting season, when grain radius increase is fastest, while the effect of solar zenith angle increases towards the end of summer. Indeed the influence of the zenith angle was found to be negligible in early June and July. The snow metamorphosis induced albedo reduction however, was also rather low (-0.04) compared to a typical drop of 0.1-0.2 within the first couple of days after snowfall, as described by Oerlemans (2010) and Doherty et al. (2010). Considering the fact that grain growth is fasted in the early stage of metamorphosis and albedo was measured on a two days old snowpack, this process might already have been underway at the time of measurement. This is supported by Warren and Wiscombe (1980) who stated the grain size of freshly fallen snow to be around 50 µm, while grain radius was found to be 280 µm on 1 June 2010. Due to the relatively high absolute detection limit of the thermo-optical EC analysis method (1 µg) and the small sample amounts of 10-40 g of snow, determination of the EC content in the surface snow layer required three to five samples representing the uppermost 30 to 50 cm of the snowpit (roughly 0.2 m weq). Warren and Wiscombe (1980) reported the particle accumulation to be concentrated in the topmost 1 cm layer, which means that highly concentrated surface snow was diluted by cleaner subsurface snow. Thus albedo-relevant EC concentrations might have been much higher than actually measured. If the total EC abundance is assumed to be concentrated in the topmost 1 cm, the resulting concentration exceeds the reliability range defined for the albedo model of Gardner and Sharp (2010). The same abundance within the uppermost 10 cm yields a concentration of 380 ppb and an albedo reduction of 0.15, which accounts for 75% of the observed discrepancy between theoretical clean snow albedo and measurements for 6 July. Additional uncertainties arise from the discrepancy between EC and BC. Since considerations on albedo naturally demand for an optical definition of soot, BC seems to be more appropriate for this purpose. This potentially leads to an overestimation of soot induced albedo reduction, when using EC instead of BC concentrations. Thus these technical constraints show counteracting uncertainties, severely restricting the model output. Additionally, the albedo model developed by Gardner and Sharp (2010) is based on the concept of the specific surface area of snow grains and therefore restricted to predicting snow albedo. In general, little effort has so far been made to model broadband albedo of glacier ice surfaces under the influence of impurities (Xu et al., 2009). As ice albedo shows large variance depending on gas content (bubble formation) and crystal structure, the effects of dust and other impurities are difficult to isolate. Moreover the albedo model of Gardner and Sharp (2010) does not account for mineral dust absorption and is designed for BC concentrations below 2 ppm. Thus the effect of mineral dust and the theoretical

albedo for 20 July and 25 August could not be simulated. Models including mineral dust absorption require its mass concentration (Aoki et al., 2011; Yasunari et al., 2011), which was not determined in the course of the present study.

6.3.2. (Spectral) reflectance of ice surface

The integral of spectral reflectance compared quite well with the measured broadband albedo (0.14 and 0.16, respectively). The small difference can be explained by the discrepancy between measured wavelength ranges (305-2800 nm for broadband albedo and 350-2500 nm for spectral reflectance), although the radiation fraction measured around the lower and upper limit of the bandwidth should only account for a few per cent.

Liquid water content

On Plaine Morte, the integrated spectral albedo of an obviously clean ice surface was measured to be 0.24. This value deviates by at least 0.1 (and up to 0.27) from typical values for clean glacier ice (Paterson, 1994). This deviation might be explained by the high liquid water content of the surface layer. Water is characterised by strong and constant absorption in the VIS wavelengths (Zeng et al., 1983) and thus shows similar absorption behaviour as soot in this spectrum. Meltwater can fill pores of surface ice, which reduces scattering and therefore decreases the surface albedo (Grenfell and Perovich, 1984). Therefore the albedo can be strongly affected by surface covering water films during melt events or the formation of streams and water ponds on the glacier surface. Satellite derived observations showed extraordinarily low albedo values for Plaine Morte glacier during the exceptionally hot summer 2003. This was presumed to be partly due to high liquid water content on the glacier surface. During the field campaign on 25 August of the present study, significant amounts of meltwater caused large scale surface runoff on the gently sloping glacier. The affected areas (especially in the vicinity of moulins) were characterised by extraordinary dark surfaces, confirming the presumption of Paul et al. (2005). Figure 21 depicts a bright and clean ice surface targeted with the sensor of the spectrometer on 25 August. In the left panel (a) mirror effects suggest presence of a water film. The picture to the right (b) illustrates colour changes due to pore-filling liquid water (porous brighter ice in the bottom and water saturated darker ice in the upper part). Additional absorption by meltwater becomes obvious when comparing the clean ice NIR spectrum with spectra

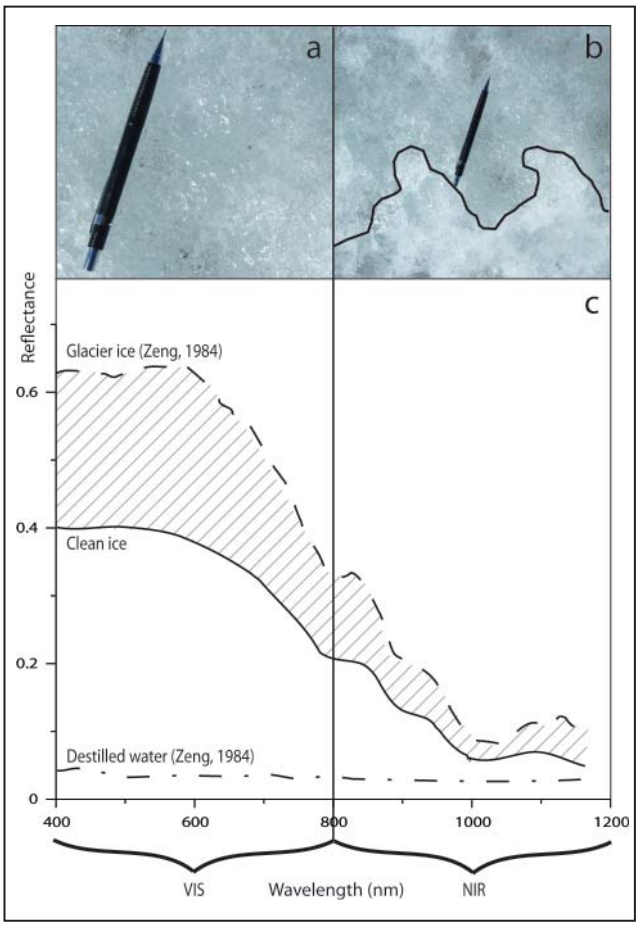

Figure 21: Pictures of clean ice, showing mirroring effects (a) and clean ice with varying liquid water content (b). The lower part of (b) shows clean white surface ice with little liquid water, while in the upper part of the picture, the ice is covered by a water film. (c) shows the measured reflectance spectrum of the clean ice target displayed in (a), which is compared to the glacier ice spectrum after Zeng (1984). The shaded area marks the reduction in reflectance in VIS and NIR. Additionally the reflectance spectrum of distilled water is displayed (Zeng 1984), illustrating the strong absorption behaviour of water.

of Zeng (1983) and Takeuchi (2009). The local maximum around 1100 nm, corresponding to the ice absorption minimum (Warren and Wiscombe, 1980), is attenuated by the presence of liquid water, which in contrast to BC (Leroux et al., 1998) also strongly reduces reflectance in NIR (c.f. Figure 21c). Since the VIS wavelengths react much more sensitively to impurities on snow and ice, while in NIR absorbance of ice is dominant (Warren and Wiscombe, 1980), this feature can exclusively be attributed to the presence of liquid water. Thus the low broadband albedo measured on the bare glacier ice on 20 July and 25 August (c.f. Figure 19), although within the range of dirty ice proposed by Patterson (1994), is partly attributable to the high liquid water content of the melting ice surface.

Mineral dust

Mineral dust was observed to be by far the most important mass contributor to the total cryoconite load. But as mentioned above, its effect on the albedo seems to be of limited importance, since cryoconite was observed to be much darker than the surrounding loose rock slopes. In snow, greyish dust was reported to show similar absorption behaviour to that of BC (Warren and Wiscombe, 1980), however with a substantially lower efficiency (factors 50-200, c.f. section 6.3.1). Considering the mass contribution to cryoconite and assuming applicability to ice surfaces, mineral dust could potentially show half to double the effect BC has on the albedo of Plaine Morte glacier. In general mineral dust, largely consisting of clay minerals, is near-transparent with the exception of strongly absorbing inclusions like iron oxides. Iron rich mineral dust (e.g. Saharan dust) is known to show a particular absorption pattern with strongest effect in the lower range (<600 nm) of the VIS spectrum leading to a yellowish to reddish colouration (Warren and Wiscombe, 1980; Collaud-Coen et al., 2004). Some of the spectra of cryoconite loaded ice showed features of iron oxide-absorption, which indicates Saharan dust deposits, although no notable SDE had been observed within the study period. It might be possible that the observed absorption features were co-determined by other impurities like brown OC showing a similar absorption pattern (see below). As mentioned above, the mean annual Saharan dust deposition in Europe might contribute roughly 2% to the total dust load observed on Plaine Morte. From a multi-annual perspective, Saharan dust might thus be a comparatively important component of cryoconite on Alpine glaciers. This is somewhat in contrast to the results of XRD analysis, which postulated predominantly local dust deposits. These inconsistencies most probably stem from the fact that Saharan dust mineralogy is not clearly distinguishable from dust deposits of local origin with the methods applied in this study. Additionally, the SDE mass input in the Alps is subject to substantial inter-annual variations. Therefore the relative contribution of Saharan dust to the total cryoconite induced albedo reduction cannot be assessed. However, the impact of Saharan dust is evident when strong SDE, regularly causing visible colouration of Alpine snow covers, temporarily reduces the albedo.

Elemental carbon

The extraordinarily high EC concentrations measured within cryoconite prefigure a substantial albedo reduction, due to the absorption efficiency of soot (c.f. section 2.5). Unfortunately quantification of this effect was not possible due to a lack in models for glacier ice albedo and the limited comparability of EC and BC (Andreae and Gelencsér, 2006; Kaspari et al., 2009; Doherty et al., 2010). Hand et al. (2010) reported internal mixing of mineral dust and BC during long-range transport. Microscopic investigations of Plaine Morte cryoconite revealed the presence of large amounts of greyish near transparent particles, which might be clay minerals with BC coating. Internal mixing was

reported to decrease the absorption efficiency of BC (Warren and Wiscombe, 1980), which might also happen in larger scales by the aggregation of cryoconite granules. However, the overall effect of BC appears to be strongly amplified by a long residence time of decades to centuries.

Biogenic matter and microorganisms

The direct effect of microorganisms is caused by pigments inducing colouration of the cells, which is almost exclusively limited to the species *Chlamydomonas nivalis* since most other algal cells were near-transparent. The features described in section 1.1 were not observed in spectra from Plaine Morte, since cell number concentrations of *Chlamydomonas nivalis* were a factor 1000 lower than observed in red stained snow (Thomas and Duval, 1995; Painter et al., 2001). Thus the direct effect of biota is negligible. However, the indirect effect seems to be extremely important. Dead algal cells are being decomposed by microbial activity and are thereby commuted to dark humic substances. This brown OC was reported to strongly absorb towards UV wavelengths (Andreae and Gelencsér, 2006) and can, as mentioned above, account for up to 40% of total absorption (Doherty et al., 2010). Thus the increase in reflectance with increasing wavelengths of the VIS spectrum observed on Plaine Morte seems to be co-determined by mineral dust absorbers and humic substances. Unfortunately with the thermo-optical method neither OC nor EC represent this organic absorber, although both sub-fractions contain part of its signal (Andreae and Gelencsér, 2006).

Surface structure

Overall, differences in cryoconite composition were rather small, whereas spectral reflectance measurements showed large differences in absorption level and behaviour. This suggests strong albedo-relevance of the surface structure of cryoconite on ice (i.e. evenly distributed versus aggregated matter forming cryoconite holes) and the absolute cryoconite load. Average integrated albedo of cryoconite matter itself was 0.03 in moist condition, which is substantially lower than the finding of Bøggild et al. (2010), who reported an albedo of 0.1 for wet cryoconite. Cryoconite loaded ice surfaces, in contrast, showed an albedo ranging from 0.03 to 0.2. In any case, cryoconite hole formation seems to be closely linked with surface runoff, as previously reported by Fountain et al. (2004). As mentioned in section 1, the importance of the surface structure on the albedo of a glacier was also investigated by Takeuchi (2009) and Bøggild et al. (2010), reporting increased broadband albedo despite high cryoconite mass on surfaces with deep cryoconite holes. Warren and Wiscombe (1980) reported decreasing albedo effect with increasing size of particulate impurities. If this is applicable to larger spatial scales, the formation of aggregated matter and cryoconite granules would significantly reduce the albedo effect of cryoconite deposits on a glacier surface.

Anthropogenic effect and feedback mechanism

The combined effect of cryoconite deposits and liquid water content caused the albedo of Plaine Morte to deviate from clean-ice albedo by more than 0.18. Based on mass-balance calculations, Oerlemans et al. (2009) found a comparable albedo reduction on Morteratsch glacier to be equivalent to a temperature increase of 1.7°C (c.f. section 1.1). Most probably, the anthropogenic impact on cryoconite accumulation on Plaine Morte is restricted to EC input from polluted PBL air masses showing decreasing emission trends in Switzerland (Fagerli et al., 2007; Legrand et al., 2007; BAFU, 2010), while local EC sources seem to be of minor importance. However the multi-annual enrichment of EC on the glacier surface suggests a memory effect, although EC emissions in Europe generally declined after the peak in the 1960s (Legrand et al., 2007). Additionally and most importantly, cryoconite seems to trigger a positive feedback mechanism, which is depicted

in Figure 22: small cryoconite induced changes in albedo cause enhanced melt via altering of the energy budget. Since liquid water is a strong absorber, additional warming of the glacier surface takes place (Wharton et al., 1985), resulting in increased surface runoff and water availability for microorganisms (Oerlemans et al., 2009). This feedback mechanism might also cause long-term albedo changes, exceeding the duration of a single ablation period, by filling pores with meltwater, which reduces the albedo of glacier ice significantly (Gardner and Sharp, 2010). Thereby the snow-albedo feedback mechanism displayed in Figure 1 could be strongly intensified.

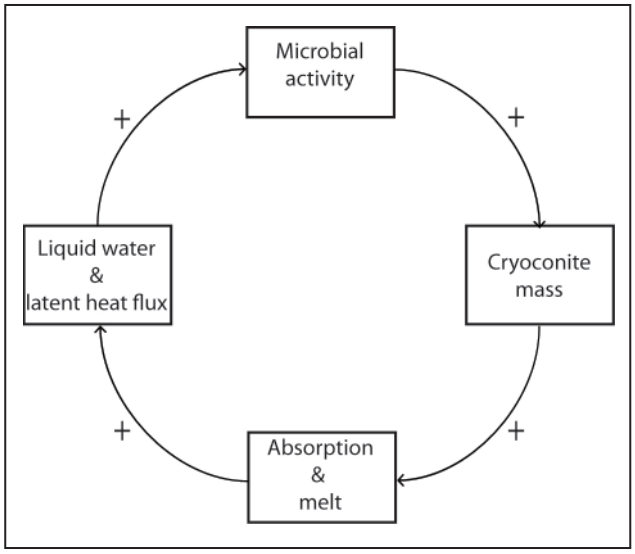

Figure 22: Schematic drawing of the cryoconite induced albedo-feedback mechanism. The symbol (+) next to the arrows indicates a positive correlation between the quantities in the adjacent boxes.

6.4. Methodological uncertainties and improvement of study setup

In general, most of the methods applied in this study showed some uncertainties.

- First of all, the limited number of ice samples severely constrained statistical analyses of the different results and therefore decreased the quantitative and informative value of the findings. Considering the heterogeneity of the glacier surface, the sample number should be substantially increased to ensure a certain degree of representativeness.
- Secondly a relatively large fraction of cryoconite matter remained unexplained. Since dust input mainly occurs in the clay fraction, XRD analyses with a focus on clay mineralogy might have provided more convincing results, with the potential to identify the mineral fraction more holistically. This should be considered in following studies.
- Thirdly the determination of the organic content and granule counting were rough estimates and did not allow the distinction of living and dead organic matter. In addition both methods were subject to major uncertainties. The limited reliability of LOI stems from the uncertainties regarding additional weight changes due to evaporation of structural water in clay minerals, loss of volatile salts or dehydration of metal oxides at temperatures below 550°C (Heiri et al., 2001). Therefore the combustion time and temperature need to be chosen carefully. Heiri et al. (2001) argued that a long exposure time (4 h) is crucial for a complete combustion of organic matter in organic-rich soils, but at the same time this increases the bias due to additional weight losses. In this case, both the temperature and ignition time were chosen at the lower limit (430°C, 2 h) in order to create a one-sided bias. Davies (1974) claimed combustion at 430°C to be convenient for both calcareous and non-calcareous soils and losses due to structural water to be minimal at this temperature. The oxidation process of organic matter might not be completed after two hours of combustion at 430°C. This suggests a tendency towards an underestimation of the organic fraction of the samples. However, Langford et al. (2010) found cryoconite from Svalbard to be largely thermo-labile, i.e. consisting predominantly of carbohydrates

which are oxidised at temperatures below 200°C. The mass loss ratio from 350-500°C amounted to less than 0.5 in that particular study. Therefore the underestimation of organic content is presumably minimal. Rather poor agreement between OC concentrations and organic matter fraction determined by the LOI method was found. As is to be expected, the OC fraction was consistently lower than that of organic matter, since during LOI not only OC but also other organic compounds are incinerated, but the extent of this deviation was not systematic. The granule counting procedure was performed on a filter section corresponding to 20% of the total filter area. The applied transect-counting is a commonly used method for large numbers of micro-sized objects (Santibáñez et al., 2008; Uetake et al., 2010), but as granules were not uniformly distributed on the filters, the results might be significantly influenced by the choice of the transects. For counting of individual cells, usage of a flow cytometer might be an option (Priscu et al., 2005).

- Further, the largest drawback of EC measurements with respect to cryoconite composition was the lack of information about particle number and size distribution, resulting from the thermo-optical analysis. Additionally for this method two known artefacts exist, concerning high mineral dust load and brown OC. Anticipated oxidation of EC at low temperatures leads to an overestimation of OC and simultaneously decreases the measured EC concentrations. This artefact arises from the release of oxygen by mineral oxides in the helium step of the NIOSH 5040 protocol (Aamaas et al., 2011). For samples with high organic content, the second artefact is caused by interference with brown OC, generating a bias in OC and EC concentrations simultaneously (Andreae and Gelencsér, 2006).
- Finally the surface structure of cryoconite loaded glacier ice was reported to notably influence the albedo (Takeuchi, 2009), especially where deep cryoconite holes are formed. The methods used in this study were not suitable to understand granule formation processes, which might be of great importance to the composition, accumulation and distribution of cryoconite on the surface of Plaine Morte glacier.

For subsequent studies more detailed analysis of the organic cryoconite fraction is desirable. Most importantly, the differentiation and identification of EPS, defragmented organic matter and humic substances or brown OC should be aimed for, along with the quantification of cyanobacteria and algal species. All of this information might be helpful to determine the nature and origin of dark colourations within cryoconite granules. However, the findings of Langford et al. (2010) and Takeuchi et al. (2001), as well as the method alternatives tested in the course of this study, illustrated the complexity of the subject and the need for further methodological research and development. Due to the setup of the field campaign, instrument availability and other constraints, no quantitative evaluation of spectral reflectance of cryoconite was possible. Therefore a qualitative assessment and comparison with results from other studies was conducted. For subsequent investigations of cryoconite induced albedo impacts, ice sample spectra should be obtained *in-situ* as well as in frozen condition, to directly relate the chemical composition to the spectral reflectance pattern and to isolate and quantify the impact of liquid water. Further, the seasonal evolution of the glacier albedo is probably of minor importance, compared to accumulative effects of cryoconite enrichment on the bare glacier surface. Although impurities accelerate snow metamorphosis and prematurely trigger the transition from snow cover to bare ice surface, the overall effect on albedo will

be similar every year (due to constant or decreasing impurity emissions (e.g. BC)). More interesting might be long-term temporal trends in cryoconite composition and impurity inputs, to understand the relation between anthropogenic and natural drivers. Therefore focus should be placed on the late ablation season, when the snowpack has melted and bare ice surface is exposed. Since no longer time series are available for the albedo, melt rates, weather conditions, and impurity deposition on Plaine Morte glacier, it is not possible to postulate a long-term trend with the current data. Therefore it remains unclear, whether the measured albedo in summer 2003 (Paul et al., 2005) and 2010 (this study) are exceptional or whether they are an expression of changing environmental conditions (e.g. dryer climate causing increased dust input, c.f. section 1.1). However it can be assumed that outcropping dust layers and accumulating EC did lead to an increased albedo forcing in the past years. Thus a more detailed study on accumulation and removal processes of different cryoconite compounds would be of great interest. Additionally it would be valuable to gain more knowledge on the formation and distribution of different surface structure types to satisfy the complexity of heterogeneous cryoconite deposits. Further studies should consider assessing and classifying different surface types, their composition, spatial dimensions and average albedo. In this respect remote sensing data might be an accurate means for large-scale investigation on the albedo of heterogeneous glacier surfaces (Paul et al., 2005). However, *in-situ* observations are indispensable in order to prevent misinterpretations regarding the causes of albedo reductions. Inter-annual variability in surface albedo might be vastly influenced by the periodical overpass of satellite sensors in combination with the temporal distribution of episodic snowfall events during the ablation season.

7. Conclusions and outlook

7.1. Conclusions

On Plaine Morte glacier in the western Swiss Alps, snowpit chemistry and the biogeochemical composition of cryoconite deposits have been investigated to identify the sources of dust inputs to the glacier, which cause surface darkening. The findings were then related to spectral reflectance and broadband albedo measurements to determine the relative contribution of different cryoconite components to observed albedo reductions during the ablation season 2010. As a result, the following major conclusions could be drawn:

- Snowpit analyses of ions, trace elements and mineralogy, indicated a predominance of local mineral dust input, with emphasis on outcropping dust layers from the melting glacier ice. Although no inventory could be obtained from available data, Saharan dust deposition during the study period was found to be below the average input rates. This might lead to an underestimation of the SDE contribution to total cryoconite accumulation. In general, the identification of mineral dust sources and their quantification proved to be difficult with the methods chosen. The organic compounds and EC concentrations showed prevailing spring and summer deposition, attributed to the rise in PBL height and enhanced biological and agricultural activity. This seasonal signal was found to overlap and attenuate the chemical footprint of ash deposits from Eyjafjalla. Local EC emissions were found to be of minor importance, since winter concentrations were below the detection limit and close to the background value. Generally particulate matter present in the snowpack could by no means account for the total cryoconite mass observed on the glacier surface. This indicates multi-annual accumulation and denotes prosecution of the enrichment process in the near future.
- The cryoconite composition was determined to be dominated by dust from LLR, showing similar mineralogy except for extremely low calcite contents and a higher organic fraction. The discrepancies compared to LLR were caused by $CaCO_3$ dissolution and by high microbial activity in the humid glacial environment, respectively. Despite the obviously heterogeneous cryoconite distribution on the glacier surface, little variation in its composition was observed, indicating uniform deposition patterns on the glacier surface with consecutive relocation processes. The dark colouration of cryoconite was partly attributable to comparatively high EC concentrations and might have been intensified by humic substances. Visual inspection revealed a diverse microbial community with various species of cyanobacteria and green algae and correspondingly strong biological activity. However, the biological analytical methods used were overall unsatisfactory, especially with respect to the characterisation of coloured organic matter (e.g. humic substances, brown OC, EPS or living organisms) and granule counting did not add information on the living organisms or their albedo effect. Therefore also the granule formation process could not be clarified, although EC can likely be excluded from controlling factors since no correlation could be detected between EC content and granule frequency/size. However, the passive integration of EC into granules might hinder its removal from the glacier surface and therefore increase its residence time.
- Strongly reduced albedo was found on Plaine Morte in comparison with clean condition model outputs and average clean ice albedo (difference of up to 0.2), suggesting strong

overall absorbance of cryoconite. Mineral dust was attributed a minor relevance with respect to observed albedo changes, since cryoconite was substantially darker than the surrounding bedrock. The modelling approach for snow albedo revealed a decreasing effect of EC, despite its increasing concentrations. This was attributed to aggregation of biogenic matter, stressing the importance of the secondary albedo effect of microorganisms. Unfortunately, the relation assessment of cryoconite constituents with spectral reflectance and broadband albedo was restricted to qualitative methods, resulting from a lack of models for glacier ice albedo and biological impurities. Additionally, overlapping spectral signatures exacerbated the identification of different absorption patterns. Nevertheless, the importance of cryoconite and the liquid water content for the albedo of the glacier could be shown, suggesting a feedback mechanism triggered by cryoconite accumulations. This albedo feedback mechanism seems to be a complex interaction between anthropogenic (EC deposition and nutrient supply) and natural effects (mineral dust outcropping, increased meltwater surface runoff and enhanced algal growth due to promoting environment). Additionally it is expected to show long-term character, when meltwater fills pores of glacier ice, permanently reducing the scattering properties, when refreezing occurs.

7.2. Outlook

Plaine Morte glacier is a suitable location for investigations on albedo changes and its impacts on the mass-balance, especially considering water supply issues in the close vicinity of the glacier. Due to its gentle base slope and the resulting high sensitivity, however, this glacier might not be representative for glaciers within the Alpine ridge, regarding both cryoconite accumulation and its implications on the mass-balance. Therefore alternative study sites should be taken into account. This study should be considered a reconnaissance project, providing preliminary results on field observations as well as methodology concerning the albedo feedback. Most methods applied did not generally meet the specific requirements of the research questions, starting with fieldwork and measurement procedures through to laboratory analyses. Subsequent studies need to thoroughly reconsider assets and drawbacks of the methodology to determine the most suitable analytical methods for the different aspects of the cryoconite induced albedo feedback. In general, sampling needs to be more extensive in terms of sample numbers as well as sample amounts. For albedo considerations sampling of comparatively large and known surface areas with shallow snow depth are recommended, since the uppermost layer of snow/ice is most relevant to albedo issues. Additionally, spectral reflectance should be measured on each ice sample *in-situ* as well as under frozen conditions to determine or exclude liquid water effects. Further, soot concentrations should be determined by an absorption-based method (BC instead of EC), while appropriate analyses or proxies for different microorganisms, humic substances, brown OC or EPS need to be found, depending on the focus of the study. Moreover, the setup of an AWS would be desirable, to compensate for the lack of representative meteorological data in the high Alpine region and to generate a continuous albedo record.

To link albedo, energy budget and melt behaviour of a glacier, longer time series of glaciological and meteorological parameters (e. g. latent heat flux from meltwater) are indispensable. Two promising approaches for further studies emerge from this preliminary investigation. For both the feedback mechanism with enhanced liquid water absorption plays a key role:

- Either the multi-annual accumulation of cryoconite on the glacier surface is brought into focus, considering annual impurity input rates, metabolism of microorganisms and redistribution and removal processes. This means the residence time of different cryoconite species could be derived, which is essential to determine long-term effects.
- Alternatively, the anthropogenic versus natural contribution might be of great interest. Therefore the provenance of impurity deposits and the relative contribution of different cryoconite components to the total albedo reduction should be studied in more detail by improved quantification methods and modelling of albedo effect and feedback mechanisms. In this respect, anthropogenic nutrient supply and changes in other limiting factors like water availability and temperature on the evolution of microbial communities might be of additional importance.

The present study showed that EC and other cryoconite components may strongly alter the energy budget of Alpine glaciers. The indicated tendency towards enhanced cryoconite accumulation illustrates the actuality of the topic, especially considering the critical state of most Alpine glaciers. Therefore closer investigations on the cryoconite induced albedo feedback mechanism are highly desirable.

Acknowledgements

This project has been supervised by Prof. Dr. Margit Schwikowski and Prof. Dr. Martin Hoelzle with assistance from Pierre-Alain Herren. Special thanks are dedicated to them for their support during fieldwork on Plaine Morte glacier and for good advice and expertise during the course of this study. I truly appreciate their helpful encouragement and constructive inputs.

Many more people have contributed to this project with professional, technical and moral support.

My sincere thanks belong to:

- Prof. Dr. Margit Schwikowski and Pierre-Alain Herren from the Laboratory of Radiochemistry and Environmental Chemistry (PSI) for offering me this great opportunity to gain insight into environmental chemistry and for reviewing my thesis
- Dr. Anita Ciric, Sabina Bruetsch and Isabel Wendl from the Laboratory of Radiochemistry and Environmental Chemistry (PSI) for introducing me to the laboratory environment and for teaching different analytical methods
- Pamela Santibáñez from the Department of Land Resources and Environmental Sciences (Montana State University, USA) and Prof. Dr. Kurt Ballmer from the Department of Biology and Chemistry (PSI) for their support with biological analyses and microscopic techniques
- Dr. Urs Eggenberger and Nicolas Greber from the Institute of Geological Sciences as well as Prof Dr. Sönke Szidat and Yanlin Zhang from the Department of Chemistry and Biochemistry (University of Berne) for providing technical requirements and knowhow for XRD and OC/EC analyses, respectively
- Leonhard Tobler from the Laboratory of Radiochemistry and Environmental Chemistry and R. Bruetsch from the Nuclear Energy and Safety Research Department (PSI) for performing ICP-MS measurements and SEM imagery
- Dr. Irene Lehner from the Institute for Atmospheric and Climate Science (ETH Zürich) and Damien Markulin and Dr. Andy Hueni from the Department of Geography (University of Zürich) for the supply of albedometer and spectrometer and for helpful technical advice
- Prof. Dr. Martin Hoelzle and Dr. Matthias Huss from the Department of Geosciences (University of Fribourg) for glaciological expertise and data
- Dr. Martine Collaud-Coen from Meteo Schweiz for providing data on SDE
- Dr. Krystyna Saunders and Dr. Christian Kamenik from the Institute of Geography (University of Berne) for reviewing my thesis, for moral support and statistical and methodological advice
- Prof. Dr. Martin Grosjean from the Oeschger Center for Climate Change Research (University of Berne) for providing a working space at the laboratories of the Lake Sediments and Paleolimnology research group
- The team of Télécabines Violettes in Crans-Montana for cooperation and technical support.

Special thanks are given to the members of the Analytical Chemistry Group at PSI and the Lake Sediments and Paleolimnology research group at the University of Berne for welcoming me with a friendly atmosphere and for sharing relaxing and entertaining coffee and lunch breaks.
Finally I would like to thank my boyfriend, family and friends for their moral support and for being there for me at all times. Thank you so much!

References

Aamaas, B., C.E. Bøggild, F. Stordal, T. Berntsen, K.I.M. Holmén and J. Ström. 2011. Elemental carbon deposition to Svalbard snow from Norwegian settlements and long-range transport. *Tellus B*, doi: 10.1111/j.1600-0889.2011.00531: 1-12.

Andreae, M.O. and A. Gelencsér. 2006. Black carbon or brown carbon? The nature of light-absorbing carbonaceous aerosols. *Atmospheric Chemistry and Physics*, **6**(10): 3131-3148.

Anesio, A.M., A.J. Hodson, A. Fritz, R. Psenner and B. Sattler. 2009. High microbial activity on glaciers: importance to the global carbon cycle. *Global Change Biology*, **15**(4): 955-960.

Aoki, T., K. Kuchiki, M. Niwano, Y. Kodama, M. Hosaka and T. Tanaka. 2011. Physically based snow albedo model for calculating broadband albedos and the solar heating profile in snowpack for general circulation models. *Journal of Geophysical Research*, **116**(D11114), doi: 10.1029/2010jd015507.

BAFU. 2010. NABEL – Luftbelastung 2009. Messresultate des nationalen Beobachtungsnetzes für Luftfremdstoffe (NABEL). Bundesamt für Umwelt (BAFU), Nr. 1016.

Bagshaw, E.A., M. Tranter, A.G. Fountain, K.A. Welch, H. Basagic and W.B. Lyons. 2007. Biogeochemical evolution of cryoconite holes on Canada Glacier, Taylor Valley, Antarctica. *Journal of Geophysical Research*, **112**(G4S35), doi: 10.1029/2007jg000442.

Baltensperger, U., H.W. Gäggeler, D.T. Jost, M. Lugauer, M. Schwikowski, E. Weingartner and P. Seibert. 1997. Aerosol climatology at the high-alpine site Jungfraujoch, Switzerland. *Journal of Geophysical Research*, **102**(D16): 19707-19715.

Bøggild, C.E., R.E. Brandt, K.J. Brown and S.G. Warren. 2010. The ablation zone in northeast Greenland: ice types, albedos and impurities. *Journal of Glaciology*, **56**(195): 101-113.

Bonriposi, M. 2011. Les usages de l'eau dans la région de Crans-Montana-Sierre en 2010, Etat des lieux (working paper). *MontanAqua*. Université de Lausanne: 1-97.

Brandt, R.E., S.G. Warren and A.D. Clarke. 2011. A controlled snowmaking experiment testing the relation between black carbon content and reduction of snow albedo. *Journal of Geophysical Research*, **116**(D08109), doi: 10.1029/2010jd015330.

Braun, L.N., M. Weber and M. Schulz. 2000. Consequences of climate change for runoff from Alpine regions. *Annals of Glaciology*, **31**: 19-25.

Brock, B.W., I.C. Willis and M.J. Sharp. 2000. Measurement and parameterization of albedo variations at Haut Glacier d'Arolla, Switzerland. *Journal of Glaciology*, **46**: 675-688.

Bukowiecki, N., P. Zieger, E. Weingartner, Z. Jurányi, M. Gysel, B. Neininger, B. Schneider, C. Hueglin, A. Ulrich, A. Wichser, S. Henne, D. Brunner, R. Kaegi, M. Schwikowski, L. Tobler, F. G. Wienhold, I. Engel, B. Buchmann, T. Peter and U. Baltensperger. Ground-based and airborne in-situ measurements of the Eyjafjallajökull volcanic aerosol plume in Switzerland in spring 2010. *Atmospheric chemistry and Physics Discussions,* **11**(10)*,* doi:10.5194/acpd-11-12949-2011: 12949–13002.

Charlson, R.J., S.E. Schwartz, J.M. Hales, R.D. Cess, J.A. Coakley, J.E. Hansen and D.J. Hofmann. 1992. Climate Forcing by Anthropogenic Aerosols. *Science*, **255**(5043): 423-430.

Ciric, A. 2009. ENSO related climate variability recorded in an ice core from Cerro Mercedario, Central Andes. (PhD. thesis, Universität Bern).

Collaud-Coen, M., E. Weingartner, D. Schaub, C. Hueglin, C. Corrigan, S. Henning, M. Schwikowski and U. Baltensperger. 2004. Saharan dust events at the Jungfraujoch: detection by wavelength dependence of the single scattering albedo and first climatology analysis. *Atmospheric Chemistry and Physics*, **4**(2465): 2465-2480.

Conway, H., A. Gades and C.F. Raymond. 1996. Albedo of dirty snow during conditions of melt. *Water Resources Research*, **32**(6): 1713–1718.

Cornelissen, G., Ö. Gustafsson, T.D. Bucheli, M.T.O. Jonker, A.A. Koelmans and P.C.M. van Noort. 2005. Extensive Sorption of Organic Compounds to Black Carbon, Coal, and Kerogen in Sediments and Soils: Mechanisms and Consequences for Distribution, Bioaccumulation, and Biodegradation. *Environmental Science & Technology*, **39**(18): 6881-6895.

Curry, J.A., J.L. Schramm, D.K. Perovich and J.O. Pinto. 2001. Applications of SHEBA/FIRE data to evaluation of snow/ice albedo parameterizations. *Journal of Geophysical Research*, **106**(D14): 15345-15355.

Dansgaard, W. 1964. Stable isotopes in precipitation. *Tellus*, **16**(4): 436-468.

Davies, B.E. 1974. Loss-on-Ignition as an Estimate of Soil Organic Matter. *Soil Sciences Society Americana Proceedings*, **38**(1): 150-151.

Doherty, S.J., S.G. Warren, T.C. Grenfell, A.D. Clarke and R.E. Brandt. 2010. Light-absorbing impurities in Arctic snow. *Atmospheric chemistry and Physics*, **10**(3), doi:10.5194/acp-10-11647-2010: 11647-11680.

Eichler, A., M. Schwikowski and H.W. Gäggeler. 2001. Meltwater-induced relocation of chemical species in Alpine firn. *Tellus B*, **53**(2), doi: 10.1034/j.1600-0889.2001.d01-15.x: 192-203.

Elster, J., R.J. Delmas, J.R. Petit and K. Řeháková. 2007. Composition of microbial communities in aerosol, snow and ice samples from remote glaciated areas (Antarctica, Alps, Andes). *Biogeosciences Discussions*, **4**(3), doi: 10.5194/bgd-4-1779-2007: 1779-1813.

EMPA. 2010. Die Aschewolken des Eyjafjallajökull – auch im Nationalen Beobachtungsnetz für Luftfremdstoffe (NABEL) klar messbar. Materials, Science and Technology (EMPA): 1-6.

Fagerli, H., M. Legrand, S. Preunkert, V. Vestreng, D. Simpson and M. Cerqueira. 2007. Modeling historical long-term trends of sulfate, ammonium, and elemental carbon over Europe: A comparison with ice core records in the Alps. *Journal of Geophysical Research*, **112**(D23S13), doi: 10.1029/2006jd008044.

Farinotti, D. 2010. Simple methods for inferring glacier ice-thickness and snow-accumulation distribution. (PhD. thesis, ETH Zürich).

Flanner, M.G., C.S. Zender, J.T. Randerson and P.J. Rasch. 2007. Present-day climate forcing and response from black carbon in snow. *Journal of Geophysical Research*, **112**(D11202), doi: 10.1029/2006JD008003.

Formenti, P., L. Schuetz, Y. Balkanski, K. Desboeufs, M. Ebert, K. Kandler, A. Petzold, D. Scheuvens, S. Weinbruch and D. Zhang. 2010. Recent progress in understanding physical and chemical properties of mineral dust. *Atmospheric Chemistry and Physics Discussions*, **10**(5194), doi: 10.5194/acpd-10-31187-2010: 31187–31251.

Forster, P., V. Ramaswamy, P. Artaxo, T. Berntsen, R. Betts, D.W. Fahey, J. Haywood, J. Lean, D.C. Lowe, G. Myhre, J. Nganga, R. Prinn, G. Raga, M. Schulz and R. Van Dorland. 2007. Changes in Atmospheric Constituents and in Radiative Forcing. *Climate Change 2007: The Physical Science Basis. Contribution of Working Group I to the Fourth Assessment Report of the Intergovernmental Panel on Climate Change*. 130-587.

Fountain, A.G., M. Tranter, T.H. Nylen, K.J. Lewis and D.R. Mueller. 2004. Evolution of cryoconite holes and their contribution to meltwater runoff from glaciers in the McMurdo Dry Valleys, Antarctica. *Journal of Glaciology*, **50**: 35-45.

Frei, C. and C. Schaer. 1998. A precipitation climatology of the Alps from high-resolution rain-gauge observations. *International Journal of Climatology*, **18**: 873-900.

Gardner, A.S. and M.J. Sharp. 2010. A review of snow and ice albedo and the development of a new physically based broadband albedo parameterization. *Journal of Geophysical Research*, **115**(01009), doi: 10.1029/2009JF001444.

Gelencsér, A. 2004. Carbonaceous Aerosol In: Mysak, L. and K. Hamilton (eds.). *Atmospheric and Oceangraphic Science Library Series,* New York, Springer.

Ginot, P., U. Schotterer, W. Stichler, M.A. Godoi, B. Francou and M. Schwikowski. 2010. Influence of the Tungurahua eruption on the ice core records of Chimborazo, Ecuador. *The Cryosphere*, **4**(5194), doi: 10.5194/tcd-4-1343-2010: 561-568.

Green, R.O., J. Dozier, D. Roberts and T. Painter. 2002. Spectral snow-reflectance models for grain-size and liquid-water fraction in melting snow for the solar-reflected spectrum. *Annals of Glaciology*, **34**: 71-73.

Grenfell, T.C. and D.K. Perovich. 1984. Spectral Albedos of Sea Ice and Incident Solar Irradiance in the Southern Beaufort Sea. *Journal of Geophysical Research*, **89**(C3), doi: 10.1029/JC089iC03p03573: 3573-3580.

Hadley, O.L., C.E. Corrigan, T.W. Kirchstetter, S.S. Cliff and V. Ramanathan. 2010. Measured black carbon deposition on the Sierra Nevada snow pack and implication for snow pack retreat. *Atmospheric Chemistry and Physics*, **10**(5194), doi: 10.5194/acp-10-7505-2010: 7505-7513.

Hand, V.L., G. Capes, D.J. Vaughan, P. Formenti, J.M. Haywood and H. Coe. 2010. Evidence of internal mixing of African dust and biomass burning particles by individual particle analysis using electron beam techniques. *Journal of Geophysical Research*, **115**(D13301), doi: 10.1029/2009JD012938.

Hansen, J. and L. Nazarenko. 2003. Soot climate forcing via snow and ice albedos. *Proceedings of the National Academy of the United States of America*, **101**(2): 423-428.

Heiri, O., A.F. Lotter and G. Lemcke. 2001. Loss on ignition as a method for estimating organic and carbonate content in sediments: reproducibility and comparability of results. *Journal of Paleolimnology*, **25**(1): 101-110.

Hinz, K.-P., A. Trimborn, E. Weingartner, S. Henning, U. Baltensperger and B. Spengler. 2005. Aerosol single particle composition at the Jungfraujoch. *Journal of Aerosol Science*, **36**(1): 123-145.

Hodson, A., K. Cameron, C. Bøggild, T. Irvine-Fynn, H. Langford, D. Pearce and S. Banwart. 2010. The structure, biological activity and biogeochemistry of cryoconite aggregates upon an Arctic valley glacier: Longyearbreen, Svalbard. *Journal of Glaciology*, **56**: 349-362.

Jacobson, M.Z. 2004. Climate response of fossil fuel and biofuel soot, accounting for soot's feedback to snow and sea ice albedo and emissivity. *Journal of Geophysical Research*, **109**(D21201), doi: 10.1029/2004jd004945.

Kandler, K., N. Benker, U. Bundke, E. Cuevas, M. Ebert, P. Knippertz, S. Rodríguez, L. Schütz and S. Weinbruch. 2007. Chemical composition and complex refractive index of Saharan Mineral Dust at Izaña, Tenerife (Spain) derived by electron microscopy. *Atmospheric Environment*, **41**(37), doi: 10.1016/j.atmosenv.2007.06.047: 8058-8074.

Kaspari, S.D., M. Schwikowski, M. Gysel, M.G. Flanner, S. Kang, S. Hou and P.A. Mayewski. 2011. Recent increase in black carbon concentrations from a Mt. Everest ice core spanning 1860-2000 AD. *Geophysical Research Letters*, **38**(L04703), doi: 10.1029/2010gl046096.

Kaspari, S.D., M. Schwikowski, M. Gysel, S. Kang, P. Mayewski and B. Grigholm. 2009. Determination of Carbonaceous Particle Concentrations in a Tibetan Plateau Ice Core. *Annual Report 2008*. Labor für Radio- und Umweltchemie, Paul Scherrer Institut (PSI): 24.

Kilbride, C., J. Poole and T.R. Hutchings. 2006. A comparison of Cu, Pb, As, Cd, Zn, Fe, Ni and Mn determined by acid extraction/ICP-OES and ex situ field portable X-ray fluorescence analyses. *Environmental Pollution*, **143**(1): 16-23.

Klok, E.J.L., W. Greuell and J. Oerlemans. 2003. Temporal and spatial variation of the surface albedo of Morteratschgletscher, Switzerland, as derived from 12 Landsat images. *Journal of Glaciology*, **49**: 491-502.

Kohshima, S. 1994. Albedo reduction by biotic impurities on a perennial snow patch in the Japan alps. *Yokohama Symposia J2 and J5*, **223**: 323-330.

Kohshima, S., K. Seko and Y. Yoshimura. 1993. Biotic Acceleration of Glacier Melting in Yala Glacier 9 Langtang Region, Nepal Himalaya. *Kathmandu Symposium*, Institute for Hydrospheric and Atmospheric Sciences, Kathmandu, **218**: 309-316.

Krivácsy, Z., A. Hoffer, Z. Sárvári, D. Temesi, U. Baltensperger, S. Nyeki, E. Weingartner, S. Kleefeld and S.G. Jennings. 2001. Role of organic and black carbon in the chemical composition of atmospheric aerosol at European background sites. *Atmospheric Environment*, **35**(36), doi: 10.1016/s1352-2310(01)00467-8: 6231-6244.

Laird, D.A., M.A. Chappell, D.A. Martens, R.L. Wershaw and M. Thompson. 2008. Distinguishing black carbon from biogenic humic substances in soil clay fractions. *Geoderma*, **143**(2): 115-122.

Langford, H., A. Hodson, S. Banwart and C. Bøggild. 2010. The microstructure and biogeochemistry of Arctic cryoconite granules. *Annals of Glaciology*, **51**(56): 87-94.

Lavanchy, V.M.H., H.W. Gäggeler, U. Schotterer, M. Schwikowski and U. Baltensperger. 1999. Historical record of carbonaceous particle concentrations from a European high-alpine glacier (Colle Gnifetti, Switzerland). Journal of Geophysical Research, 104(D17): 21227-21236.

Legrand, M. and P. Mayewski. 1997. Glaciochemistry of polar ice cores: A review. *Reviews of Geophysics*, **35**(3): 219-243.

Legrand, M., S. Preunkert, M. Schock, M. Cerqueira, A. Kasper-Giebl, J. Afonso, C. Pio, A. Gelencsér and I. Dombrowski-Etchevers. 2007. Major 20th century changes of carbonaceous aerosol components (EC, WinOC, DOC, HULIS, carboxylic acids, and cellulose) derived from Alpine ice cores. *Journal of Geophysical Research*, **112**(D23), doi: 10.1029/2006jd008080: D23S11.

Leroux, C., J.-L. Deuzé, P. Goloub, C. Sergent and M. Fily. 1998. Ground measurements of the polarized bidirectional reflectance of snow in the near-infrared spectral domain: Comparisons with model results. *Journal of Geophysical Research*, **103**(D16), doi: 10.1029/98jd01146: 19721-19731.

Leya, T., A. Rahn, C. Lütz and D. Remias. 2009. Response of arctic snow and permafrost algae to high light and nitrogen stress by changes in pigment composition and applied aspects for biotechnology. *FEMS Microbiology Ecology*, **67**(3), doi: 10.1111/j.1574-6941.2008.00641.x: 432-443.

Li, Z., R. Edwards, E. Mosley-Thompson, F. Wang, Z. Dong, X. You, H. Li, C. Li and Y. Zhu. 2006. Seasonal variability of ionic concentrations in surface snow and elution processes in snowfirn packs at the PGPI site on Urumqi glacier No. 1, eastern Tien Shan, China. *Annals of Glaciology*, **43**, doi: 10.3189/172756406781812069: 250-256.

Liu, Y., T. Yao, S. Kang, N. Jiao, Y. Zeng, S. Huang and T. Luo. 2007. Microbial community structure in major habitats above 6000 m on Mount Everest. *Chinese Science Bulletin*, **52**(17), doi: 10.1007/s11434-007-0360-4: 2350-2357.

Maire, R. 1978. Les karsts sous-glaciaires et leurs relations avec le karst profond. *Reveue de géographie alpine*, **2**(66): 139-148.

Marshall, S. and R.J. Oglesby. 1994. An improved snow hydrology for GCMs. Part 1: snow cover fraction, albedo, grain size, and age. *Climate Dynamics*, **10**(1): 21-37.

Ming, J., C. Xiao, H. Cachier, D. Qin, X. Qin, Z. Li and J. Pu. 2009. Black Carbon (BC) in the snow of glaciers in west China and its potential effects on albedos. *Atmospheric Research*, **92**(1), doi: 10.1016/j.atmosres.2008.09.007: 114-123.

Moreno, T., X. Querol, S. Castillo, A. Alastuey, E. Cuevas, L. Herrmann, M. Mounkaila, J. Elvira and W. Gibbons. 2006. Geochemical variations in aeolian mineral particles from the Sahara-Sahel Dust Corridor. *Chemosphere*, **65**(2): 261-270.

Moune, S., P.-J. Gauthier, S.R. Gislason and O. Sigmarsson. 2006. Trace element degassing and enrichment in the eruptive plume of the 2000 eruption of Hekla volcano, Iceland. *Geochimica et Cosmochimica Acta*, **70**(2): 461-479.

Müller, T., W. Bleiß, C.D. Martin, S. Rogaschewski and G. Fuhr. 1998. Snow algae from northwest Svalbard: their identification, distribution, pigment and nutrient content. *Polar Biology*, **20**(1): 14-32.

Negi, H.S. and A. Kokhanovsky. 2011. Retrieval of snow albedo and grain size using reflectance measurements in Himalayan basin. *The Cryosphere*, **5**(1): 203-217.

Oerlemans, J. 2010. *The Microclimate of Valley Glaciers.* Institute for Marine and Atmospheric Research, Utrecht Univeristy, Utrecht Publishing & Archiving Services.

Oerlemans, J., R.H. Giesen and M.R. Van Den Broeke. 2009. Retreating alpine glaciers: increased melt rates due to accumulation of dust (Vadret da Morteratsch, Switzerland). *Journal of Glaciology*, **55**: 729-736.

Painter, T.H., B. Duval, W.H. Thomas, M. Mendez, S. Heintzelman and J. Dozier. 2001. Detection and Quantification of Snow Algae with an Airborne Imaging Spectrometer. *Applied Environmental Microbiology*, **67**(11), doi: 10.1128/aem.67.11.5267-5272.2001: 5267-5272.

Paterson, W.S.B. 1994. *The Physics of Glaciers.* Third Edition ed. Oxford, UK, Butterworth - Heinemann.

Paul, F., H. Machguth and A. Kääb. 2005. On the Impact of Glacier Albedo under Conditions of Extreme Glacier Melt: The Summer of 2003 in the Alps. *EARSeL eProceedings*, **4**: 139-149.

Perron, N. 2010. Radiocarbon-supported source apportionment of carbonaceous aerosols. (PhD thesis, Universität Bern).

Priscu, J.C., B.C. Christner and C.M. Foreman. 2005. Biological Material in Ice Cores. *Encyclopedia of Quaternary Sciences*, **2**: 1156-1166.

Ramanathan, V., M.V. Ramana, G. Roberts, D. Kim, C. Corrigan, C. Chung and D. Winker. 2007. Warming trends in Asia amplified by brown cloud solar absorption. *Nature*, **448**(7153), doi: 10.1038/nature06019: 575-578.

Reznichenko, N., T. Davies, J. Shulmeister and M. McSaveney. 2010. Effects of debris on ice-surface melting rates: an experimental study. *Journal of Glaciology*, **56**: 384-394.

Roedel, W. 1994. *Die Physik unserer Umwelt: Die Atmosphäre.* 3 ed. Heidelberg, Springer.

Rose, N. 2001. Fly-Ash Particles. In: Last, W.M. and J.P. Smol (eds.). *Tracking Environmental Change Using Lake Sediments, Physical and Geochemical Methods*. London, Kluwer Academic Publishers: 319-350.

Santibáñez, P., S. Kohshima, R. Scheihing, J. Jaramillo, T. Shiraiwa, S. Matoba, D. Kanda, P. Labarca and G. Casassa. 2008. Glacier mass balance interpreted from biological analysis of firn cores in the Chilean lake district. *Journal of Glaciology*, **54**(186): 452-462.

Schimel, D., D. Alves, I. Enting, M. Heimann, F. Joos, D. Raynaud, T. Wigley, M. Prather, R. Derwent, D. Ehhalt, R. Eraser, E. Sanhueza, X. Zhou, R. Jonas, R. Charlson, H. Rodhe, S. Sadasivan, K.R. Shine, Y. Fouquart, V. Ramaswamy, S. Solomon, J. Srinivasan, D. Albritton, R. Derwent, L. Isaksen, M. Lal and D. Wuebbels. 1995. Climate Change 1995, The Science of Climate Change. *Climate Change 1995:The Science of Climate Change. Contribution of Working Group I to the Second Assessment Report of the Intergovernmental Panel on Climate Change*. Intergovernmental Panel on Climate Change: 1-531.

Schneider, F. 2010. Water Scarcity in Inner-Alpine Regions Options for sustainable water use in the Crans-Montana-Sierre region (Valais). *Swiss Geoscience Meeting, Symposium 18: Troubling water*, Fribourg, Switzerland, **8**: 342.

Schotterer, U., K. Fröhlich, H.W. Gäggeler, S. Sandjordj and W. Stichler. 1997. Isotope Records from Mongolian and Alpine Ice Cores as Climate Indicators. *Climatic Change*, **36**(3): 519-530.

Schotterer, U., W. Stichler and P. Ginot. 2004. The influence of post-depositional effects on ice core studies: examples from the Alps, Andes and Altai. In: Cecil, L.D., L.G. Thompson and E.J. Steig (eds.). *Earth paleoenvironments: records preserved in mid and low latitude glaciers*. London, Kluwer Academic Publishers: 39-59.

Schwikowski, M., S. Brütsch, H.W. Gäggeler and U. Schotterer. 1999. A high-resolution air chemistry record from an Alpine ice core: Fiescherhorn glacier, Swiss Alps. *Journal of Geophysical Research*, **104**(D11), doi: 0148-0227/99/1998JD100112: 13'709-13'719.

Schwikowski, M. and A. Eichler. 2010. Alpine Glaciers as Archives of Atmospheric Deposition. In: Bundi (ed.), U. *Alpine Waters*. Berlin, Heidelberg, Springer-Verlag: 141-150.

SCNAT. 2011. Gletscherberichte (1881-2009) "Die Gletscher der Schweizer Alpen". *Jahrbücher der Expertenkommission für Kryosphärenmessnetze der Akademie der Naturwissenschaften Schweiz (SCNAT)*.

Spreafico, M. and R. Weingartner. 2005. Hydrologie der Schweiz – Ausgewählte Aspekte und Resultate. Bundesamt für Wasser und Geologie.

Stephenson, P.J. 1967. Some considerations of snow metamorphism in Antarctic ice sheet in the light of ice crystal studies. In: Oura (ed.), H. *Physics of snow and ice*. Institute for Low Temperature Sciences, Hokkaido University. Part II).

Stibal, M., M. Tranter, J. Telling and L. Benning. 2008. Speciation, phase association and potential bioavailability of phosphorus on a Svalbard glacier. *Biogeochemistry*, **90**(1): 1-13.

Stocker, T. 2009. Introduction to climate modelling. Script to the lecture: Introduction to climate modelling. Physics Institute, University of Bern, Bern. 1-148.

Takeuchi, N. 2001. The Altitudinal Distribution of Snow Algae on an Alaska Glacier (Gulkana Glacier in the Alaska Range). *Eastern Snow Conference*, Ottawa, Ontario, Canada.

Takeuchi, N., S. Kohshima and K. Seko. 2001. Structure, Formation, and Darkening Process of Albedo-Reducing Material (Cryoconite) on a Himalayan Glacier: A Granular Algal Mat Growing on the Glacier. *Arctic Antarctic and Alpine Research*, **33**(2): 115-122.

Takeuchi, N. 2002a. Optical characteristics of cryoconite (surface dust) on glaciers: the relationship between light absorbency and the property of organic matter contained in the cryoconite. *Annals of Glaciology*, **34**: 409-414.

Takeuchi, N. 2002b. Surface albedo and characteristics of cryoconite (biogenic surface dust) on an Alsaka glacier, Gulkana Glacier in the Alaska Range. *Bulletin of Glaciological Research*, **19**: 63-70.

Takeuchi, N. 2009. Temporal and spatial variations in spectral reflectance and characteristics of surface dust on Gulkana Glacier, Alaska Range. *Journal of Glaciology*, **55**: 701-709.

Taylor, S.R. and S.M. McLennan. 1995. The geochemical evolution of the continental crust. *Reviews of Geophysics*, **33**(2): 241-265.

Thomas, W.H. and B. Duval. 1995. Sierra Nevada, California, U.S.A., Snow Algae: Snow Albedo Changes, Algal-Bacterial Interrelationships, and Ultraviolet Radiation Effects. *Arctic Antarctic and Alpine Research*, **27**(4): 389-399.

Tobler, L., R. Bruetsch, S. Bruetsch, N. Bukowiecki and M. Schwikowski. 2011. Volcanic ash from the Eyjafjalla detected in surface snow and aerosol samples from Jungfraujoch. *Annual Report 2010*. Labor für Radio- und Umweltchemie, Paul Scherrer Institut (PSI): 29.

Uetake, J., T. Naganuma, M.B. Hebsgaard, H. Kanda and S. Kohshima. 2010. Communities of algae and cyanobacteria on glaciers in west Greenland. *Polar Science*, **4**(1): 71-80.

Uetake, J., A. Sakai, Y. Matsuda, K. Fujita, H. Narita, S. Matoba, K. Duan, M. Nakawo and T. Yao. 2006. Preliminary observations of sub-surface and shallow ice core at July 1st Glacier, China in 2002-2004. *Bulletin of Glaciological Research*, **23**: 85-93.

Voinesco, A. Thesis in preparation. Ice thickness distribution of Glacier de la Plaine Morte. (Master thesis, University of Fribourg).

Wagenbach, D., K.O. Münnich, U. Schotterer and H. Oeschger. 1988. The anthropogenic impact on snow chemistry at Colle Gnifetti. Swiss Alps. *Annals of Glaciology*, **10**: 183-187.

Warren, S.G. and W.J. Wiscombe. 1980. A Model for the Spectral Albedo of Snow. II: Snow Containing Atmospheric Aerosols. *Journal of the Atmospheric Sciences*, **37**(12), doi: 0022-4928/80/122734-12: 2734-2745.

Weingartner, R. 2007. Hydrologie- im Wasserschloss Europas. In: Wallner, A., E. Bäschlin, M. Grosjean, T. Labhart, U. Schüpbach and U. Wiesmann (eds.). *Welt der Alpen, Erbe der Welt, Jungfrau Aletsch Bietschhorn*. Bern, Haupt Verlag: 73-90.

Wenk, H. and A. Bulakh. 2004. *Minerals: their constitution and origin*. Cambridge, Cambridge University Press: 646.

Wharton, R.A. Jr., C.P. McKay, G.M. Simmons Jr. and B.C. Parker. 1985. Cryoconite Holes on Glaciers. *BioScience*, **35**(8): 499-503.

Wientjes, I.G.M. and J. Oerlemans. 2010. An explanation for the dark region in the western melt zone of the Greenland ice sheet. *The Cryosphere*, **4**(3): 261-268.

Wientjes, I.G.M., R.S.W. Van de Wal, G.J. Reichart, A. Sluijs and J. Oerlemans. 2011. Dust from the dark region in the western ablation zone of the Greenland ice sheet. *The Cryosphere*, **5**(559), doi: 10.5194/tc-5-589-2011: 589-601.

Wiscombe, W.J. and S.G. Warren. 1980. A Model for the Spectral Albedo of Snow. I: Pure Snow. *Journal of the Atmospheric Sciences*, **37**: 2712-2745.

Wyer, H. 2008. Die Nutzung der Wasserkraft im Wallis. *Geschichte - Recht - Heimfall*, Visp, Rotten Verlag AG 1-267.

Xu, B., J. Cao, J. Hansen, T. Yao, D.R. Joswia, N. Wang, G. Wu, M. Wang, H. Zhao, W. Yang, X. Liu and J. He. 2009. Black soot and the survival of Tibetan glaciers. *Proceedings of the National Academy of Sciences*, **106**(52), doi: 10.1073/pnas.0910444106: 22114-22118.

Yasunari, T.J., P. Bonasoni, P. Laj, K. Fujita, E. Vuillermoz, A. Marinoni, P. Cristofanelli, R. Duchi, G. Tartari and K.-M. Lau. 2010. Estimated impact of black carbon deposition during pre-monsoon season from Nepal Climate Observatory – Pyramid data and snow albedo changes over Himalayan glaciers. *Atmospheric Chemistry and Physics*, **10**(5194): 6603-6615.

Yasunari, T.J., R.D. Koster, K.M. Lau, T. Aoki, Y.C. Sud, T. Yamazaki, H. Motoyoshi and Y. Kodama. 2011. Influence of dust and black carbon on the snow albedo in the NASA Goddard Earth Observing System version 5 land surface model. *Journal of Geophysical Research*, **116**(D2): D02210.

Zeng, Q., M. Cao, X. Feng, F. Liang, X. Chen and W. Sheng. 1983. A study of spectral reflection characteristics for snow, ice and water in the north of China. *Hamburg Symposium*, Hamburg, Germany: 451-462.

Appendix A

Table A1: Snowpit data: Depth in m weq, density in g/cm³ and the $\delta^{18}O$ value in ‰

Snowpit 1	Depth (m weq)	Density (g/cm³)	$\delta^{18}O$ (‰)
PM 01	0.03	0.30	-14.81
PM 02	0.05	0.23	-12.31
PM 03	0.10	0.47	-11.92
PM 04	0.14	0.41	-12.35
PM 05	0.20	0.50	-14.02
PM 06	0.24	0.41	-13.78
PM 07	0.29	0.52	-14.89
PM 08	0.34	0.51	-17.93
PM 09	0.40	0.47	-17.91
PM 10	0.45	0.50	-18.83
PM 11	0.49	0.43	-18.03
PM 12	0.54	0.42	-20.16
PM 13	0.59	0.48	-18.07
PM 14	0.64	0.54	-13.69
PM 15	0.70	0.61	-19.65
PM 16	0.75	0.48	-22.99
PM 17	0.82	0.72	-21.28
PM 18	0.88	0.52	-18.01
PM 19	0.93	0.55	-25.27
PM 20	0.98	0.52	-23.36
PM 21	1.04	0.54	-13.70

Snowpit 2	Depth (m weq)	Density (g/cm³)	$\delta^{18}O$ (‰)
PM 25	0.06	0.58	-15.82
PM 26	0.12	0.56	-17.19
PM 27	0.16	0.46	-16.81
PM 28	0.21	0.50	-17.98
PM 29	0.27	0.56	-23.76
PM 30	0.31	0.55	-21.41
PM 31	0.37	0.56	-14.84
PM 32	0.43	0.60	-12.55
PM 33	0.48	0.56	-14.09
PM 34	0.54		-13.69
PM 35	0.60		-14.64

Table A2: Snowpit data: Ion concentrations in µeq

Snowpit 1	Na^+ (µeq)	NH_4^+ (µeq)	K^+ (µeq)	Mg^{2+} (µeq)	Ca^{2+} (µeq)	Cl^- (µeq)	NO_3^- (µeq)	SO_4^{2-} (µeq)
PM 01	0.18	0.68	0.06	0.36	0.64	0.31	0.85	0.60
PM 02	0.05	1.90	0.06	0.55	0.56	0.35	1.70	1.67
PM 03	0.10	2.09	0.09	0.49	1.59	0.44	2.07	1.51
PM 04	0.09	3.16	0.09	0.38	0.76	0.39	2.17	1.79
PM 05	0.10	5.17	0.17	0.60	1.41	0.46	2.79	0.82
PM 06	0.52	8.18	0.15	0.68	2.59	0.99	5.13	1.88
PM 07	1.12	3.13	0.15	0.67	2.81	1.66	4.03	1.81
PM 08	0.37	1.52	0.06	0.39	0.82	0.69	4.07	0.80
PM 09	0.27	1.18	0.01	0.42	0.60	0.66	2.47	1.05
PM10	0.31	1.19	0.03	0.39	0.80	0.74	5.59	1.43
PM11	0.08	0.52	0.01	0.32	0.59	0.32	1.92	0.97
PM12	0.10	0.90	0.05	0.29	0.92	0.44	3.14	0.66
PM13	0.20	0.38	0.01	0.27	0.31	0.43	0.96	0.57
PM14	0.87	0.60	0.04	0.46	1.31	1.14	1.54	1.06
PM15	0.39	0.43	0.01	0.42	1.41	0.67	2.57	0.80
PM16	0.20	0.27	0.01	0.39	1.02	0.49	2.57	0.77
PM17	0.31	0.89	0.08	0.74	3.48	0.53	3.31	0.90
PM18	0.10	0.20	0.01	0.30	0.37	0.32	0.96	0.56
PM19	0.15	0.54	0.01	0.37	1.50	0.35	1.67	0.80
PM20	0.08	0.29	0.02	0.45	7.22	0.31	2.03	0.93
PM21	0.83	2.25	0.10	0.89	7.37	1.11	3.48	2.58

Snowpit 2	Na^+ (µeq)	NH_4^+ (µeq)	K^+ (µeq)	Mg^{2+} (µeq)	Ca^{2+} (µeq)	Cl^- (µeq)	NO_3^- (µeq)	SO_4^{2-} (µeq)
PM25	0.61	1.10	0.09	0.50	2.02	0.90	2.05	0.99
PM26	0.24	0.72	0.06	0.41	1.21	0.46	1.60	0.66
PM27	0.44	2.95	0.27	0.59	1.33	0.90	2.29	0.69
PM28	0.10	0.55	0.06	0.37	0.54	0.26	1.05	0.66
PM29	0.13	0.60	0.04	0.33	0.76	0.29	1.39	0.73
PM30	0.55	1.38	0.39	0.53	2.00	0.86	1.38	0.52
PM31	0.21	0.97	0.05	0.49	2.56	0.40	1.24	0.95
PM32	1.18	3.92	0.13	0.97	3.33	1.59	2.16	0.72
PM33	0.23	1.03	0.01	0.32	0.52	0.42	0.73	0.25
PM34	1.15	1.24	0.60	0.79	3.28	1.20	1.36	1.07
PM35	0.48	2.47	0.18	2.55	12.28	0.69	2.77	3.01

Table A3: Snowpit data: Ion concentrations in ppb

Snowpit 1	Na^+ (ppb)	NH_4^+ (ppb)	K^+ (ppb)	Mg^{2+} (ppb)	Ca^{2+} (ppb)	Cl^- (ppb)	NO_3^-(ppb)	SO_4^{2-} (ppb)
PM 01	4.16	12.34	2.32	4.36	12.85	10.86	52.95	28.69
PM 02	1.24	34.35	2.34	6.63	11.32	12.29	105.31	80.11
PM 03	2.27	37.63	3.53	5.93	31.78	15.49	128.19	72.73
PM 04	2.06	57.01	3.43	4.60	15.15	13.86	134.26	86.17
PM 05	2.41	93.33	6.51	7.33	28.26	16.47	173.04	39.33
PM 06	11.96	147.54	5.74	8.31	51.98	35.19	318.02	90.27
PM 07	25.79	56.43	5.72	8.10	56.36	58.92	250.00	87.13
PM 08	8.60	27.41	2.16	4.77	16.34	24.51	252.28	38.21
PM 09	6.25	21.34	0.40	5.10	11.93	23.53	153.30	50.48
PM10	7.10	21.47	1.27	4.79	16.07	26.12	346.79	68.71
PM11	1.83	9.34	0.40	3.84	11.83	11.27	118.85	46.70
PM12	2.35	16.29	1.80	3.47	18.53	15.51	194.73	31.94
PM13	4.49	6.77	0.40	3.30	6.31	15.15	59.58	27.14
PM14	19.97	10.77	1.49	5.55	26.33	40.46	95.27	50.87
PM15	8.86	7.73	0.40	5.06	28.25	23.60	159.56	38.63
PM16	4.55	4.83	0.40	4.76	20.46	17.50	159.29	36.94
PM17	7.11	16.13	2.97	8.94	69.77	18.72	205.33	43.43
PM18	2.36	3.65	0.40	3.61	7.47	11.33	59.52	27.08
PM19	3.50	9.75	0.40	4.54	30.07	12.46	103.84	38.61
PM20	1.77	5.24	0.93	5.51	144.61	10.92	125.91	44.74
PM21	19.04	40.68	3.81	10.83	147.69	39.49	215.59	123.76

Snowpit 2	Na^+ (ppb)	NH_4^+ (ppb)	K^+ (ppb)	Mg^{2+} (ppb)	Ca^{2+} (ppb)	Cl^- (ppb)	NO_3^-(ppb)	SO_4^{2-} (ppb)
PM25	14.12	19.80	3.67	6.09	40.55	32.02	126.83	47.44
PM26	5.42	13.00	2.16	4.97	24.24	16.31	99.00	31.75
PM27	10.04	53.16	10.37	7.18	26.68	31.85	142.04	32.98
PM28	2.28	9.90	2.31	4.52	10.75	9.31	65.13	31.91
PM29	3.08	10.77	1.37	4.01	15.16	10.14	86.31	35.15
PM30	12.68	24.85	15.38	6.47	40.14	30.44	85.78	25.16
PM31	4.83	17.50	2.11	5.94	51.37	14.16	77.13	45.57
PM32	27.18	70.79	5.11	11.76	66.72	56.30	134.10	34.40
PM33	5.30	18.67	0.40	3.92	10.37	14.80	45.46	11.78
PM34	26.38	22.41	23.62	9.59	65.70	42.38	84.56	51.53
PM35	11.00	44.47	7.00	31.02	246.15	24.48	171.90	144.68

Table A4: Snowpit data: Raw data of trace elements for snowsamples in pg/ml and for ice samples in ng/ml

Snowpit 1	Li (pg/ml)	Rb (pg/ml)	Sr (pg/ml)	Zr (pg/ml)	Mo (pg/ml)	Ag (pg/ml)	Cd (pg/ml)
PM 01		4.63	46.80	8.65	4.13	1.40	1.76
PM 02		4.28	36.67	2.47	3.32	0.73	1.64
PM 03	13.66	43.78	246.69	20.53	12.99	0.72	2.11
PM 04	6.08	17.05	123.04	8.61	12.47	0.91	3.47
PM 05	6.15	18.28	76.71	12.61	9.68	1.29	1.43
PM 06	8.53	25.84	138.38	3.41	5.65	0.91	1.98
PM 07	0.56	12.65	144.98	2.85	4.28	0.23	1.32
PM 08		4.04	53.24	0.84	2.58	0.12	0.98
PM 09		3.54	28.24	0.53	2.86	0.06	0.95
PM10		4.38	64.59	1.27	3.13	0.37	2.24
PM11		1.34	18.42	0.40	1.28	0.09	0.88
PM12		4.70	117.67	2.60	2.46	0.80	3.28
PM13	5.75	0.69	11.49	0.14	4.56	0.00	0.18
PM14	10.25	1.84	75.64	0.21	0.44	0.00	0.41
PM15		2.43	45.11	0.31	0.47	0.10	0.25
PM16		2.47	39.13	0.11	0.89		0.34
PM17	3.46	13.41	123.19	0.59	1.45	0.89	0.87
PM18		1.04	20.26	0.22	0.91	0.07	1.16
PM19		1.99	57.84	0.10	0.95		0.51
PM20	3.63	18.30	304.98	0.89	1.38	0.47	0.51
PM21	5.98	26.22	627.14	6.18	4.46	0.26	3.21

Snowpit 2	Li (pg/ml)	Rb (pg/ml)	Sr (pg/ml)	Zr (pg/ml)	Mo (pg/ml)	Ag (pg/ml)	Cd (pg/ml)
PM25	30.71	90.93	160.78	11.51	11.22	2.54	1.29
PM26	2.91	12.00	40.66	2.82	3.14	2.02	0.73
PM27	3.13	12.05	57.23	4.53	23.28	3.73	6.45
PM28	0.87	3.63	27.62	0.77	1.40	0.29	1.06
PM29		3.21	32.84	0.68	1.04	0.20	0.95
PM30	19.08	59.82	162.31	3.25	33.82	2.78	9.28
PM31	2.60	5.58	85.00	0.38	1.09	0.18	1.03
PM32	11.95	31.37	194.53	3.12	5.57	1.07	1.19
PM33	2.26	6.71	16.73	0.17	0.80	0.21	0.34
PM34	8.70	19.15	143.60	0.86	2.94	0.91	2.01
PM35	8.26	5.26	544.30	0.37	5.65	0.32	0.54

Ice samples	Li (ng/ml)	Rb (ng/ml)	Sr (ng/ml)	Zr (ng/ml)	Mo (ng/ml)	Ag (ng/ml)	Cd (ng/ml)
IS1	29.05	7.51	67.11	0.56	0.17	0.08	2.14
IS2	3.24	2.75	10.12	0.18	0.24	0.05	0.19
IS3	5.26	2.78	10.57	0.21	0.12	0.05	0.40
IS4	4.25	3.74	11.52	0.32	0.07	0.06	0.23
IS5	31.40	12.21	77.92	1.08	0.68	0.06	1.18
IS6	51.22	15.13	143.62	4.15	1.11	0.91	2.24
IS7	93.02	26.01	241.87	3.31	1.01	0.76	3.83

Table A4 continued

Snowpit 1	Sb (pg/ml)	Cs (pg/ml)	Ba (pg/ml)	La (pg/ml)	Ce (pg/ml)	Pr (pg/ml)	Nd (pg/ml)
PM 01	11.74	1.09	119.64	1.34	2.45	0.44	1.32
PM 02	8.88	0.79	53.04	0.86	1.81	0.24	0.89
PM 03	40.47	5.18	274.32	38.88	84.38	10.40	42.04
PM 04	23.14	2.21	189.39	14.74	30.21	4.31	17.23
PM 05	28.39	2.52	126.31	20.84	44.46	5.41	21.34
PM 06	15.09	3.04	189.39	16.34	35.91	4.67	18.57
PM 07	9.49	1.20	99.74	5.29	10.68	1.31	5.80
PM 08	7.85	0.77	125.10	0.80	1.69	0.21	0.90
PM 09	11.67	0.49	43.94	0.82	1.66	0.19	0.75
PM10	11.88	0.59	188.18	1.16	2.43	0.29	1.13
PM11	6.47	0.29	40.67	0.39	0.83	0.12	0.52
PM12	12.90	3.26	236.71	2.21	2.57	0.33	1.51
PM13	4.81	0.22	51.59	0.11	0.23	0.03	0.09
PM14	6.22	0.28	36.18	0.68	1.23	0.19	0.76
PM15	5.01	0.43	29.38	0.49	1.06	0.14	0.61
PM16	6.05	0.42	27.69	0.49	1.05	0.12	0.53
PM17	7.65	1.65	52.92	3.37	6.10	0.89	3.78
PM18	6.69	0.42	90.41	0.30	0.53	0.05	0.24
PM19	5.34	0.32	32.66	0.47	1.14	0.17	0.85
PM20	7.79	2.56	125.10	3.54	10.19	1.78	8.91
PM21	13.18	2.70	513.31	32.42	67.28	8.71	36.82

Snowpit 2	Sb (pg/ml)	Cs (pg/ml)	Ba (pg/ml)	La (pg/ml)	Ce (pg/ml)	Pr (pg/ml)	Nd (pg/ml)
PM25	24.64	9.57	328.91	32.80	70.32	9.14	39.76
PM26	10.52	1.67	81.06	6.22	12.47	1.50	5.92
PM27	13.18	1.39	89.68	7.79	15.72	1.75	6.97
PM28	7.79	0.39	37.63	0.79	1.31	0.15	0.69
PM29	6.63	0.27	32.78	0.53	1.13	0.14	0.54
PM30	11.88	6.31	216.08	11.40	26.60	4.00	19.51
PM31	6.83	1.33	150.57	2.89	5.95	0.87	3.63
PM32	9.83	7.32	322.84	41.16	82.86	11.27	43.87
PM33	6.22	3.32	34.84	3.44	7.74	1.04	4.49
PM34	9.56	4.74	113.33	5.15	11.08	1.58	6.86
PM35	8.47	1.30	161.49	0.47	0.93	0.16	0.65

Ice samples	Sb (ng/ml)	Cs (ng/ml)	Ba (ng/ml)	La (ng/ml)	Ce (ng/ml)	Pr (ng/ml)	Nd (ng/ml)
IS1	0.70	0.71	178.11	32.64	96.54	13.31	69.96
IS2	0.76	0.37	72.52	5.73	14.88	1.91	8.84
IS3	0.55	0.38	22.66	6.63	17.71	2.41	12.49
IS4	1.07	0.34	51.81	10.15	25.84	3.29	15.52
IS5	0.65	0.52	228.62	61.69	162.61	19.41	97.08
IS6	1.41	0.54	301.38	104.38	284.11	35.98	172.74
IS7	1.33	0.85	522.35	186.72	539.26	66.36	317.37

Table A4 continued

Snowpit 1	Sm (pg/ml)	Eu (pg/ml)	Yb (pg/ml)	W (pg/ml)	Tl (pg/ml)	Pb (pg/ml)	Bi (pg/ml)
PM 01	0.37	0.27	0.23	2.23	0.49	40.77	2.62
PM 02	0.23	0.14	0.10	0.92	0.36	211.84	1.52
PM 03	8.97	1.96	2.36	2.41	0.86	592.47	24.77
PM 04	3.85	0.96	1.10	1.86	0.73	411.22	19.75
PM 05	4.46	1.14	1.38	1.55	0.32	457.54	9.97
PM 06	3.94	0.90	1.09	0.85	0.52	365.51	2.90
PM 07	1.15	0.30	0.38	0.48	0.28	224.45	1.57
PM 08	0.17	0.08	0.06	0.51	0.17	222.98	1.41
PM 09	0.15	0.06	0.07	0.37	0.15	218.14	1.11
PM10	0.28	0.11	0.08	1.18	0.26	260.40	1.77
PM11	0.14	0.04	0.04	0.28	0.12	195.36	1.05
PM12	0.38	0.14	0.13	1.65	1.73	236.68	3.85
PM13	0.02	0.04	0.01	0.22	0.07	173.28	0.80
PM14	0.15	0.06	0.06	0.18	0.14	3328.49	1.78
PM15	0.18	0.06	0.09	0.07	0.08	181.93	1.27
PM16	0.13	0.05	0.08	0.08	0.10	186.13	0.98
PM17	0.93	0.24	0.49	0.27	0.19	233.95	1.70
PM18	0.06	0.07	0.02	0.37	0.14	703.23	1.41
PM19	0.29	0.07	0.09	0.11	0.10	190.15	0.93
PM20	2.89	0.59	1.23	0.14	0.20	217.87	1.23
PM21	7.77	1.66	2.12	0.72	0.75	346.82	1.92

Snowpit 2	Sm (pg/ml)	Eu (pg/ml)	Yb (pg/ml)	W (pg/ml)	Tl (pg/ml)	Pb (pg/ml)	Bi (pg/ml)
PM25	9.21	1.71	2.74	1.73	0.80	13735.66	19975.98
PM26	1.15	0.27	0.37	0.93	0.17	269.02	5.60
PM27	1.47	0.30	0.42	8.22	0.23	383.93	12.53
PM28	0.17	0.05	0.04	0.36	0.14	200.63	2.12
PM29	0.13	0.04	0.04	0.29	0.08	201.01	1.54
PM30	5.45	1.15	1.88	4.74	0.53	6536.63	14.73
PM31	0.89	0.20	0.25	0.16	0.12	234.23	1.15
PM32	9.03	1.93	2.10	0.49	0.36	330.61	1.72
PM33	1.04	0.24	0.32	0.14	0.11	219.70	1.35
PM34	1.87	0.36	0.43	0.41	0.18	284.76	2.12
PM35	0.20	0.08	0.06	0.20	0.20	176.86	0.86

Ice samples	Sm (ng/ml)	Eu (ng/ml)	Yb (ng/ml)	W (ng/ml)	Tl (ng/ml)	Pb (ng/ml)	Bi (ng/ml)
IS1	20.77	4.20	5.66	0.14	0.17	666.92	2.45
IS2	2.27	0.48	0.61	0.15	0.08	223.01	1.62
IS3	4.09	0.68	0.88	0.14	0.08	300.24	1.51
IS4	3.94	0.77	1.03	0.20	0.13	393.14	2.33
IS5	25.84	5.37	7.47	0.30	0.40	1740.76	4.77
IS6	43.78	9.19	13.07	0.48	0.58	3088.53	6.66
IS7	80.69	17.20	23.61	0.50	0.91	5819.09	9.31

Table A4 continued

Snowpit 1	Th (pg/ml)	U (pg/ml)	Na (pg/ml)	Mg (pg/ml)	Al (pg/ml)	Ca (pg/ml)	Sc (pg/ml)
PM 01	0.75	0.43	6688.43	3059.91	2957.26	14662.30	0.56
PM 02	0.32	0.17	1413.93	7503.51	2067.06	7428.00	0.17
PM 03	2.93	1.96	8305.63	19090.71	31179.76	48916.30	2.06
PM 04	1.84	1.18	3852.13	8424.91	11394.76	21675.30	1.63
PM 05	1.26	1.24	3354.53	10550.71	16579.76	19018.30	0.88
PM 06	1.25	2.01	8753.53	8850.11	18315.76	27729.30	0.65
PM 07	0.74	0.67	19178.13	4916.71	4595.86	35406.30	0.68
PM 08	0.19	0.17	8579.33	2358.31	2035.26	11414.30	0.08
PM 09	0.18	0.27	6066.43	1933.01	1555.96	7501.80	0.03
PM10	0.30	0.18	12038.13	3676.51	11345.76	17246.30	0.08
PM11	0.10	0.06	1849.33	1351.91	3324.16	6350.20	0.08
PM12	0.36	0.34	5519.13	2723.21	6136.66	128274.30	0.13
PM13	0.08	0.06	3056.03	625.45	592.33	1854.40	
PM14	0.08	0.05	19128.13	2549.61	971.36	25957.30	0.23
PM15	0.21	0.21	6141.13	1252.71	1575.46	16065.30	0.13
PM16	0.54	0.31	3329.73	1440.51	1465.46	9125.90	0.06
PM17	0.88	3.32	5270.33	5483.71	4155.66	43379.30	0.70
PM18	0.07	0.09	2732.53	1110.91	5892.06	4283.20	0.00
PM19	0.21	0.07	2657.93	1096.71	3006.16	16729.30	0.41
PM20	1.83	1.82	1821.93	4137.11	4424.66	98746.30	2.06
PM21	3.39	3.43	24801.13	14625.71	19220.76	187334.30	4.86

Snowpit 2	Th (pg/ml)	U (pg/ml)	Na (pg/ml)	Mg (pg/ml)	Al (pg/ml)	Ca (pg/ml)	Sc (pg/ml)
PM25	3.48	2.74	18556.13	23272.71	36560.76	63090.30	1.68
PM26	0.44	0.44	3528.73	3375.31	6650.16	9568.90	0.25
PM27	1.05	0.67	8355.43	8460.31	72511.76	15843.30	0.54
PM28	0.15	0.09	3031.13	1635.41	2468.16	7428.00	0.02
PM29	0.18	0.11	4001.43	1568.01	4767.06	10454.30	0.06
PM30	3.46	2.77	15819.13	17212.71	40228.76	63090.30	3.11
PM31	0.40	0.29	3528.73	3534.71	6161.06	31346.30	0.47
PM32	1.65	2.52	16143.13	12393.71	22155.76	42863.30	1.84
PM33	0.13	0.39	2832.13	1238.51	3788.76	4312.70	0.18
PM34	0.27	0.86	16566.13	5058.51	6161.06	35849.30	0.70
PM35	0.22	0.27	5767.93	14165.71	570.32	114984.30	0.15

Ice samples	Th (ng/ml)	U (ng/ml)	Na (ng/ml)	Mg (ng/ml)	Al (ng/ml)	Ca (ng/ml)	Sc (ng/ml)
IS1	0.78	2.72	235.57	6862.82	20123.49	14050.60	0.52
IS2	0.07	0.62	56.69	1186.02	3659.25	1807.52	0.02
IS3	0.12	0.73	68.02	1445.78	4746.29	2378.76	0.05
IS4	0.10	1.03	70.54	1736.42	5686.69	2451.52	0.04
IS5	1.17	6.87	317.44	12475.62	39543.09	18707.80	0.69
IS6	2.32	11.67	489.08	20914.74	69661.08	33771.75	1.26
IS7	3.74	21.34	851.68	38451.29	126643.03	58417.68	2.14

Table A4 continued

Snowpit 1	V (pg/ml)	Cr (pg/ml)	Mn (pg/ml)	Fe (pg/ml)	Co (pg/ml)	Ni (pg/ml)	Cu (pg/ml)	Zn (pg/ml)
PM 01	4.67	8.63	93.54	1353.32	1.56	51.25	190.39	331.43
PM 02	4.93	6.58	78.72	796.09	0.61	23.62	32.60	215.09
PM 03	36.45	50.31	639.19	22104.12	11.92	63.69	283.68	387.21
PM 04	60.31	19.49	271.95	10881.12	5.28	35.04	153.98	401.55
PM 05	40.83	26.84	391.55	23290.12	7.12	25.84	233.05	266.09
PM 06	37.55	20.42	309.01	13311.12	7.50	31.72	122.42	356.93
PM 07	13.80	11.67	253.42	3234.32	3.31	11.00	244.84	172.06
PM 08	4.47	6.31	79.73	971.95	1.53	13.30	22.09	109.26
PM 09	10.49	5.09	56.48	877.10	1.30	6.99	15.26	151.34
PM10	12.33	5.41	122.35	987.72	1.24	10.83	57.92	310.71
PM11	3.38	1.80	35.59	367.32	0.62	3.50	11.06	116.12
PM12	5.41	13.35	116.46	1712.92	11.81	40.67	70.40	65328.59
PM13	2.33	50.08	15.16	252.72	0.30	5.12	25.49	51.73
PM14	4.71	8.70	50.92	991.72	1.47	1.62	55.49	157.71
PM15	3.09	0.18	66.93	979.82	1.23	0.77	7.25	89.82
PM16	2.52	7.78	85.29	817.83	2.22	2.05	7.80	131.42
PM17	6.73	7.53	317.43	6198.22	7.19	24.81	60.69	237.40
PM18	1.34	5.94	48.56	468.09	0.31	8.78	113.75	2535.59
PM19	1.95	2.39	144.59	460.19	2.74	1.54	17.51	67.99
PM20	10.01	4.97	674.57	6850.22	13.09	29.08	27.40	157.71
PM21	55.72	17.24	1176.54	10604.12	16.00	27.63	47.51	229.43

Snowpit 2	V (pg/ml)	Cr (pg/ml)	Mn (pg/ml)	Fe (pg/ml)	Co (pg/ml)	Ni (pg/ml)	Cu (pg/ml)	Zn (pg/ml)
PM25	52.43	119.82	864.93	68735.12	15.78	98.15	359.98	662.92
PM26	11.78	10.91	161.10	10664.12	4.64	15.86	157.79	267.68
PM27	20.74	205.90	7933.54	38109.12	11.64	327.51	918.33	2264.59
PM28	2.41	4.33	52.10	1321.72	1.14	10.15	35.37	1289.29
PM29	2.87	5.50	56.82	1428.42	0.92	8.61	52.37	514.71
PM30	31.64	232.60	7175.44	28822.12	30.47	486.96	1074.37	3380.19
PM31	5.19	7.30	129.26	2029.02	2.74	12.96	37.11	1595.29
PM32	43.46	24.77	1456.24	22499.12	16.73	33.60	96.76	436.61
PM33	4.95	5.94	202.88	2740.42	3.86	8.27	20.70	243.77
PM34	7.67	22.46	378.08	3925.92	6.84	32.83	130.40	1278.09
PM35	9.11	95.42	202.88	853.39	3.36	13.56	44.74	140.98

Ice samples	V (ng/ml)	Cr (ng/ml)	Mn (ng/ml)	Fe (ng/ml)	Co (ng/ml)	Ni (ng/ml)	Cu (ng/ml)	Zn (ng/ml)
IS1	48.62	30.84	4517.52	44316.52	65.02	66.52	152.36	457.90
IS2	10.08	7.24	69.40	6771.72	1.71	8.21	24.89	73.27
IS3	10.86	7.75	82.11	9130.92	2.86	12.72	30.35	69.39
IS4	16.08	9.66	99.92	11558.52	2.35	10.37	46.41	97.36
IS5	116.27	72.95	1894.20	75808.52	38.69	77.89	328.18	7130.38
IS6	198.38	111.79	3281.79	122468.57	59.61	121.71	533.15	755.00
IS7	363.26	198.94	5870.00	217353.79	107.68	220.78	962.88	1401.89

Appendix B

Table B1: Cryoconite composition data: Mineralogy raw data for samples of PM, ice samples and LLR with uncertainties for each mineral. Each sample was measured twice (measurements a, b)

Samples of PM	Quartz	Quartz uncert.	Calcite	Calcite uncert.	Dolomite	Dolomite Uncert.	Kalifeldspars	Kalif. uncert.	Plagioclase	Plagiocl. uncert.
LLRa	27.4	0.7	42	1	0.11	0.07	0.07	0.2	2.8	0.2
LLRb	25.4	0.6	40	1	0.15	0.07	0.2	0.2	2.7	0.2
PM44a	32	0.8	6.4	0.3	0.06	0.07	0.8	0.2	4.1	0.2
PM44b	37.4	1	8.2	0.3	0		1.4	0.3	4.4	0.2
PM45a	32.3	0.8	0.08	0.09	0.08	0.07	2.5	0.3	5.5	0.2
PM45b	30.8	0.8	0.02	0.09	0.2	0.08	2.7	0.3	5.7	0.3
PM46a	35.4	0.9	0		0		2.6	0.3	6.9	0.3
PM46b	36.2	0.9	0.3	0.1	0.15	0.08	4.2	0.4	7.3	0.3
PM47a	37.2	1	3	0.2	0.03	0.08	3.3	0.3	6.2	0.3
PM47b	32.7	0.8	2.4	0.2	0.06	0.07	1.5	0.3	5.5	0.2
PM49a	34.7	0.9	0.5	0.1	0.02	0.08	4	0.3	7	0.3
PM49b	25.9	0.6	0.03	0.08	0		2.3	0.2	6.6	0.2
PM50a	39	1	0.6	0.1	0.2	0.08	1.8	0.3	4.9	0.3
PM50b	40	1	0.9	0.1	0.05	0.09	1.7	0.3	4.5	0.3
PM52a	33.8	0.9	0	0.1	0		1.8	0.3	4.7	0.3
PM52b	24.3	0.5	0.09	0.08	0.01	0.06	1.7	0.2	3.3	0.2

Ice samples	Quartz	Quartz uncert.	Calcite	Calcite uncert.	Dolomite	Dolomite uncert.	Kalifeldspars	Kalif. uncert.	Plagioclase	Plagiocl. uncert.
IS1a	29	0.6	0.2	0.08	0		1.2	0.2	4.1	0.2
IS1b	37.5	0.9	0.1	0.1	0		1.4	0.3	5.4	0.3
IS4a	38	1	0.3	0.1	0.05	0.08	2.3	0.3	6	0.3
IS4b	28.5	0.6	0.25	0.09	0		2.2	0.3	4.1	0.2
IS5a	35.7	0.9	0.4	0.1	0		2.9	0.3	6.1	0.3
IS5b	34.9	0.9	0.3	0.1	0		3.4	0.3	8.4	0.3
IS6a	37	1	0.3	0.1	0.09	0.08	3.1	0.3	7	0.3
IS6b	31.1	0.7	0		0.08	0.07	3	0.3	4.8	0.2
IS7a	32.3	0.8	0.1	0.1	0		2.4	0.3	5.5	0.3
IS7b	33.1	0.9	0.4	0.1	0		2.6	0.3	4.8	0.2

Table B2: Cryoconite composition: Organic fraction of ice samples, samples of PM and LLR from loss on ignition measurements in comparison with the OC fraction from OC/EC analysis

Samples of PM	Dry weight (g)	Organic matter (%)	OC (%)
PM43	0.22	14.45	
PM44	7.98	3.77	
PM45	4.29	10.11	
PM46	11.94	9.23	
PM47	9.03	4.84	
PM49	5.76	9.34	
PM50	7.22	5.23	
PM52	3.18	8.85	
LLR	9.46	1.38	

Ice samples	Dry weight (g)	Organic matter (%)	OC (%)
IS1	3.14	6.38	3.00
IS2			5.21
IS3	0.56	7.13	5.06
IS4	2.88	8.48	2.61
IS5	2.62	9.21	3.77
IS6	6.20	9.16	6.43
IS7	3.17	9.18	2.32

Table B3: Cryoconite composition: Raw data from OC/EC analysis in (µg/cm²) including uncertainty ranges for OC, EC and total carbon (TC) and the EC to TC ratio

Ice samples	OC (µg/cm²)	OC uncert.	EC (µg/cm²)	EC uncert.	TC (µg/cm²)	TC uncert.	EC/TC ratio
IS1	22.50	1.33	3.11	0.36	25.61	1.58	0.12
IS2	11.13	0.76	3.46	0.37	14.59	1.03	0.24
IS3	10.22	0.71	3.03	0.35	13.25	0.96	0.23
IS4	14.07	0.90	5.70	0.48	19.77	1.29	0.29
IS5	29.95	1.70	7.25	0.56	37.20	2.16	0.19
IS6	51.31	2.77	11.70	0.79	63.02	3.45	0.19
IS7	14.64	0.93	5.72	0.49	20.36	1.32	0.28

Snowpit 1	OC (µg/cm²)	OC uncert.	EC (µg/cm²)	EC uncert.	TC (µg/cm²)	TC uncert.	EC/TC ratio
PM 01-03	19.56	1.18	1.50	0.28	21.06	1.35	7.14E-2
PM 04-06	31.71	1.79	3.45	0.37	35.16	2.06	9.82E-2
PM 07-09	16.33	1.02	1.01	0.25	17.34	1.17	5.81E-2
PM 10-12	9.55	0.68	0.27	0.21	9.82	0.79	2.72E-2
PM 13-15	8.98	0.65	0.48	0.22	9.47	0.77	5.11E-2
PM 16-18	8.43	0.62	3.87E-4	0.20	8.44	0.72	4.59E-5
PM 19-21	16.60	1.03	-5.95E-2	0.20	16.54	1.13	-3.60E-3

Snowpit 2	OC (µg/cm²)	OC uncert.	EC (µg/cm²)	EC uncert.	TC (µg/cm²)	TC uncert.	EC/TC ratio
PM 25-29	58.99	3.15	14.01	0.90	73.00	3.95	0.19
PM 30-32	12.48	0.82	0.18	0.21	12.67	0.93	1.44E-2
PM 33-35	9.41	0.67	0.42	0.22	9.84	0.79	4.32E-2

Samples of PM	OC (µg/cm²)	OC uncert.	EC (µg/cm²)	EC uncert.	TC (µg/cm²)	TC uncert.	EC/TC ratio
PM 48	10.91	0.75	0.16	0.21	11.07	0.85	0.01
PM 45	14.44	0.92	2.31E-3	0.20	14.45	1.02	1.60E-4
PM 46	21.97	1.30	6.26	0.51	28.22	1.71	0.22
PM 49	41.55	2.28	33.11	1.86	74.66	4.03	0.44

Table B4: Cryoconite composition: Data from granule counting of all ice samples expressed as surface area per ml, surface area per cm², number per ml and number per cm²

Surface area per ml				
Sample number	**Chlamydomonas nivalis**	**Black opaque granules**	**Thick brown granules**	**Networks**
IS1		192.0	144.2	13.6
IS2		86.4	92.5	0.7
IS3		102.0	9.8	8.6
IS4		10.7	12.1	2.0
IS5		84.6	99.1	66.1
IS6		341.3	341.2	95.0
IS7		19.9	24.1	15.0

Surface area per cm²				
Sample number	**Chlamydomonas nivalis**	**Black opaque granules**	**Thick brown granules**	**Networks**
IS1		382.3	287.1	27.2
IS2		207.9	222.4	1.7
IS3		239.7	23.1	20.3
IS4		27.7	31.1	5.2
IS5		163.4	191.5	127.8
IS6		782.0	781.9	217.7
IS7		36.2	44.0	27.4

Number per ml				
Sample number	**Chlamydomonas nivalis**	**Black opaque granules**	**Thick brown granules**	**Networks**
IS1	300	3556.2	3240.1	
IS2	34	2623.7	2307.6	
IS3	15	948.3	237.1	
IS4	70	869.3	948.3	
IS5	360	7270.4	9325.1	
IS6	210	24814.2	23707.8	
IS7	25	2054.7	3240.1	

Number per cm²				
Sample number	**Chlamydomonas nivalis**	**Black opaque granules**	**Thick brown granules**	**Networks**
IS1	597.4	7081.9	6452.4	2203.2
IS2	81.8	6311.8	5551.3	684.4
IS3	35.3	2228.5	557.1	1114.3
IS4	180.2	2237.8	2441.2	203.4
IS5	695.3	14042.3	18010.7	9463.3
IS6	481.2	56860.0	54324.8	10865.0
IS7	45.5	3742.5	5901.6	863.6

Appendix C

Table C1: Albedo raw data (10 minute mean) from all field campaign dates (1 June, 6 July, 20 July and 25 August)

Time	1 June	6 July	20 July	25 August
9:40	0.73			
9:50	0.78			
10:00	0.78			
10:10	0.78			
10:20	0.77		0.24	0.17
10:30	0.76	0.53	0.23	0.17
10:40	0.76	0.54	0.23	0.17
10:50	0.75	0.53	0.22	0.16
11:00	0.74	0.52	0.22	0.15
11:10	0.73	0.52	0.22	0.16
11:20	0.73	0.52	0.22	0.15
11:30	0.72	0.51	0.22	0.16
11:40	0.70	0.50	0.21	0.16
11:50	0.66	0.50	0.21	0.16
12:00	0.67	0.50	0.20	0.15
12:10	0.69	0.50	0.20	0.15
12:20	0.68	0.51		0.15
12:30	0.67	0.51		0.14
12:40	0.67	0.52		0.14
12:50	0.70	0.54		0.14
13:00	0.68	0.56		0.14
13:10	0.68	0.58		0.14
13:20	0.67			0.13
13:30	0.66			0.13
13:40	0.65			0.13
13:50	0.66			0.13
14:00				0.13
14:10				0.13
14:20				0.13
14:30				0.13
14:40				0.13
14:50				0.13
15:00				0.13